UNIVERSITÉ DE MONTRÉAL

DOUBLE U-TUBE GEOTHERMAL BOREHOLE OPERATION UNDER PHASE CHANGE CONDITIONS

PARHAM ESLAMI NEJAD

DÉPARTEMENT DE GÉNIE MÉCANIQUE

ÉCOLE POLYTECHNIQUE DE MONTRÉAL

THÈSE PRÉSENTÉE EN VUE DE L'OBTENTION

DU DIPLÔME DE PHILOSOPHIAE DOCTOR

(GÉNIE MÉCANIQUE)

DÉCEMBRE 2011

UNIVERSITÉ DE MONTRÉAL

ÉCOLE POLYTECHNIQUE DE MONTRÉAL

Cette thèse intitulée:

DOUBLE U-TUBE GEOTHERMAL BOREHOLE OPERATION UNDER PHASE CHANGE CONDITIONS

présentée par: ESLAMI NEJAD Parham

en vue de l'obtention du diplôme de : Philosophiae doctor

a été dûment acceptée par le jury d'examen constitué de :

M. PELLETIER Dominique, Ph.D., président

M. BERNIER Michel, Ph.D., membre et directeur de recherche

M. MARCOTTE Denis, Ph.D., membre

M. YAVUZTURK Cenk Cy, Ph.D., membre

DÉDICACE

I dedicate this thesis to Samira for her unconditional love during these years

REMERCIEMENTS

I would like to convey my sincere gratitude to those who helped me to complete this study. First of all, I am genuinely grateful to my supervisor, Professor *Michel Bernier*, for his friendly guidance, substantial support, and precious advice. It was a great pleasure for me to work under his supervision. He was an endless source of encouragement to me throughout this period. His exceptional high standards inspired me to improve my skills throughout my research at École Polytechnique de Montréal. I am deeply indebted to him for his availability at any time for consultations and discussions on my research.

I take great pleasure in acknowledging all present and former students of my supervisor and of course my good friends, *Ali Salim-Shirazi*, *Simon Chapuis*, *Antoine Langlois*, and *Yannick Allard*, who created lots of memorable moments for me during these years and helped me to integrate into the group. I would also like to extend my thanks to *Ali Salim-Shirazi* for his assistance in calibrating the thermocouples used in my experiments.

I am deeply indebted to Professors *B. R. Baliga* and *A. Teyssedou* for the knowledge I acquired throughout their incredibly valuable lectures. I am also thankful to Professor *M. Kummert* for all the encouragement, support, and friendly advice I received from him.

I like to extend my thanks to the technical and administrative staff of the Mechanical Engineering Department. Special thank to Mr. *Jean-Marie Béland* for his marvellous work on my experimental set-up.

I made many friends in Montreal, and it gives me great pleasure to acknowledge the encouragement, support, and love that I received from them. They were with me in sad and happy moments and made all these years memorable for me. I refrain from acknowledging them individually because that would take many pages, and for fear that I may inadvertently miss some of them. However, I can not help mentioning the name of my best friends, *Mahnaz*, *Ravid*, *Azin*, *Naser*, *Arezou*, *Alireza*, *Sara*, *Ali*, *Maryam and Farhad* who were with me during the most tragic moment of my life when I lost my father.

I would like to thank colleagues of the “Course de Mardi” for bringing joy during days that I was doing experiments and writing my thesis. I had a wonderful jogging experience with them along Mont Royal Park which kept me physically and mentally in shape.

I owe special gratitude to my father and my mother for their pray, unconditional love, support, and encouragement throughout my entire life. I am deeply indebted to them for every success I have ever achieved. I wish my father was alive to see this moment that he was always hopping for. I would also thank my brother for his support, love, and guidance. He provided a great deal of encouragement to me during my bachelor studies and I am grateful to him.

I would like to send a heartfelt acknowledgement to my Family-in-law for the support and love I received from them.

I would also like to acknowledge *Canada*, the province of *Québec*, and *École Polytechnique de Montréal* for giving me the opportunity to continue my studies. It is with great pleasure that I express my thanks to *Montrealers* for their kindness.

I would like to convey my gratitude to Dr. *Pelletier*, Dr. *Marcotte*, and Dr. *Yavuzturk* for accepting to be a jury member.

The financial support provided by the NSERC *Solar Building Research Network (SBRN)* and *Electricité de France*, under the guidance of Dr. Odile Cauret, is greatly acknowledged.

Last, but most importantly, I would like to express my special gratitude to my lovely wife, *Samira*, for her patience, love, and support. She was an endless source of inspiration to me for achieving my goals. She was genuinely caring during these years and I am deeply indebted to her for every single second of our life.

Parham ESLAMI NEJAD

École Polytechnique de Montréal

Montréal, Québec, Canada

December 2011

RÉSUMÉ

Les systèmes de pompe à chaleurs couplées à des échangeurs géothermiques verticaux constituent des alternatives intéressantes pour la climatisation/chauffage des espaces et le chauffage de l'eau chaude en raison de leur haute efficacité et de leur faible impact sur l'environnement. Cependant, les coûts de forage demeurent un obstacle à leur utilisation généralisée. Les coûts de forage sont directement reliés à la profondeur des puits. Dans le cas d'installations avec puits unique, la profondeur dépend principalement de l'extraction maximale de la chaleur du sol pendant le pic des charges de chauffage du bâtiment.

Pour diminuer l'extraction maximale de chaleur du sol, il a été suggéré de recharger le sol en utilisant l'énergie solaire. Cependant, dans les installations à simple puits, l'injection de chaleur solaire ne réduit pas la longueur de forage de façon significative puisque l'injection solaire ne coïncide pas nécessairement avec le pic de charge du bâtiment. Par ailleurs, la chaleur solaire injectée se dissipe dans le sol sans faire augmenter la température du sol à proximité du puits de façon significative.

Dans ce projet, une nouvelle alternative est proposée pour réduire la longueur de forage dans les installations avec puits unique. Il s'agit d'une pompe à chaleur géothermique couplée avec un système solaire dont l'échangeur géothermique est constitué d'un puits à deux tubes en U avec deux circuits indépendants entouré par un anneau de sable saturé. Cette configuration est utilisée pour l'extraction de la chaleur dans un circuit, combiné avec une pompe à chaleur, et l'injection thermique dans l'autre circuit en utilisant l'énergie solaire. Dans cette configuration, l'échangeur géothermique agit comme un échangeur de chaleur entre le capteur solaire et la pompe à chaleur. Lors des périodes de pointe de chauffage du bâtiment, généralement la nuit lorsque l'énergie solaire n'est pas disponible, la pompe à chaleur extrait l'énergie du sol et, dans certains cas, le sable saturé gèle en formant un anneau autour du puits. Cela a pour effet de ralentir la baisse de la température de retour à la pompe à chaleur et tire parti de la teneur en énergie relativement élevée associée à la chaleur latente de fusion de l'eau dans le sable. Lorsque l'énergie solaire est disponible, la chaleur solaire est injectée dans le second tube en U pour faire fondre l'anneau de glace.

Pour évaluer précisément les conséquences de l'utilisation du système proposé, des modèles théoriques pour les puits et le sol sont développés dans cette étude. Le modèle du puits tient

compte des deux tubes en U avec deux circuits indépendants et le modèle numérique du sol permet de prédire le gel et le dégel de l'anneau de sable saturé autour du puits ainsi que le transfert de chaleur par conduction dans le sol.

Un modèle analytique est d'abord développé pour prédire le transfert de chaleur en régime permanent des puits à double tube en U sans l'anneau de sable saturé. Le modèle tient compte de la résistance thermique des tubes et de l'interaction thermique entre ceux-ci. Il permet de prédire les profils de température du fluide dans les deux circuits le long de la profondeur du puits, y compris la température des deux fluides en sortie. La nouvelle configuration de puits est évaluée en utilisant des simulations annuelles d'une pompe à chaleur pour un bâtiment résidentiel situé à Montréal. Les résultats indiquent que la recharge solaire hivernale en utilisant la configuration proposée réduit la quantité d'énergie extraite du sol de manière significative. Cependant, les diminutions de la longueur nécessaire du puits et de la consommation d'énergie de la pompe à chaleur sont relativement faibles.

Enfin, les conséquences thermiques du gel de l'anneau de sable saturé sont examinées. Un modèle numérique unidimensionnel radial est développé pour évaluer le transfert de chaleur de la paroi du puits vers le sol. Le modèle est en mesure de tenir compte de couches multiples du sol et le changement de phase est traité en utilisant la méthode des capacités thermiques équivalentes. Une installation expérimentale à échelle réduite a également été construite. Elle a été utilisée pour valider avec succès le modèle numérique. Ce modèle numérique du sol est par la suite combiné avec le modèle du puits afin d'examiner différents scénarios d'opération typiques. Les résultats montrent que la température de la paroi du puits demeure autour de 0 º C pendant plusieurs jours lorsque l'anneau de sable gèle alors qu'elle serait ramené à des valeurs beaucoup plus faibles sans la présence de l'anneau de sable saturé. Le gel est limité à quelques centimètres autour du puits. Lorsque l'énergie solaire est disponible, il est possible de faire fondre la glace et de «recharger» le sol pour le prochain cycle de gel. En utilisant cette approche, la profondeur du forage peut être réduite de 38% dans certains cas.

ABSTRACT

Conventional ground coupled heat pump systems with vertical ground heat exchangers constitute attractive alternatives for space conditioning and domestic hot water heating due to their high efficiency and environmental friendliness. However, borehole costs remain a barrier for their widespread utilization. Borehole costs are mainly driven by borehole depths which, in single borehole installations, are mainly dependent on peak ground load heat extraction during peak building heating loads.

To mitigate the peak ground heat removal, it has been suggested to recharge the ground using solar energy. However, in single borehole installations, solar heat injection does not reduce the borehole length significantly since solar energy injection is not necessarily coincident with the peak building load. Furthermore, the injected solar heat dissipates into the ground without making notable increases on ground temperature near the borehole.

In this work, a new solar assisted ground coupled heat pump alternative is proposed to reduce the borehole length in single borehole installations. The system under study consists of a double U-tube borehole with two independent circuits surrounded by a saturated sand ring. This configuration is used for heat extraction in one circuit, combined with a heat pump, and simultaneous thermal recharging in the other circuit using solar energy. In effect, it acts as a heat exchanger between the solar thermal collector and the heat pump. During peak building loads, usually at night when solar energy is unavailable, the heat pump extracts energy from the ground and in some cases the saturated sand freezes. This slows down the decrease in the return temperature to the heat pump and takes advantage of the relatively high energy content associated with the latent heat of fusion of water in the sand. When solar energy is available, solar heat is injected in the second U-tube to melt the frozen saturated ring.

To evaluate precisely the expected consequences of using the proposed system, theoretical models for the borehole and the ground are developed in this study. The borehole model accounts for the double U-tube with two independent circuits and the numerical ground model can handle freezing and thawing in the saturated region in the immediate vicinity of the borehole as well as pure conduction heat transfer in the ground.

An analytical model is first developed for the borehole to predict steady-state heat transfer in double U-tube geothermal boreholes without the saturated sand ring. The model accounts for fluid and pipe thermal resistance and thermal interaction among pipes, and it predicts the fluid temperature profiles in both circuits along the borehole depth, including the exit fluid temperature. The effect of the new borehole configuration is evaluated using annual simulations of a heat pump for a typical residential building located in Montreal. Results indicate that winter solar recharging using the proposed configuration reduces the amount of energy extracted from the ground significantly. However, the decreases in the required borehole length and heat pump energy consumption are relatively small.

Finally, the thermal consequences of freezing the saturated sand ring are examined. A one-dimensional radial numerical heat transfer model is developed to evaluate heat transfer from the borehole wall to the ground. The model can account for multiple ground layers and phase change is handled using the effective capacity method. A small-scale experimental set-up is also built. It was used to successfully validate the numerical model. The numerical ground model is combined with the borehole model to examine various scenarios involving typical heat pump operation. Results show that the borehole wall temperature remains around 0ºC for several days when the ground freezes while it would drop to much lower values without the presence of the saturated sand ring. Freezing is restricted to a few centimetres around the borehole. When solar energy is available, it is possible to melt the ice and "recharge" the ground for the next freezing cycle. Using this approach, borehole depth can be reduced by as much as 38% in some cases.

TABLE DES MATIÈRES

LISTE DES TABLEAUX

LISTE DES FIGURES

LISTE DES SIGLES ET ABRÉVIATIONS

$2D$	Shank spacing between the U-tubes (m)
a, b, c, d	Dimensionless parameters, defined in Eq. (3.8)
C	Fluid specific heat ($J \cdot kg^{-1} \cdot K^{-1}$)
c_s	Soil specific heat ($J \cdot kg^{-1} \cdot K^{-1}$)
c_i	Ice specific heat ($J \cdot kg^{-1} \cdot K^{-1}$)
c_w	Water specific heat ($J \cdot kg^{-1} \cdot K^{-1}$)
G	Solar radiation ($W \cdot m^{-2}$)
$G_{ij}, G'_{ij}, G''_{ij}$	Dimensionless parameters, defined in Eq. (4.A.1)
h_i	Fluid convective heat transfer coefficient, inside surface of the pipes ($W \cdot m^{-2} \cdot K^{-1}$)
H	Required borehole length (m)
k	Thermal conductivity ($W \cdot m^{-1} \cdot K^{-1}$)
k_b	Grout thermal conductivity ($W \cdot m^{-1} \cdot K^{-1}$)
k_g	Ground thermal conductivity ($W \cdot m^{-1} \cdot K^{-1}$)
k_r	Saturated sand ring thermal conductivity ($W \cdot m^{-1} \cdot K^{-1}$)
L	Latent heat per unit mass ($J \cdot kg^{-1}$)
$\dot{m}$	Mass flow rate of the circulating fluid ($kg \cdot s^{-1}$)
N, S	Two adjacent neighbours of a central control volume (shown in Figure 5-2)
n, s	Control volume faces (shown in Figure 5-2)
P	Central control volume represented by node P (shown in Figure 5-2)
p	Laplace transform operator
q_b	Extracted energy from the ground (kWh)
q_{solar}	Solar energy injected into the borehole (kWh)
r	Radial distance from the center (m)

r_b	Borehole radius (m)
r_{int}	Freezing interface radius in the saturated region (m)
r_{intmax}	Maximum radius of the frozen region (m)
r_p	Pipe external radius (m)
r_{sr}	Saturated sand ring radius (m)
R	Thermal resistance, defined in Eq. (3.1) ($m \cdot K \cdot W^{-1}$)
R^{Δ}	Thermal resistance, defined in Eq. (3.4) ($m \cdot K \cdot W^{-1}$)
R^{*}	Dimensionless thermal resistance
R_{pipe}	Combined thermal resistance of the fluid and pipe wall ($m \cdot K \cdot W^{-1}$)
T_a	Ambient temperature (^oC)
T_b	Borehole wall temperature (^oC)
T_f	Fluid temperature (^oC)
T_f', T_f''	Inlet fluid temperatures (^oC)
T_{inhp}	Inlet fluid temperature to the heat pump (^oC)
T_{ouths}	Outlet fluid temperature from the heat source (^oC)
T_m	Melting temperature (^oC)
T_{mean}	Solar collector mean fluid temperature (^oC)
$(U_T)_c$	Uncertainty of the temperature measurement (^oC)
$(U_T)_r$	Uncertainty associated with the probe location accuracy (^oC)
U_r	Uncertainty of the thermocouple tip location (m)
U_T	Global temperature uncertainty (^oC)
W_{hp}	Annual heat pump energy consumption (kWh)
z	Axial coordinate along the borehole depth (m)
Z	Dimensionless z coordinate

Δt	Time interval (s)

Greek symbols

2δ	Phase change temperature range (^{o}C)
α	Ratio of thermal capacities (defined in Eq. (4.9))
$\beta, \varepsilon, \gamma, \eta$	Dimensionless parameters in Eq. (3.A.1)-(3.A.3)
γ, η	Dimensionless parameters in Eq. (4.A.1)
θ	Dimensionless fluid temperature
$\bar{\theta}$	Laplace transform of θ
ϕ	Soil porosity
ρc	Heat capacity ($J \cdot m^{-3} \cdot K^{-1}$)
ρ_{sp}	Density of soil particles ($kg \cdot m^{-3}$)
ρ_{w}	Density of water and ice ($kg \cdot m^{-3}$)

Subscripts

is	bulk average values of the frozen regions
ws	bulk average values of the unfrozen regions
1-3	1-3 circuit in the 1-3,2-4 configuration
2-4	2-4 circuit in the 1-3,2-4 configuration

Abbreviations

1-D	One-dimensional
2-D	Two-dimensional
3-D	Three-dimensional
CHS	Cylindrical heat source
DST	Duct ground heat storage model
GCHP	Ground coupled heat pump

GHE	Ground heat exchanger
HDPE	High density polyethylene
LHEST	Latent heat energy storage tank
SAGCHP	Solar assisted ground coupled heat pump
SCHP	Solar coupled heat pump
TC	Thermocouples

INTRODUCTION

Ground coupled heat pump systems (GCHPs) are attractive alternatives to conventional air conditioning systems due to their high efficiency and environmental friendliness. This study concentrates on the ground part of GCHPs and more specifically on vertical ground heat exchangers (GHEs) as presented schematically in Figure 1. In heating mode, the heat pump extracts heat from the ground while in cooling mode it rejects heat to the ground. Typically, this can be accomplished with a coefficient of performance (COP) of about 3. With such a COP, in heating, two units of energy are collected from the ground and three are delivered in the house with one unit provided by the heat pump compressor.

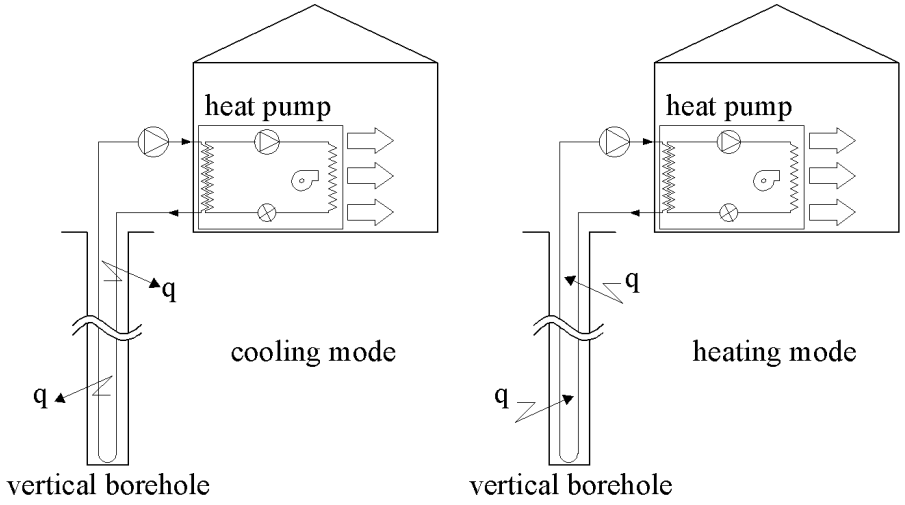

Figure1: Schematic representation of a GCHP system in heating and cooling modes

However, in heating dominated climates (e.g. Canada), the performance of the ground coupled heat pump decreases gradually over time. This is due to the fact that more heat is extracted from the ground than the amount rejected during the cooling season (if the heat pump is used for cooling). The ground temperature reduction in the vicinity of the borehole over the years results in a decrease in the inlet temperature to the heat pump, which translates into a reduction in the coefficient of performance (COP). In some extreme cases, for undersized boreholes, heat pumps cease to operate due to inlet temperatures that are below their recommended operating limit.

Typically, two alternatives are used to avoid this situation. The first one is to use longer boreholes to overcome the peak building load of future years. However, high borehole drilling costs are often a barrier to the use of longer boreholes. The second alternative is to use an

auxiliary source of energy, electric heating, to supplement the heat pump output during peak building loads. This reduces the overall seasonal COP of the system.

Other alternatives have been examined to improve system performance and reduce borehole length. One such alternative uses a free and renewable source of energy such as solar energy to assist GCHP systems. These solar assisted ground coupled heat pumps (SAGCHPs) use solar heat to either increase the inlet temperature to the heat pump or to recharge the ground or a combination of the two.

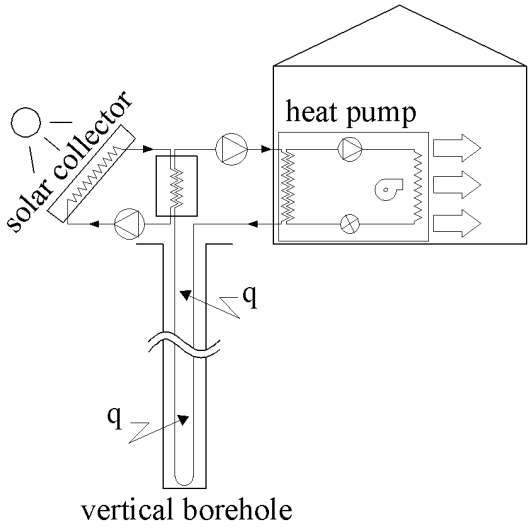

Figure 2: Schematic representation of a solar-assisted ground coupled heat pump system

Figure 2 shows one possible configuration for a SAGCHP with an intermediate heat exchanger. Even though, the additional heat exchanger may add to the complexity of the system, several studies indicate that it is a viable option for multiple borehole installations in heating-dominated climates. However, in single borehole installations (typically for residential buildings), studies have shown that solar heat injection into the borehole does not reduce the borehole length significantly since it is not necessarily coincident with the peak building load. Furthermore, the injected solar heat dissipates into the ground without making notable increases on ground temperature near the borehole. Consequently, borehole length can not be reduced and the heat pump energy consumption reduction is minimal.

In this research, a new SAGCHP alternative is proposed to reduce the borehole length in single borehole installations. The system under study is presented schematically in Figure 3. It consists of a double U-tube borehole with two independent circuits surrounded by a saturated sand ring.

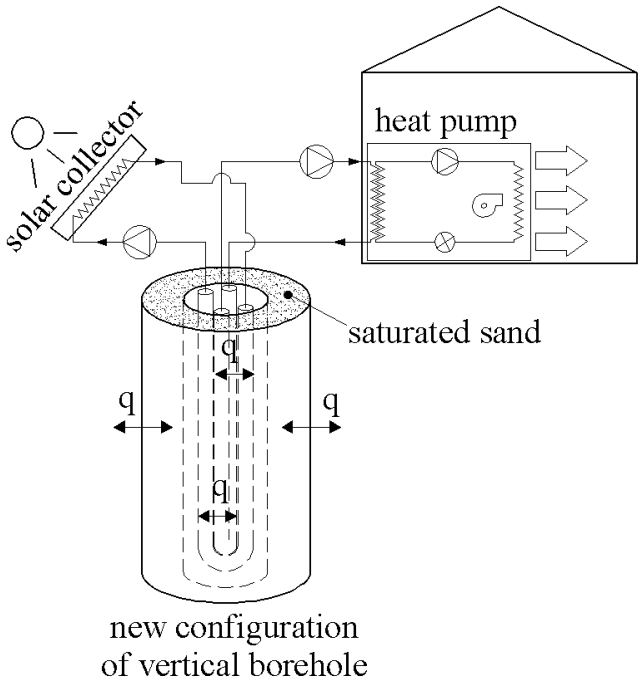

Figure 3: Schematic presentation of the proposed system

As shown in Figure 3, one circuit is linked to a heat pump and the other is connected to thermal solar collectors. In effect, the borehole in this configuration acts as a heat exchanger between the solar thermal collectors and the heat pump. Three modes of operation are possible: heat pump operation only, solar recharging with the heat pump off, and combined operation of the heat pump and solar collectors.

During peak building loads, usually at night when solar energy is unavailable, the heat pump extracts energy from the ground and in some cases the saturated sand freezes. This slows down the decrease in the return temperature to the heat pump and takes advantage of the relatively high energy content associated with the latent heat of fusion of water in the sand. When solar energy is available, solar heat is injected in the second U-tube to melt the frozen saturated ring and recharge the ground for the next freezing cycle.

To evaluate the merits of the proposed system, theoretical models for the borehole and the ground are developed in this study. The borehole model accounts for the double U-tube with two independent circuits configuration and the numerical ground model can handle freezing and thawing in the saturated region in the immediate vicinity of the borehole as well as the conduction heat transfer in the ground. A small-scale experimental set-up which mimics the behaviour of a geothermal borehole is built to validate the numerical model. Based on

temperature measurements in the sand, the numerical ground model is validated under freezing and non-freezing conditions.

Finally, the ground and borehole models are coupled and used in several simulations with real heat pump operation to evaluate the effects of this new system on borehole length and heat pump energy consumption. The optimum saturated sand ring radius is also evaluated for different ground thermal conductivites.

CHAPITRE 1 LITERATURE REVIEW

Overview

This study examines a borehole configuration for solar assisted ground coupled heat pump systems. It consists of two U-tubes with two independent fluid circuits. Solar collectors are connected to one circuit for solar recharging while the heat pump is linked to other circuit. The borehole is surrounded with a relatively small saturated (with water) region in its immediate vicinity. To our knowledge this configuration has not yet been studied. The following literature review describes previous work related to the modeling of geothermal boreholes, ground freezing, and solar recharging of geothermal boreholes.

1.1 Borehole and ground Models

Heat transfer to and from the ground in the vicinity of vertical ground heat exchangers (GHEs) is rather complicated. Several thermo-physical processes are involved such as multidimensional heat and moisture transfer, ground water movement, possible freezing and thawing, and frost expansion.

Several models have been developed for the design and simulation of vertical GHEs. However, each considered different assumptions to facilitate the calculations, particularly in geothermal engineering applications. This subsection describes briefly the existing models used to analyse vertical U-tube GHEs. Before introducing existing borehole and ground models, vertical U-tube borehole characteristics and configurations are presented here.

For vertical U-tube boreholes two major configurations are typically encountered, double U-tubes (popular in Europe) and single U-tubes (used in North-America) as shown in Figure 1-1. The U-tubes are made of high density polyethylene (HDPE) pipes with a U-bend at the end to reverse the direction of the flow. The space between the pipes and the borehole wall is usually filled with a grout. The grout is used to prevent contamination of aquifers and to augment heat transfer from the fluid to the ground. The circulating fluid flowing in the U-tubes is either water or a water-antifreeze mixture. The double U-tube configuration has a smaller borehole thermal resistance which usually leads to shorter boreholes.

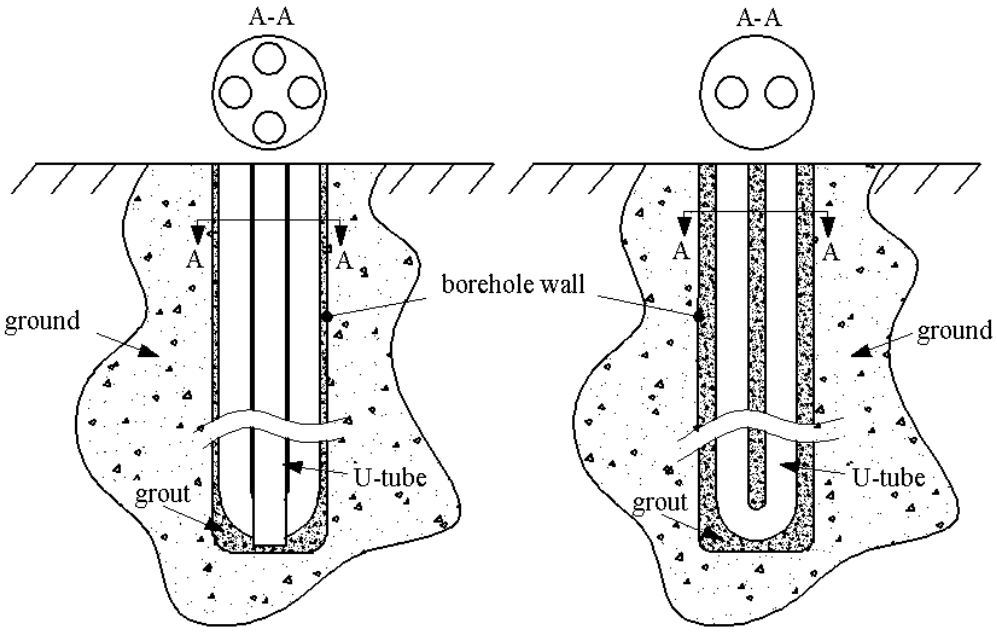

Double U-tube GHE Single U-tube GHE

Figure 1-1: Schematic representation of single and double U-tube GHEs

A two dimensional horizontal cross section of a single U-tube borehole is presented schematically in Figure 1-2. It consists of two pipes with a center-to-center distance 2D, often called the shank spacing.

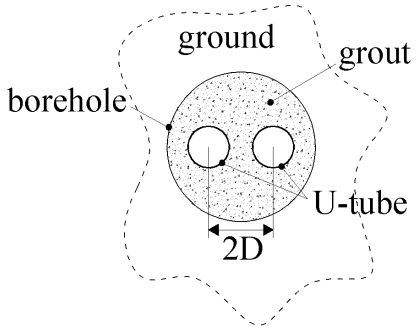

Figure 1-2: Borehole cross section

Due to the relatively high drilling cost of vertical GHEs, the initial investment associated to GCHP systems is relatively high. Therefore, it is important to estimate the required borehole length as accurately as possible. Several tools have been developed by many researchers to model the borehole and the ground in order to calculate the required length. These models are mainly based on analytical or numerical approaches.

1.1.1 Analytical models

One of the most basic transient analytical one-dimensional solutions that can be used for geothermal applications is the line source theory which was first proposed by Kelvin in 1882. Figure 1-3 presents schematically the line source model where the borehole geometry is neglected and approximated using an infinite line source or sink surrounded by an infinite homogeneous medium (ground). Pure heat conduction in the radial direction is solved in the ground. As reported by many researchers, ground temperature predictions using the line source equation are inaccurate for short time periods. For example, for a typical borehole, the line source equation is valid for times greater than approximately 10 hours.

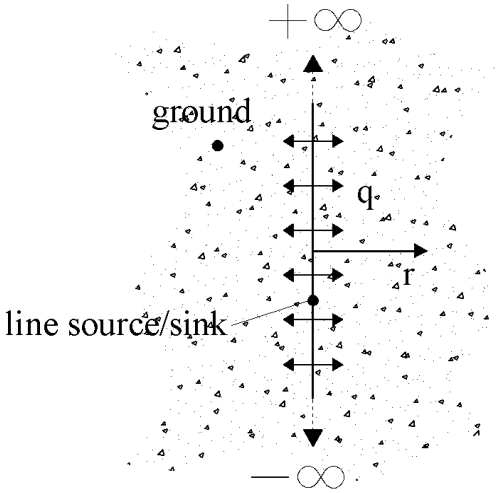

Figure 1-3: Schematic representation of the line source model

Zeng et al. (2002) developed a finite line source model in a semi-infinite medium to evaluate more precisely the two-dimensional temperature response of the vertical boreholes (Figure 1-4).

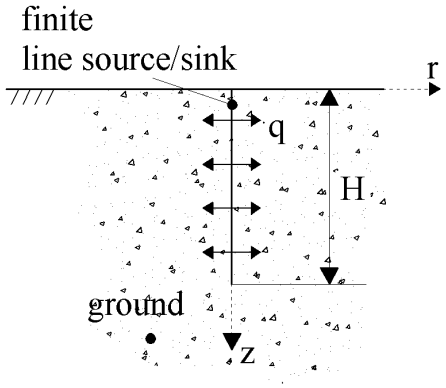

Figure 1-4: Schematic representation of the finite line source model

The other well-known one-dimensional analytical model is the cylindrical heat source (CHS) model for a finite diameter cylindrical source or sink embedded in an infinite homogeneous medium (Figure 1-5). The proposed solution (Carslaw and Jaeger, 1947) is a rather complicated indefinite integrals of Bessel functions. Ingersoll (1954) presented pre-calculated values for the integrals and used them for GCHP case studies.

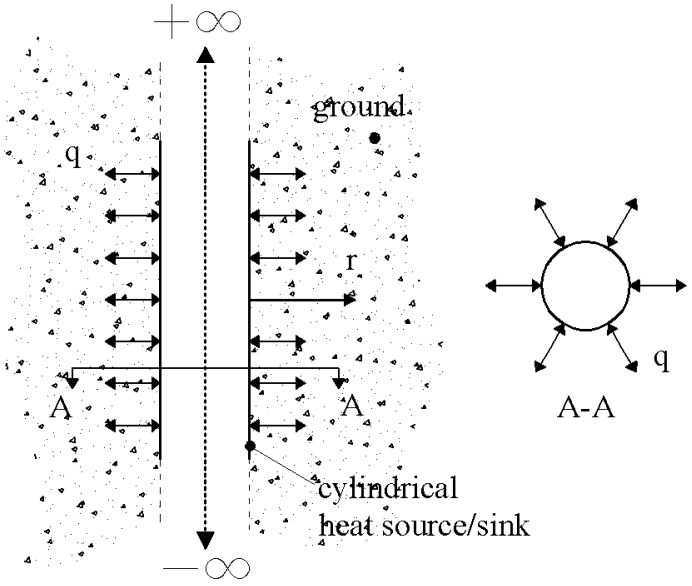

Figure 1-5: Schematic representation of the cylindrical heat source model

A more complex model is the buried cable model developed by Carslaw and Jaeger (1947). It is an analytical model used to calculate the heat flow out of an infinite cable buried in the ground.

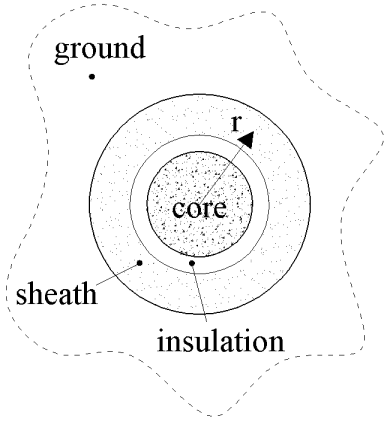

Figure 1-6: Cross section of a buried cable

As shown in Figure 1-6, the cable, consist of multi layer cylinder with a metal core, insulation, and an outer protective sheath. The most significant difference between this model and the line source and cylindrical source is that it accounts for the thermal capacity of the core and the sheath. However, due to the high thermal conductivities of the core and the sheath, the thermal resistance of these regions is neglected. The insulation ring has a thermal resistance but its thermal capacity is neglected.

Young (2004) evaluated analytically the short time response of boreholes based on the "buried cable" solution. He replaced the core and the sheath in the buried cable model with the fluid and grout of real boreholes. Thus, the model accounts for the grout and the fluid thermal capacities. Furthermore, he placed the overall borehole thermal resistance between the grout and the fluid (insulation region of the buried cable model). In order to use the buried cable model for the single U-tube borehole configuration, equivalent borehole and pipe diameters are calculated. To improve the model, he moved part of the grout capacity to the core region (fluid) by defining a so called grout allocation factor. He compared his model against the line source model in an hourly annual simulation of a small office building. He concluded that the heat pump energy consumption calculated by the line source model is as accurate as his proposed model. However, he indicated that line source over predicts the peak outlet fluid temperatures from the borehole by as much as 1.3ºC for short duration peak loads.

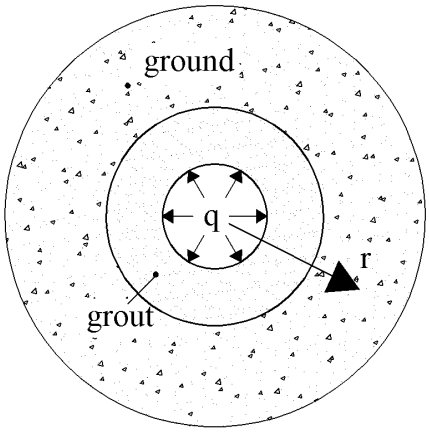

Figure 1-7: Schematic representation of the model developed by Lamarche and Beauchamp (2007)

Lamarche and Beauchamp (2007) approximated the short-time response of single U-tube boreholes using an analytical solution to the unsteady one-dimensional heat conduction problem

of concentric annuli where the inner and the outer annuli represent the grout and the ground respectively. Better results for the short time response were reported compared to other analytical solutions since the model accounts for the heat capacity of the grout. An equivalent pipe diameter technique was used to approximate the U-tube configuration with a single pipe (Figure 1-7).

Man et al. (2010) developed analytical models for both infinite (1-D) and finite (2-D) cylindrical heat sources. The model accounts for the heat capacity of boreholes by assuming a homogeneous medium for the whole calculation domain including the cylindrical region inside the heat source (Figure 1-8). The infinite heat source model was validated against the classical line source and "hollow" cylindrical source models.

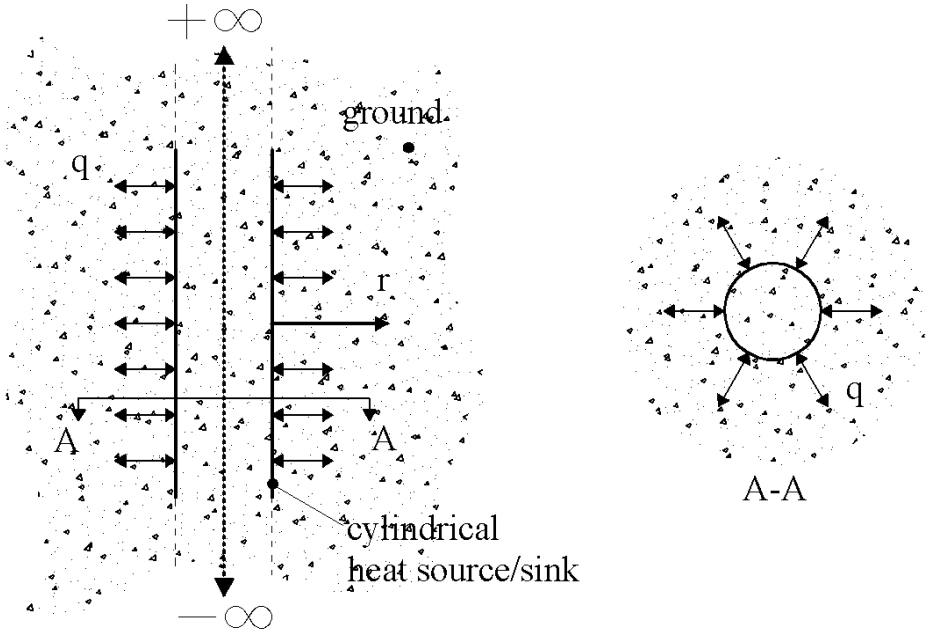

Figure 1-8: Schematic representation of the model developed by Man et al. (2010)

1.1.2 Numerical and combined numerical and analytical models

Almost all analytical models do not account for the borehole geometry since this makes the task of finding a suitable analytical model impossible. They basically replace the boreholes with cylindrical or line heat sources or heat sinks to examine the heat transfer in the ground. In other words, thermal properties of the borehole elements, pipe thermal interactions in the borehole and borehole-to-borehole thermal interferences are not taken into account. Eskilson (1987) and Hellström (1991) are at the origin of some of the earlier works on detailed modeling of boreholes and bore fields. Eskilson calculated the temperature response of multiple boreholes based on

dimensionless temperature response factors, called *g-functions*. He used a combination of analytical and numerical techniques. The numerical model is transient and two dimensional in a radial-axial cylindrical coordinate system developed for a single borehole. The borehole thermal resistance and capacitance are neglected (see Figure 1-9 for schematic presentation of the calculation domain). A spatial superposition technique is used to obtain the response of the whole bore field.

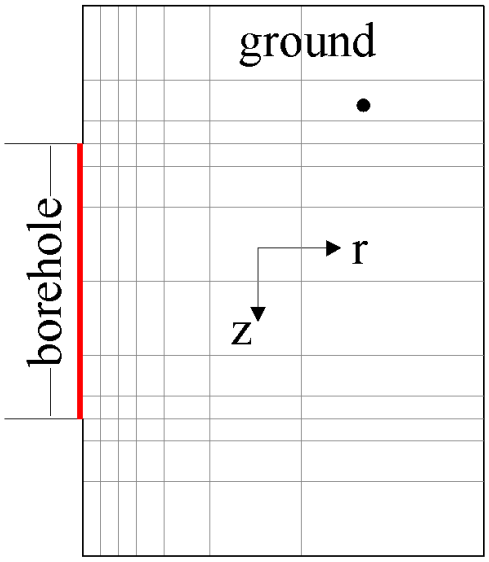

Figure 1-9: Schematic presentation of the numerical 2-D (radial-axial) calculation domain for the borehole and the surrounding ground

Hellström derived steady-state two-dimensional analytical solutions for borehole thermal resistances with an arbitrary number of pipes. Theses solutions account for thermal interactions between pipes in the borehole. He also developed a well-known simulation model for seasonal thermal energy storage which is called duct ground heat storage model, or DST, (Hellström, 1989). This model is also a combination of analytical and numerical approaches for the borehole and the ground, respectively. The model predicts temperature distribution and heat transfer over the whole calculation domain. It accounts for multiple boreholes using superposition techniques. The DST model has been implemented in TRNSYS and is often considered to be a benchmark for other models.

For annual hourly simulation of GCHP systems, Bernier et al. (2004) developed an algorithm to aggregate heating/cooling loads in conjunction with the cylindrical heat source method. They referred to this algorithm as a “multiple load aggregation algorithm”. In order to reduce

calculation time, they used “past” and “immediate” thermal history periods. Immediate thermal history is not aggregated, while past thermal history is aggregated and subdivided into four time periods of the order of a day, a week, a month, and years. For single borehole installations, they performed an analysis to find a fixed duration for each period in order to have relatively accurate results as well as relatively short calculation time. For multiple boreholes in a bore field, a numerical two-dimensional model was developed to calculate the resulting temperature field. A schematic representation of the bore field used by Bernier et al. is shown in Figure 1-10. The model accounts for the borehole interaction using the temperature penalty concept. This temperature corrects the borehole wall temperature calculated based on the CHS model.

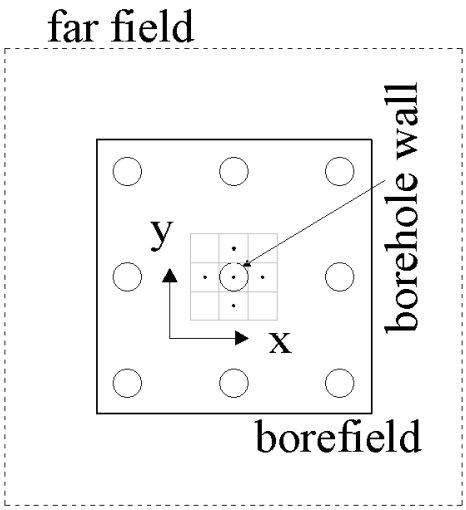

Figure 1-10: Schematic representation of the 3×3 bore field used by Bernier et al. (2004)

Marcotte and Pasquier (a2008) used the fast Fourier transform (FFT) technique to evaluate the convolution product in time of incremental heat load and the analytical model response to a unit heat load. They also proposed a subsampling of the analytical function at a certain selected times according to a geometric sequence and then using good interpolation method such as cubic spline to obtain more reduction in computing time. They reported a reduction of one to two orders of magnitude in computing time compared to time-domain approaches with load aggregation.

Muraya (1995) used a transient two-dimensional finite element model for single U-tube boreholes to analyse thermal interaction between the U-tube legs. He defined a heat exchanger effectiveness to quantify thermal interaction. He also evaluated the equivalent diameter of a single tube at the borehole center that could produce the same heat transfer as a U-tube heat exchanger.

Rottmayer et al. (1997) developed a three-dimensional finite difference model for the simulation of a single vertical borehole and its neighbouring ground. This model is proposed for a single U-tube borehole but pipes in the borehole are approximated using “pie sectors”. The model accounts for fluid, pipe wall, and grout thermal resistance. To increase the calculation speed and thus reduce the simulation time, two time steps, one for the fluid transport and the other for the heat transfer to the ground, were used.

Wetter and Huber (1997) modeled the transient behaviour of a double U-tube borehole. However, they simplified the calculations by combining the pipes and treat them as a single element. They used a numerical model to simulate the ground next to the borehole while the outer boundaries of the simulation area was handled using the analytical line source approach. They accounted for variable heat extraction by superposing constant heat extraction starting at different time steps. They implemented this model into TRNSYS and it is known as Type 451.

Yavuzturk et al. (1999) developed a two-dimensional fully implicit finite volume model for single U-tube boreholes. They extended Eskilson’s work to calculate dimensionless temperature response factors, *g-functions*, for short time scales.

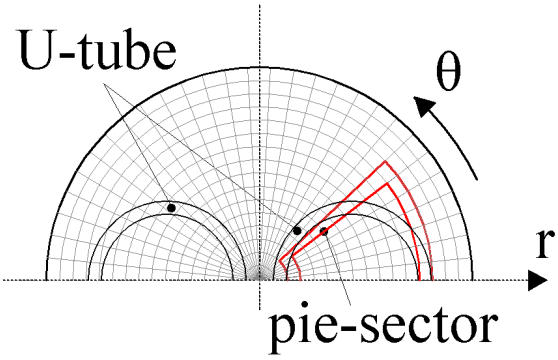

Figure 1-11: Schematic representation of the pie-sector approximation

The model accounts for thermal resistances of the grout and pipes, and the convective thermal resistance of the circulating fluid. Temperature variations along borehole depth and three-dimensional effects at the bottom of the U-tube and the ground surface are neglected. The cross section of the U-tube is approximated using “pie sectors” as shown in Figure 1-11. The pie-shaped wedge shown in this figure represents one leg of the U-tube.

Al-Khoury and Bonnier (2006) applied a three-dimensional finite element method to develop a transient flow and heat transfer model for double U-tube boreholes and the surrounding ground. The U-tubes were simulated using a single line (1-D) finite element representation. Both inlet temperatures are equal which implies a parallel arrangement for the double U-tubes.

Marcotte and Pasquier (b2008) proposed a so-called “p-linear” average temperature using a 3-D numerical simulation to evaluate the borehole thermal resistance from experimental data. They reported that the assumptions of constant heat flux along the borehole length or constant borehole wall temperature result in overestimated borehole thermal resistances. They also evaluated the economic impact of using overestimated borehole length in a case study with multiple boreholes.

He et al. (2009) developed a finite-volume-based three dimensional model to simulate the short time scale dynamic behaviour of the circulating fluid as well as transient heat transfer in and around single U-tube boreholes. The model predicts a delay for the response of the outlet temperature to a step change of inlet temperature. Contrary to analytical and simplified numerical models, three-dimensional models cannot realistically be used in annual hourly GCHP system simulations. This is due to the fact that the time required for simulation of the whole system would be very long.

Zeng et al. (2003) used Hellström’s work to establish an analytical steady-state quasi-three dimensional model for single and double U-tube configurations arranged either in parallel or in series (see Figure 1-12).

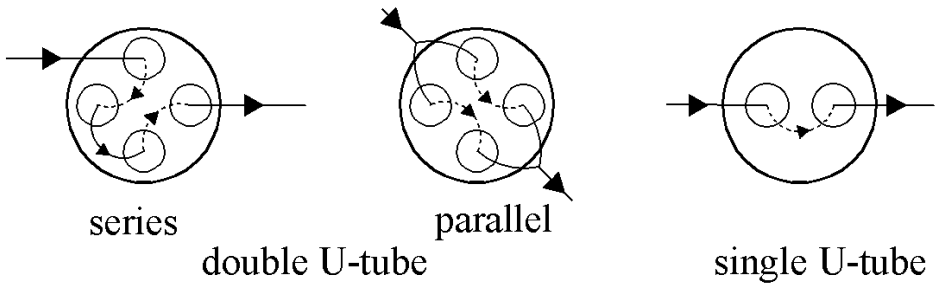

Figure 1-12: Schematic presentation of single and double U-tube boreholes

Equivalent borehole thermal resistances were calculated for several combinations of circuit arrangements. The model accounts for thermal interaction between U-tube legs. Diao et al. (2004) combined this analytical borehole model and the finite-line source model developed by Zeng (2002) to predict heat transfer inside the borehole and in the ground.

In a review study, Lamarche et al. (2010) compared different existing approaches to calculate borehole thermal resistance including thermal short-circuit between pipes. They also performed an unsteady 3-D numerical simulation of a standard single U-tube borehole. A good agreement for the axial fluid temperature distribution of a single U-tube borehole was reported between the approach proposed by Zeng et al. (2003) and the three-dimensional simulation results.

Different studies were performed to calculate steady state borehole thermal resistances. For example, Bennet et al. (1987) developed the so-called “multi-pole” analytical solution method to solve the steady state two-dimensional heat conduction equation for pipes of different radii located inside a homogenous circular region. The circular region which represents the grout is surrounded by an outer homogenous circular region which represents the ground. They calculated temperature distribution as well as the steady state borehole thermal resistance based on a constant fluid temperature along the pipe. As shown in Figure 1-13, the multi-pole method is general and pipe symmetry is not required.

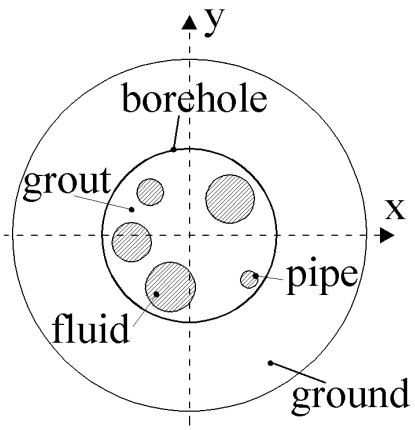

Figure 1-13: Schematic representation of the multi-pole method geometry

Steady state borehole thermal resistance was evaluated experimentally and numerically by Paul (1996). Shape factor correlations for single U-tube boreholes were developed to calculate steady state borehole thermal resistance as a function of the shank spacing, pipe diameter, borehole diameter, and grout thermal conductivity.

Gu and O'Neal (1998) calculated steady state borehole thermal resistances using an equivalent diameter method. They proposed an algebraic equation to approximate the single U-tube configuration using one circular pipe in the middle of the borehole. The circular pipe diameter (equivalent diameter) was calculated based on the diameter of the U-tube and shank spacing.

Remund (1999) proposed a set of relationships for different single U-tube borehole configurations to calculate the steady-state borehole thermal resistances based on conduction shape factors obtained from empirical data.

Al- Khoury and Bonnier (2005) developed a three-dimensional steady state flow and heat transfer model for single U-tube boreholes and the surrounding ground. The model accounts for ground water flow. Model validation did not correspond to the single U-tube borehole embedded in the ground. It was performed in two separate steps: examining heat flow in a 3-D ground structure without the borehole and examining heat flow in a single heat pipe.

1.2 Ground Freezing

Artificial ground freezing, which is commonly used for construction and mining purposes, has been reported in several studies. They mainly evaluated frost expansion, soil temperature distribution and required refrigeration capacity.

1.2.1 Artificial ground freezing for construction or mining purposes

In an early study, Hashemi and Sliepcevich (1973) developed a 2-D numerical model to evaluate the effect of ground water flow (seepage flow) on artificial ground freezing. Mass and energy conservation equations as well as Darcy's equation for unidirectional velocity field were solved simultaneously based on a finite difference method to calculate the temperature and velocity fields around a row of freeze-pipes.

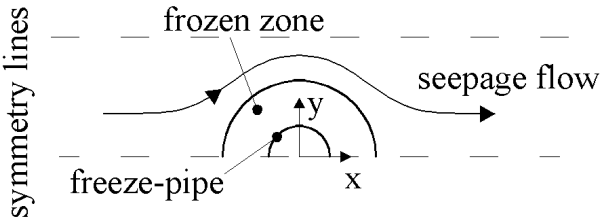

Figure 1-14: Schematic representation of the 2-D model developed by Hashemi and Sliepcevich (1973)

The effective capacity method is used to account for the latent heat of the water. Bulk average values of thermal conductivity and specific heat of the wet soil vary with temperature in the calculation domain. The authors indicated that a relatively small ground water flow perpendicular

to the freeze-pipes axis has no significant effect on the ice interface growth in the horizontal direction.

Giudice et al. (1977) developed a 2-D finite-element ground freezing model to model freezing under roads. Different properties for frozen and unfrozen materials as well as different soil layers are considered in their study. However, water and soil elements are not specified separately and therefore the soil porosity did not appear in the formulations. Consequently, unfrozen and frozen soils are considered as two materials with their own thermal conductivity and heat capacity. An effective capacity method was used to handle the latent heat effect.

Newman and Wilson (1997) developed a 1-D model (in the ground depth direction) for freezing unsaturated soil. They combined heat and mass transfer equations by using soil-freezing and soil-water characteristic curve data generated by other researchers. They calculated temperature evolutions as well as unfrozen water content and suction for the nodes positioned at or behind the frost front in the unfrozen soil region. Ice content values are computed using permeability versus suction relationships of unsaturated soil. They compared computed results with existing experimental results and good agreement was reported.

Frivik and Comini (1982) developed a 2-D finite element model of ground freezing in the presence of ground water flow for saturated soils. In this model, coupled velocity and temperature fields were calculated using energy and mass conservation equations. They accounted for the latent heat of fusion of water using a temperature dependent specific heat for the ground. A small convection contribution to the total energy transfer was reported due to a very low value of permeability. No ground water flow was assumed at the frozen soil region. An experimental set-up of a soil freezing plant was built to validate the computed results. Good agreement was found between predicted and measured temperature fields.

Mikkola and Hartikainen (2001) modeled the heat and mass transfer involved in freezing a saturated soil. They developed a 2-D model based on the mass, momentum, and energy conservation equations as well as entropy inequality equation for soil, water, and ice. The constitutive equations of the porous medium were derived based on the theory of mixtures with the concept of molar volume fractions and on the basic principles of continuum mechanics and macroscopic thermodynamics. The results were validated against 2-D experimental data and good agreement was reported.

Sres et al. (2006) and Sres and Anagnostou (2007) developed a 3-D numerical model based on the finite element method to evaluate freezing around concentric cylinder embedded in the ground. The model accounted for ground deformation and ground water flow. In this model, coupled temperature and velocity fields were calculated using the energy and mass conservation equations. The latent heat effect during freezing and thawing of the ground was handled using a temperature dependent specific heat of the soil. Simplified numerical techniques were implemented to increase computational efficiency. The results were validated against experimental data from a freezing process laboratory and showed a good agreement.

1.2.2 Natural freezing in soil around a buried pipeline

Lu and Wang (2008) developed a 2-D flow and heat transfer model for ground freezing around a buried crude oil pipeline during a shutdown period. . The model includes natural convection effects in the solidifying crude oil (Figure 1-15).

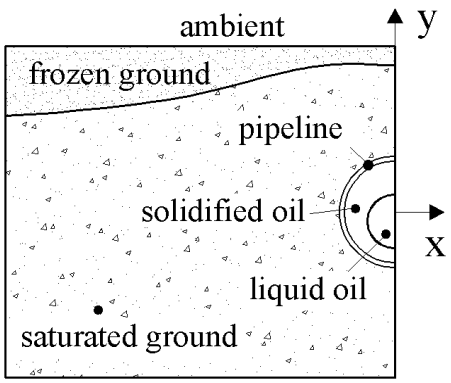

Figure 1-15: Schematic representation of the 2-D model developed by Lu and Wang (2008)

The enthalpy method was used to calculate the temperature and flow fields as well as the frozen-unfrozen soil and crude oil interfaces. Mass, momentum, and energy conservation equations were discritized and solved using on a fully implicit finite difference scheme based on the control volume method.

1.2.3 Freezing in porous media

Since soils can be considered as a porous material, the methods used to handle solidification and melting in porous media can be applied for soil-water media as well. However, heat transfer modes in porous media can be different. Freezing and melting in a porous medium is commonly classified into three categories; pure conduction, combined conduction and forced convection,

and combined conduction and natural convection models. Pure conduction and combined conduction and natural convection models are of interest to this study and a few studies in these areas will now be reviewed.

Weaver and Viskanta (1985) performed a 1-D numerical study of the solidification of saturated porous media in a cylindrical capsule. Heat is extracted from the outer surface of the capsule using a copper heat exchanger wrapped and soldered around the outside of the capsule (see Figure 1-16).

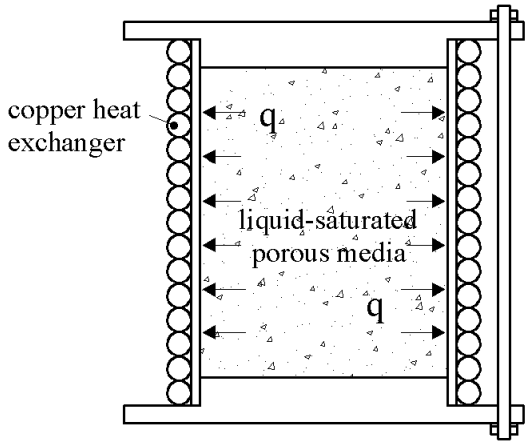

Figure 1-16: Experimental set-up built to validate the 1-D numerical model of Weaver and Viskanta (1985)

The pure conduction energy equation for the solid and liquid are solved based on a finite difference method for a fixed grid system. The latent heat effect is taken into account using an interfacial energy balance equation. The effective thermal conductivity of the porous media and of the phase change material (PCM) is calculated using empirical formulations. An experimental validation for water-glass beads and water-aluminum beads, were performed and good agreement between predicted and measured data for the water-glass beads is reported. However, due to large differences between the properties of aluminum and water, the local temperature equilibrium assumption was violated and poor agreement was reported for the water-aluminum beads.

Wang et al. (1990) evaluated the effect of natural convection on solidification of a superheated liquid-saturated porous media around a cold vertical cylinder. A 2-D model was developed to solve the energy equation in the solid and liquid regions, the momentum equations in the liquid region and the energy balance equation at the solid-liquid interface. Thicknesses of the frozen layer, temperature distributions, and velocity fields were obtained. The energy equation in the

solid region around cylinder was solved in the cylindrical coordinate systems while the Cartesian coordinate system was used in the liquid region. Consequently, the radial curvature effects were neglected in the liquid region. The authors did not validate the predicted values against experimental data. They reported significant convection effects under high values of the Rayleigh numbers and liquid superheat.

Rattanadecho and Wongwises (2008) developed a 2-D freezing model of water-saturated porous media using a moving mesh technique. The unsteady conduction equation was solved iteratively together with a moving boundary condition using an implicit-finite difference method. A rectangular cavity filled with water-saturated glass beads was modeled with different boundary conditions (see Figure 1-17). Bulk average values of thermal conductivity, density, and thermal heat capacity for two frozen and unfrozen regions were considered. Predicted values were validated against experimental measurements and available analytical solution and good agreement was reported.

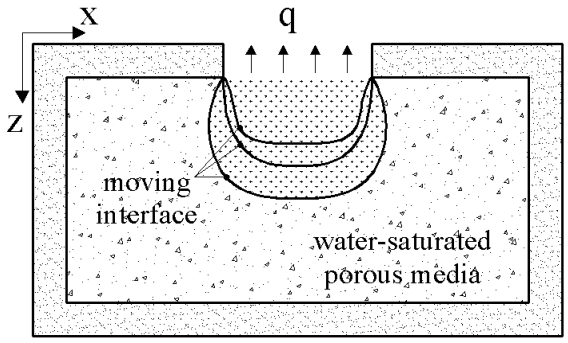

Figure 1-17: Rectangular cavity filled with water-saturated glass beads modeled numerically by Rattanadecho and Wongwises (2008)

1.2.4 Freezing in geothermal energy utilization

A few researchers evaluated the effect of groundwater advection on boreholes and GCHP performance and a few studies have also developed models to account for ground freezing in geothermal energy utilization. However none of them focused on ground freezing effects on system performance. Furthermore, they have not evaluated the effect of ground freezing on borehole length reduction.

For example Diao et al. (2004) developed an analytical model based on the line source approximation to account for coupled conduction and advection in a saturated soil but without

any change of phase. Wang et al. (a2009) conducted a thermal performance experiment of a borehole under groundwater flow in a city in China. A simplified theoretical model was developed to estimate the characteristics of the groundwater flow based on ground temperature profile measurements. Raymond et al. (2011) developed a method to analyze thermal response tests under more realistic conditions such as significant groundwater flow, high geothermal gradient, or heterogeneous distribution of surface properties.

Mei and Emerson (1985) are at the origin of some of the earlier works on modeling ground freezing in geothermal applications. They developed a numerical 1-D flow and heat transfer model for buried horizontal single coil connected to a heat pump.

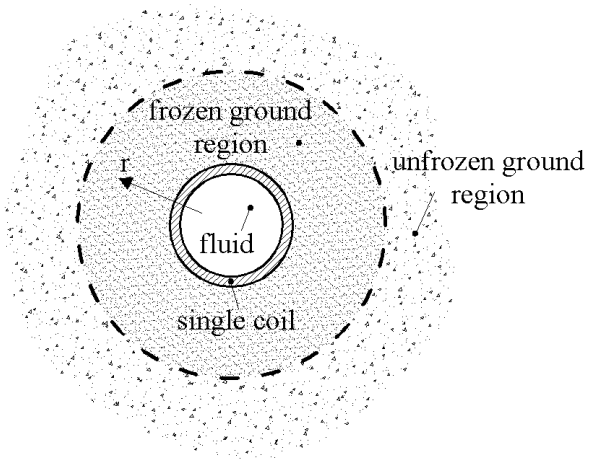

Figure 1-18: Schematic representation of the geometry modeled by Mei and Emerson (1985)

The model accounted for heat pump cyclic operation and ground freezing around the coil. The governing equations are coupled using the boundary conditions at the outer pipe surface and at the frozen/unfrozen interface. Results indicated that when the fluid inlet temperature is much lower than the ground freezing point, the total energy extracted from the ground comes mainly from the latent heat of fusion of the water in the ground.

Fukusako and Seki (1986) investigated the heat transfer characteristics of a concentric-tube thermosyphon connected to a heat pump. The concentric-tube thermosyphon was placed vertically in the ground to exchange thermal energy by free convection of the working fluid. Momentum and energy equations in the pipe and annulus were solved as well as the heat conduction equation in the ground for both the frozen and unfrozen regions by using a finite-

difference method. The model accounted for the latent heat effect using an energy balance equation at the annulus wall and at the frozen area interface.

Fan et al. (2007) developed a model to evaluate the impact of groundwater advection on the borehole and GCHP performance. The model accounted for a 2-D heat conduction and unidirectional groundwater advection in a saturated ground. Multiple boreholes in a bore field were considered while each borehole was approximated using an equivalent single pipe. The latent heat of fusion of the ground water was accounted for using an inner source term in the energy conservation equation. The results indicated that a relatively high ground water flow has a significant impact on the ground temperature field and the working fluid temperature. However, the effect of ground freezing on system design and performance was not evaluated in this study.

Nordell and Alström (2006) reported that in certain unusual cases, water-filled borehole freezing causes a high pressure that deforms the pipes in the borehole thus stopping the working fluid circulation. They also suggested some solutions such as replacing the water with cement or sand to solve the problem.

Marcotte et al. (2010) examined the effects of axial heat conduction by comparing the results obtained using the finite and infinite line source method. In one of their test cases they evaluated the effect of axial heat conduction on the energy required to freeze the ground for environmental purposes.

Recently, Fontaine et al. (2011) combined steady state results for fluid temperature inside horizontal pipes and transient ground temperature calculated based on the finite line source to develop a complete heat transfer model for both the fluid and the ground. The model accounts for phase change in the ground. A case study of horizontal pipes with spiral pattern was studied. The effect of different parameters of the borehole such as length, spacing and buried depth on the amount of heat extracted from the ground and on the ground temperature was evaluated. Results indicated that increasing length, spacing and buried depth increases the amount of energy extracted from the ground. Furthermore, they concluded that increasing buried depth can keep the ground frozen around the pipes while increasing length and spacing enhances the risk of thawing around the pipes.

1.3 Ground Solar Recharging

Despite the fact that GCHP systems are attractive options for heating and cooling applications, several studies have reported that in heating dominated climates, the performance of conventional GCHP system decreases gradually over time. This is due to the fact that the ground temperature in the vicinity of the borehole decreases over the years since more heat is extracted from the ground than the amount rejected during the cooling season. Bernier (2000) indicated that for a typical constant heat extraction of 37.5 W/m, the borehole wall temperature decreases by approximately 5ºC over a 24 hour period. Trillat-Berdal et al. (2007) also reported a reduction of 2ºC of the soil temperature in the vicinity of double U-tube borehole over twenty years of heat pump operation. The ground temperature reduction results in a decrease in the inlet temperature to the heat pump which translates into a reduction in the coefficient of performance (COP).

One possible strategy to increase the ground temperature is to combine a supplementary source of energy such as solar energy with conventional GCHP systems. These systems are usually known as solar assisted ground coupled heat pump (SAGCHP) systems or hybrid GCHP systems. This idea was first introduced by Penrod and Prasanna (1962, 1969) who proposed a system that utilizes both solar collectors and the ground as the heat source for the heat pump. In other words, they let the ground temperature recover from heat extraction by using available solar energy.

In a more recent study performed by Yang et al. (2006) a numerical simulation was conducted to find the optimum operating time of ground coupled heat pump (GCHP) and solar coupled heat pump (SCHP) systems in alternate operation mode. A vertical geothermal borehole was approximated by an equivalent cylindrical heat source/sink and the heat transfer process in the borehole surrounding was calculated using a 2-D heat conduction model. The optimum heat pump operation time was obtained based on the mean earth temperature at the end of the GCHP off period and system monetary savings. They recommended using the SCHP and GCHP systems alternately for a period of 10-14 hours a day to achieve a 30-60% recovery-rate for the ground temperature. They also evaluated different alternatives for combination of geothermal boreholes, solar collector, and heat pump. Results indicated that solar heat injection into the borehole is one of the energy efficient options.

The other possible strategy to increase the ground temperature is to inject heat into the ground using geothermal boreholes. Many researchers indicated that recharging the ground is a viable

option to make the GCHP system economically attractive since solar heat injection into the ground balances the ground loads in heating-dominated buildings and therefore reduces the borehole size (H. Yang et al., 2010). When a supplementary source of energy is combined with a GCHP system there are different options to improve overall system efficiency.

Chiasson and Yavuzturk (2003) performed a 20-year life-cycle cost analysis to evaluate the economics of SAGCHP systems for six different heating dominated climates in the U.S. In their study, solar heat is injected into the GCHP loop using a heat exchanger (see Figure 1-19).

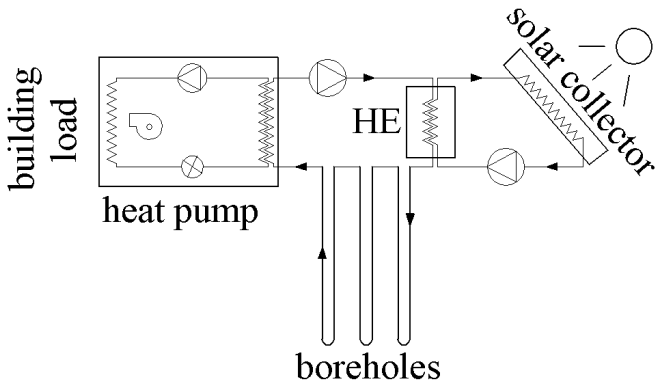

Figure 1-19: Schematic representation of the system studied by Chiasson and Yavuzturk (2003)

A relatively complicated control system is used to couple the solar and heat pump loops. The simulations were performed in the TRNSYS environment and the boreholes were simulated using the DST model. Results indicated that for multiple borehole installations the borehole length reduction due to the solar heat injection can cut the project cost significantly.

Ozgener and Hepbasli (2005) performed an experimental study to investigate the performance of a SAGCHP system for greenhouse heating based on the exergy analysis method. As shown in Figure 1-20, the circulating fluids in the right loop (solar and borehole loop) and the left loop (heat pump loop) exchange heat in heat pump evaporator. The exergy transports between the components for a steady-state steady-flow condition were determined for the average measured parameters obtained from the experimental results. The exergy efficiency for each component and the improvement potential were reported.

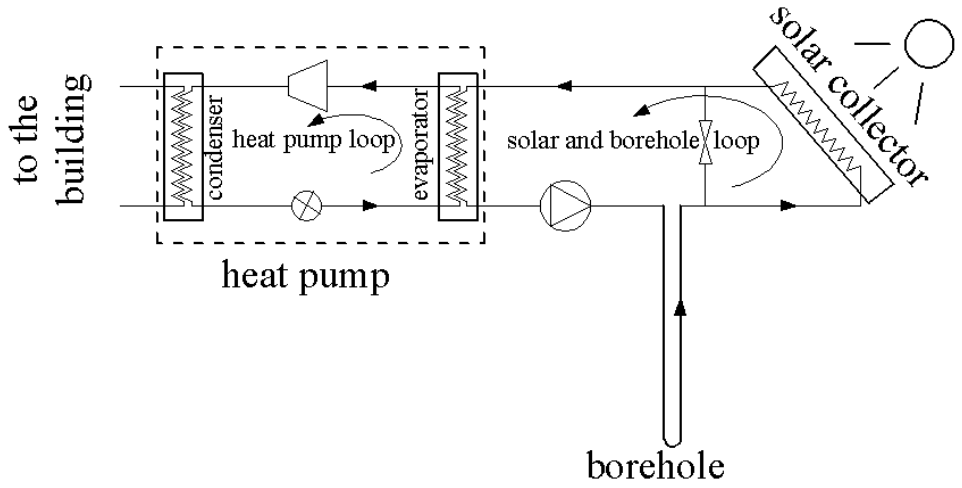

Figure 1-20: Schematic presentation of the system studied by Ozgener and Hepbasli (2005)

Trillat-Berdal et al. (2007) performed an experimentally validated simulation to investigate a SAGCHP system for air conditioning and domestic hot water production. They proposed solar heat injection into the borehole and the operation of the heat pump in cooling mode to increase ground temperature for the next heating season. They evaluated using solar energy for domestic hot water production, space heating, and ground recharging as three possible alternatives.

Han et al. (2008) investigated different operation modes of a SAGCHP system in the presence of a latent heat energy storage tank (LHEST) in heating dominated climate. A year was divided into two different periods with and without heat pump operation. With favourable weather when the heat pump is not working, the priority is given to charging the storage tank followed by solar energy injection into the borehole. A vertical single U-tube geothermal borehole was approximated using an equivalent cylindrical heat source/sink and the 2-D heat conduction energy equation was solved in the ground. They reported a 12.3% increase in system COP for a combined SAGCHP/LHEST system compared to SAGCHP without a LHEST.

Wang et al. (b2009) simulated the operational performance of a SAGCHP system for residential buildings. The system mainly consists of a solar collector, heat pump, ground heat exchanger, and water storage tank. The solar energy was first injected into the water storage tank and then into the ground. In heating mode, the heat pump was used to provide space heating when the water storage tank can not satisfy the building load. A short period of simulation was validated against experimental data. Results indicated that the system performance depends strongly on the solar collector area and water storage tank volume.

Kjellsson et al. (2010) evaluated five SAGCHP alternatives and compared them against a base case without solar collectors. They indicated that the best option with the highest reduction in electricity consumption is a SAGCHP system with solar heat injection into the boreholes in winter combined with solar domestic hot water production during the summer. They used the DST model in TRNSYS to simulate the borehole.

Stojanovic and Akander (2010) conducted a long-term performance test of a SAGCHP system for residential heating in Nordic climatic conditions. They evaluated the heat pump and the whole system performance using seasonal performance factors. Solar energy is injected into the ground when the heat pump is off while it is used to increase the heat pump evaporator temperature using a heat exchanger when the heat pump is working. A compact horizontal ground heat exchanger is used. Results indicated that despite unfavourable building conditions, the proposed system succeeded to provide 2-year heating requirements. The seasonal performance of the heat pump and the whole system were reported to be 2.85 and 2.09, respectively.

Wang et al. (2010) performed an experimental study of a SAGCHP, located in a cold climate, with solar energy storage in the ground during summer. In the summer, solar heat is injected into the ground using 12 vertical single U-tube boreholes. During winter, solar heat is used in priority to heat the building and only when the solar heat is not sufficient, the heat pump is activated to provide the heating requirements. Results indicated that the energy extracted from the ground in winter is 75.5% of the heat injected into the ground in summer. The average system COP of the system was equal to 6.55.

W. Yang et al. (2010) investigated the effect of different SAGCHP alternatives on ground temperature recovery in the vicinity of geothermal boreholes. A 2-D numerical heat transfer model, including ground freezing was developed. The vertical geothermal borehole was approximated as a cylindrical heat source/sink and its diameter was calculated using the equivalent diameter approach. Solar heat is injected into the borehole when the heat pump is not operating. Transient borehole wall temperatures were calculated to evaluate how fast the ground temperature recovered in different alternatives. The effect of ground freezing on system design and performance was not evaluated in this study.

All studies reviewed in this section used either single U-tube or double U-tube borehole configurations with series or parallel circuit arrangements. Since simultaneous charging and

discharging of the ground are not possible for these configurations, storage tanks or additional heat exchangers are required, which adds to the complexity of the system. In order to reduce the relative complexity of the system presented in Figures 1-19 and 1-20 and to make simultaneous heat injection and heat extraction possible, double U-tube borehole with two independent circuits can be used. In this configuration one circuit is linked to a heat pump and the other is connected to thermal solar collectors. In effect, this configuration with two independent circuits acts as a heat exchanger between the solar thermal collector and the heat pump and reduces the complexity of the system.

Chapuis and Bernier (2008, 2009) are at the origin of two studies that attempted to model double U-tubes in conjunction with seasonal storage. In the first study, Chapuis and Bernier (2008) used an external heat exchanger combined with the DST model to mimic simultaneous charging and discharging in the ground heat exchanger. Later, they modified the DST model to handle double U-tube boreholes with two independent circuits (Chapuis and Bernier, 2009). However, the thermal interaction between the U-tubes in the borehole was not taken into account.

Kummert and Bernier (2008) proposed a new system for space conditioning and domestic hot water heating in a Canadian climate using a gas-fired absorption heat pump coupled with a vertical geothermal borehole with two independent circuits linked, respectively, to the evaporator and the condenser of the heat pump. They considered three modes of operations, including heating only, cooling only, and simultaneous heating/cooling. The ground heat exchanger was modeled using the DST model, which precluded any studies on simultaneous flows in the two independent circuits.

Bernier and Salim Shirazi (2007) and Eslami nejad et al. (2009) evaluated the impact of solar heat injection on borehole length and heat pump energy consumption. However, they approximated the double U-tube configuration with a single U-tube based on a simple approach which assumed that the heat transferred into the ground is the sum of the solar heat injection and the heat pump extraction/rejection. Depending on the magnitude of these two terms, the value of the heat transferred into the ground can either be positive or negative. Furthermore, both outlet fluid temperatures were assumed equal. Results indicated that, for single borehole installations, solar heat injection can not reduce the borehole length or heat pump energy consumption

significantly. This is due to the fact that the solar heat is not necessarily coincident with the peak building load and therefore it dissipates rapidly into the ground without making notable effects.

This last finding corroborates the findings of Georgiev et al. (2006) who indicated that only a small portion of solar energy injected into the ground can be extracted due to the heat dissipation into the ground and heat losses from the surface.

In this research, a new SAGCHP alternative is proposed to reduce the borehole length for single borehole installations. It consists of a double U-tube borehole with two independent circuits surrounded by a saturated sand ring. Such a configuration has not yet been analysed and reported in the literature.

CHAPITRE 2 OBJECTIVES AND THESIS ORGANISATION

Solar heat injection into boreholes has been proposed to balance the annual ground load in heating dominated climates or to reduce the impact of continuous heat extraction during peak building loads. In this research, a new borehole configuration is proposed to combine solar collectors and GCHP systems. Contrary to most systems, the new double U-tube borehole with two independent circuits configuration can be used for simultaneous heat extraction in one circuit and thermal recharging in the other. In addition it is proposed to surround the borehole with a small saturated sand ring. In peak heating conditions this ring would be allowed to freeze in order to take advantage of the relatively high energy content associated with the latent heat of fusion of water during freezing and thawing of the borehole surroundings. A model for this new borehole configuration is developed and used with other system components including heat pumps and solar collector.

Based on the expertise gained during this work, Electricité de France solicited the author and his supervisor to undertake a study on various similar borehole configurations. This work was the subject of a confidential report (Eslami-nejad et al. 2010) and will not be presented in this thesis.

2.1 Thesis objectives

The main objective of this work is to assess the applicability and benefits of the double U-tube with two independent circuit configuration equipped with a saturated ring both in terms of heat pump energy consumption and borehole length reduction. In order to achieve this overall goal, it is necessary to achieve a number of specific objectives:

- Develop an analytical heat transfer model for double U-tube boreholes with two independent circuits.
- Evaluate the effect of solar heat injection into a borehole on borehole length and heat pump energy consumption using the new borehole configuration but without the saturated ring.
- Develop a numerical heat transfer model which accounts for freezing and thawing in the immediate vicinity of a borehole.

- Design and build a small-scale experimental set-up to mimic the behaviour of a geothermal borehole to validate the ground model under freezing and thawing conditions.
- Combine the ground and borehole models into a single model.
- Perform annual simulations of the coupled model in conjunction with the operation of heat pump and solar collectors.
- Perform a parametric analysis to optimize the sand ring radius as a function of ground thermal conductivity.

2.2 Thesis organization

This dissertation includes six chapters and is submitted as a "thesis by articles". The first chapter describes previous work related to the modeling of geothermal boreholes, ground freezing, and solar recharging of geothermal boreholes. The second chapter clarifies the objectives of this study and presents the organisation of this dissertation. The next three chapters present three journal articles. The next chapter presents the first article entitled “Heat transfer in double U-tube boreholes with two independent circuits”. It was published in the *ASME Journal of Heat Transfer* (Eslami nejad and Bernier, a2011). This paper addresses the first specific objective mentioned earlier. It presents the development of an analytical model to predict steady-state heat transfer in double U-tube geothermal boreholes equipped with two independent circuits. The model accounts for thermal interaction among pipes and it predicts the fluid temperature profiles in both circuits along the borehole depth including the exit fluid temperature. Different circuit configurations are assessed under typical borehole operating conditions.

The fourth chapter is the second article entitled “Coupling of geothermal heat pumps with thermal solar collectors using double U-tube boreholes with two independent circuits” published in the *Applied Thermal Engineering* journal (Eslami nejad and Bernier, b2011). This chapter addresses the second specific objective. This study presents an analytical model to predict steady-state heat transfer in double U-tube boreholes with two independent circuits operating with unequal mass flow rates and inlet temperatures. The proposed model is used to study double U-tube borehole configurations with one circuit linked to a heat pump operating in heating mode and the other to thermal solar collectors. The performance of this configuration is compared to a conventional GCHP (without thermal recharge of the borehole) and to a single-circuit SAGCHP

system. All three systems are simulated over a 20-year period for a single borehole installation typically encountered in residential buildings.

The fifth chapter presents the last article “Freezing of geothermal borehole surroundings: A numerical and experimental assessment with application” which was recently submitted to the *Applied Energy* journal. The principal objective of this thesis as well as most specific objectives are addressed in this chapter. It examines the thermal consequences of freezing the ground in the immediate vicinity of geothermal boreholes. First, a one-dimensional radial numerical heat transfer model is developed to evaluate heat transfer from the borehole wall to the ground. A small-scale experimental set-up is also built and used to successfully validate the numerical model. The numerical ground model is coupled to the borehole model developed in previous chapters to examine various scenarios involving typical heat pump operation.

These three chapters (articles) are followed at the end by a general discussion and recommendations for future studies which form the last chapter of this work.

CHAPITRE 3 SCIENTIFIC ARTICLE 1: HEAT TRANSFER IN DOUBLE U-TUBE BOREHOLES WITH TWO INDEPENDENT CIRCUITS

Abstract

This study presents the development of an analytical model to predict steady-state heat transfer in double U-tube geothermal boreholes equipped with two independent circuits. Such boreholes can be used for heat extraction in one circuit, combined with a heat pump, for example, and simultaneous thermal recharging in the other circuit. The model accounts for a thermal interaction among pipes, and it predicts the fluid temperature profiles in both circuits along the borehole depth, including the exit fluid temperature. Different circuit configurations are assessed under typical borehole operating conditions. For a typical borehole geometry, results show that double U-tube boreholes with two independent circuits connected to a relatively low temperature heat source are superior to single U-tube and regular (one circuit) double U-tube boreholes. The axial variation in fluid temperature and the heat exchange among pipes show that most of the heat transfer occurs in the downward legs. Furthermore, in some cases, the fluid in the heat extraction leg gets cooled as it flows upward, which is contrary to the desired effect.

3.1 Introduction

Vertical geothermal boreholes that are linked to ground source heat pumps (GSHPs) are widely used for space conditioning and domestic hot water heating. Three conventional configurations are shown in Figure 3-1: (a) single U-tube and double U-tube arrangements either (b) in parallel or (c) in series.

In heating dominated climates, the performance of a GSHP that uses conventional U-tube configurations decreases gradually over time. This is due to the fact that more heat is extracted from the ground than the amount rejected during the cooling season. For example, Bernier (2000) indicated that for a typical constant heat extraction of 37.5 W/m, the borehole wall temperature decreases by approximately 5°C over a 24 h period. Yang et al. (2006) recommended an off-period of 10–14 h a day for GSHP systems to achieve a 30–60% recovery rate for the ground temperature in the vicinity of the borehole. The ground temperature reduction in the vicinity of

the borehole over the years results in a decrease in the inlet temperature to the heat pump, which translates into a reduction in the coefficient of performance (COP). In some extreme cases, heat pumps cease to operate due to inlet temperatures that are below their recommended operating limit. One strategy used to alleviate this problem is to combine a supplementary source of energy such as solar energy with conventional GSHP systems. These systems are usually known as solar-assisted GSHP systems or hybrid GSHP systems. This concept was first introduced by Penrod and Prasanna (1962, 1969), who proposed a system that utilized both solar collectors and the ground as the heat source for the heat pump.

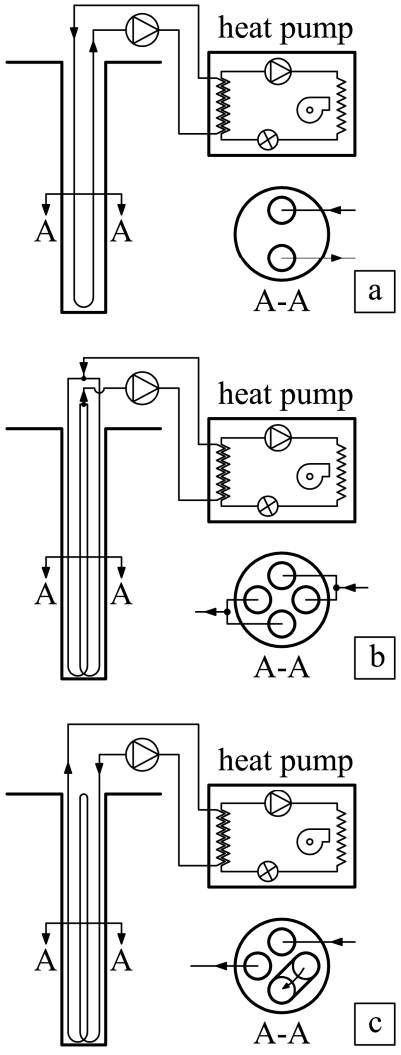

Figure 3-1: Schematic representation of conventional U-tube configurations

This paper proposes a new type of hybrid GSHP with boreholes equipped with two independent circuits, as shown in Figure 3-2. With this configuration, the borehole has two U-tubes, each

forming an independent circuit with different inlet conditions. Furthermore, this configuration offers the advantage of decoupling the heat source and heat pump circuits, allowing the use of different fluids in each circuit.

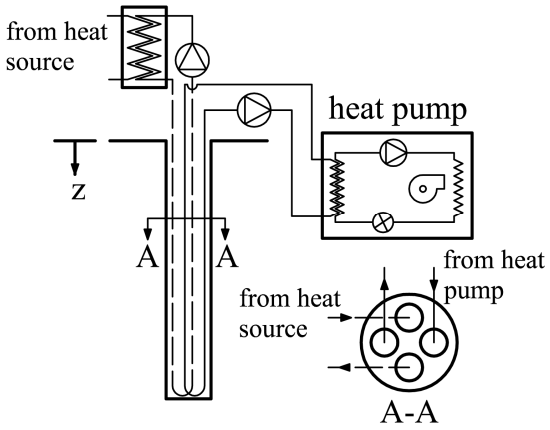

Figure 3-2: Schematic representation of a double U-tube borehole with two independent circuits

Three modes of operation are possible: heat pump circuit only, heat source circuit only, and simultaneous heat extraction for the heat pump and heat injection from the heat source. This paper is concerned with this last mode of operation. The objective is to predict the outlet fluid temperature of both circuits as well as the fluid temperature profile along the borehole depth for given inlet conditions (temperature and mass flow rate) and borehole wall temperatures. The steady-state heat flow balance equations for each pipe are first introduced as a function of the borehole wall and fluid temperatures along the borehole depth using thermal resistances among pipes and between pipes and the borehole wall. These equations are nondimensionalized and then changed, using Laplace transforms, from a set of linear first order differential equations to a set of linear algebraic equations, which can easily be solved. Finally, the Laplace inverse method is used to retransfer the equations to their original form to obtain the temperature distribution along the borehole depth as well as the outlet temperature of each circuit.

3.2 Previous Studies

When a supplementary source of energy such as solar energy is combined with a GSHP system, there are different options to improve the overall system efficiency. Kjellsson et al. (2010) indicated that the best option with the highest reduction in electricity consumption is a hybrid GSHP system with solar heat injection into the boreholes in winter combined with solar domestic

hot water production during the summer. Chiasson and Yavuzturk (2003) performed a 20 year life-cycle cost analysis to evaluate the economics of GSHP systems coupled with thermal solar collectors for six different climates in the U.S. They concluded that GSHP systems combined with solar collectors are economically viable for heating dominated climates. Stojanović and Akander (2010) conducted a 2 year performance test on a full-scale solar-assisted heat pump system for a residential building in a Nordic climate. They indicated that despite unfavorable building conditions, the proposed system succeeded in fulfilling the heating requirements. A Swedish manufacturer (website, 2009) is also proposing a hybrid GSHP system that uses a supplementary heat source coming from a house exhaust air system and connected to a compact collector composed of a series of short closely packed plastic pipes. This system supplies heat continuously to the ground heat exchanger, which enables a reduction in its overall length.

In northern climates, heat injection into boreholes can also be used in a seasonal storage system for domestic hot water or space heating. Typically, single U-tubes are used in such systems. Since simultaneous charging and discharging of the ground are not possible in a single U-tube configuration, transition tanks or additional heat exchangers are required, which adds to the complexity of the system (Sibbitt et al., 2007). Wang et al. (2010) performed an experimental study of a ground coupled heat pump system linked to a seasonal borehole storage. Solar energy was stored in the summer using 12 single U-tube boreholes. They indicated that the operation of such a system significantly improves the heat pump heating COP. Chapuis and Bernier (2008, 2009) are at the origin of two studies that attempted to model double U-tubes in conjunction with seasonal storage. In the first study, Chapuis and Bernier (2008) used an external heat exchanger combined with the duct ground heat storage (DST) model (1989) to mimic simultaneous charging and discharging in the ground heat exchanger. Later, they modified the DST model to handle double U-tube boreholes with two independent circuits (2009). However, the thermal interaction between the U-tubes in the borehole was not taken into account.

Kummert and Bernier (2008) proposed a new system for space conditioning and domestic hot water heating in a Canadian climate using a gas-fired absorption heat pump coupled with a vertical geothermal borehole with two independent circuits linked, respectively, to the evaporator and the condenser of the heat pump. They considered three modes of operations, including heating only, cooling only, and simultaneous heating/cooling. The ground heat exchanger was

modeled using the DST model, which precluded any studies on simultaneous flows in the two independent circuits.

Bernier and Salim Shirazi (2007) and Eslami nejad et al. (2009) evaluated the impact of solar heat injection on borehole length and heat pump energy consumption. However, they approximated the double U-tube configuration with a single U-tube based on a simple approach, which assumed that the heat transferred into the ground is the sum of the solar heat injection and the heat pump extraction/rejection. Depending on the magnitude of these two terms, the value of the heat transferred into the ground can either be positive or negative. Furthermore, both outlet fluid temperatures were assumed equal.

Several numerical and analytical models have been developed to simulate heat transfer inside single U-tube boreholes and in the ground. He et al. (2009) developed a finite-volume-based threedimensional model to simulate the dynamic response of the circulating fluid as well as transient heat transfer in and around boreholes. However, they provided a limited number of results. Furthermore, contrary to analytical models such as the one reported in this paper, three-dimensional models cannot realistically be used in annual hourly GSHP system simulations. Young (2004) analytically evaluated the short-time response of the borehole based on the “buried cable” solution given by Carslaw and Jaeger (1947), which accounts for the grout and fluid thermal capacity. Lamarche and Beauchamp (2007) approximated the short-time response of single U-tube boreholes using an analytical solution to the unsteady one-dimensional heat conduction problem of concentric cylinders. Recently, Man et al. (2010) developed an analytical model, which accounts for borehole heat capacity. However, identical properties for the grout and ground are assumed, limiting the applicability of their model. Remund (1999) proposed a set of relationships for different single U-tube borehole configurations to calculate the steady-state borehole thermal resistances based on conduction shape factors obtained from empirical data. Marcotte and Pasquier (b2008) proposed a so-called “p-linear” temperature average using a three-dimensional numerical simulation to evaluate the borehole resistance from an experimental thermal response test.

A few studies have also modeled double U-tube boreholes. Al- Khoury and Bonnier (2006) applied the three-dimensional finite element method to analyze transient heat transfer in a double U-tube with a parallel arrangement (Figure 3-1(*b*)). Hellström (1991) derived steady-state two-

dimensional analytical solutions for borehole thermal resistances with an arbitrary number of pipes. Zeng et al. (2003) used Hellström's work to establish an analytical quasi-threedimensional model for single and double U-tube configurations arranged either in parallel or in series. Diao et al. (2004) used this approach to simulate heat transfer inside the borehole, which they combined with the finite-line source solution to predict heat transfer in the ground. Although their model takes into account the interaction between pipes in the borehole, the two U-tubes are connected either in parallel or in series, as shown in Figure 3-1(*b*) and Figure 3-1(*c*). Wetter and Huber (1997) modeled the transient behavior of a borehole with a double U-tube configuration with a single equivalent pipe diameter, which precludes any possibility of modeling the two independent circuits in a borehole with their approach.

It is apparent from this review that there are no reported studies on heat transfer modeling of double U-tube geothermal boreholes with two independent circuits.

3.3 Problem Formulation

A cross section of a double U-tube borehole is presented schematically in Figure 3-3. It consists of four pipes, which are inserted over the full depth of the borehole and connected at the bottom to form two U-tubes (see Figure 3-2) and two independent circuits with different inlet temperatures $(T_f' \neq T_f'')$. The space between the pipes is filled with a grout. The borehole is subjected to a constant borehole wall temperature T_b at the borehole radius r_b.

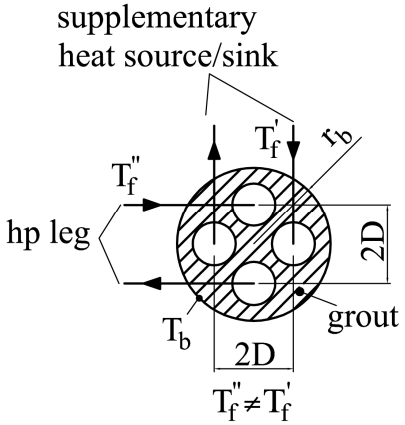

Figure 3-3: Cross section of a double U-tube borehole with two independent circuits

Pipes are disposed symmetrically with identical center-to-center distance (2D) between two opposing pipes. The three possible inlet/outlet configurations are presented schematically in

Figure 3-4. In the following description, the pipes are numbered clockwise, and the various options are classified with a four digit notation separated by a comma. For example, for the 1-2,3-4 configuration, the fluid from the first circuit enters pipe 1, goes to the bottom of the borehole, and then up to pipe 2. Similarly, the fluid from the second circuit enters pipe 3, goes to the bottom of the borehole, and then up to pipe 4.

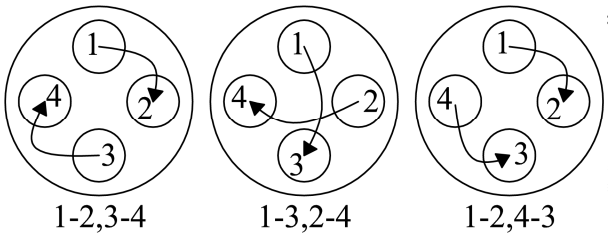

Figure 3-4: Possible piping configurations

The objective of this study is to model steady-state heat transfer in boreholes with two independent circuits. The model considers the thermal interaction among pipes and the axial temperature variation along the depth of the borehole. To make the model analytically manageable, the following assumptions are used: (i) The heat capacities of the materials inside the borehole (aside from the fluid) are neglected, (ii) the ground and the grout are homogeneous, and their thermal properties are constant, (iii) the borehole wall temperature (T_b in Figure 3-3) is constant along the borehole's depth, (iv) heat conduction in the axial direction is neglected, and (v) mass flow rates are equal in each circuit. The first four assumptions have been used in the past by a number of researchers (e.g., Zeng et al., 2003; Hellström, 1991). More recently, Lamarche et al. (2010) compared borehole thermal resistance calculation methods against an unsteady three-dimensional numerical borehole model. A good agreement for the axial fluid temperature distribution of a single U-tube borehole was reported between the approach proposed by Zeng et al. (2003), which uses the first four assumptions mentioned above, and the three-dimensional simulation results. Yang et al. (2009) coupled a steadystate single U-tube borehole model, assuming a uniform T_b, to an unsteady one-dimensional ground heat transfer model based on the cylindrical heat source approach. This two-region model was validated experimentally. Results indicated that the calculated fluid outlet temperature is in very good agreement with experimental data in the steady-state regime.

3.4 Heat Flow Balance Equations

The difference between the borehole wall temperature and the fluid temperatures in each circuit is caused by the net heat flows per unit length, q_1,q_2,q_3, and q_4 in and out of the four pipes. Thus, with reference to Figure 3-5 and based on the approach proposed by Hellström (1991) and Zeng et al. (2003), the following heat flow balances are obtained:

$$\begin{aligned} T_{f1}(z) - T_b &= R_{11}q_1 + R_{12}q_2 + R_{13}q_3 + R_{14}q_4 \\ T_{f2}(z) - T_b &= R_{21}q_1 + R_{22}q_2 + R_{23}q_3 + R_{24}q_4 \\ T_{f3}(z) - T_b &= R_{31}q_1 + R_{32}q_2 + R_{33}q_3 + R_{34}q_4 \\ T_{f4}(z) - T_b &= R_{41}q_1 + R_{42}q_2 + R_{43}q_3 + R_{44}q_4 \end{aligned} \tag{3.1}$$

In Eq. (3.1), $T_{fi}(z)$ (i=1,2,3,4) represents the fluid temperature at a certain borehole depth z, R_{ii} (i=1,2,3,4) is the thermal resistance between the fluid in pipe i and the borehole wall, and R_{ij} (i, j=1,2,3,4) is the thermal resistance between pipes i and j.

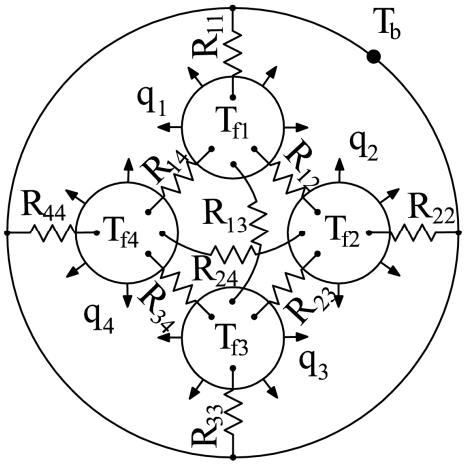

Figure 3-5: Presentation of terms used in Eq. (3.1)

Since pipes are assumed to be disposed symmetrically in the borehole, R_{ij}=R_{ji}, R_{ii}=R_{jj}, R_{24}=R_{13}, and R_{23}=R_{14}=R_{34}=R_{12}. Thus, only three thermal resistances, R_{11}, R_{12}, R_{13}, need to be evaluated. Hellström (1991) presented a technique to evaluate R_{ii} and R_{ij} based on the line source solution for each pipe which are then superimposed. This leads to:

$$R_{11} = \frac{1}{2\pi k_b}\left[\ln\left(\frac{r_b}{r_p}\right) - \frac{k_b - k}{k_b + k}\ln\left(\frac{r_b^2 - D^2}{r_b^2}\right)\right] + R_{pipe}$$
$$R_{12} = \frac{1}{2\pi k_b}\left[\ln\left(\frac{r_b}{\sqrt{2}D}\right) - \frac{k_b - k}{2(k_b + k)}\ln\left(\frac{r_b^4 + D^4}{r_b^4}\right)\right] \quad (3.2)$$
$$R_{13} = \frac{1}{2\pi k_b}\left[\ln\left(\frac{r_b}{2D}\right) - \frac{k_b - k}{k_b + k}\ln\left(\frac{r_b^2 + D^2}{r_b^2}\right)\right]$$

Where k and k_b are the ground and grout thermal conductivities, respectively, r_p is the outer radius of the pipe, R_{pipe} is an overall thermal resistance (considered constant along the borehole depth) which combines the fluid convective resistance, the conduction resistance in the pipe and a contact resistance associated with gaps between the pipes and the grout :

$$R_{pipe} = \frac{1}{2\pi h_i r_{i,p}} + \frac{\ln\left(\frac{r_p}{r_{i,p}}\right)}{2\pi k_p} + R_{air} \quad (3.3)$$

Where $r_{i,p}$ is the inner pipe radius, k_p is the pipe thermal conductivity, h_i is convective heat transfer coefficient inside the U-tubes, and R_{air} is a contact resistance at the grout/pipe interface. This last resistance was set to zero in this work. However, it could easiliy be included in the value of R_{pipe} if required. The reader is referred to the work of Philippacopoulos and Berndt (2001) for a discussion on the effect air-filled gaps at the grout/pipe interface. Finally, the value of h_i is assumed to be the same in both circuits and constant along the depth of the borehole.

Equation (3.1) can be rearranged in terms of the net heat flows in each pipe as follows:

$$q_1 = \frac{T_{f1} - T_b}{R_1^\Delta} + \frac{T_{f1} - T_{f2}}{R_{12}^\Delta} + \frac{T_{f1} - T_{f3}}{R_{13}^\Delta} + \frac{T_{f1} - T_{f4}}{R_{12}^\Delta}$$
$$q_2 = \frac{T_{f2} - T_{f1}}{R_{12}^\Delta} + \frac{T_{f2} - T_b}{R_1^\Delta} + \frac{T_{f2} - T_{f3}}{R_{12}^\Delta} + \frac{T_{f2} - T_{f4}}{R_{13}^\Delta} \quad (3.4)$$
$$q_3 = \frac{T_{f3} - T_{f1}}{R_{13}^\Delta} + \frac{T_{f3} - T_{f2}}{R_{12}^\Delta} + \frac{T_{f3} - T_b}{R_1^\Delta} + \frac{T_{f3} - T_{f4}}{R_{12}^\Delta}$$
$$q_4 = \frac{T_{f4} - T_{f1}}{R_{12}^\Delta} + \frac{T_{f4} - T_{f2}}{R_{13}^\Delta} + \frac{T_{f4} - T_{f3}}{R_{12}^\Delta} + \frac{T_{f4} - T_b}{R_1^\Delta}$$

where

$$R_1^{\Delta} = R_{11} + R_{13} + 2R_{12}$$
$$R_{12}^{\Delta} = \frac{R_{11}^2 + R_{13}^2 + 2R_{11}R_{13} - 4R_{12}^2}{R_{12}}$$
$$R_{13}^{\Delta} = \frac{(R_{11} - R_{13})(R_{11}^2 + R_{13}^2 + 2R_{11}R_{13} - 4R_{12}^2)}{R_{13}^2 + R_{11}R_{13} - 2R_{12}^2}$$

As the fluid temperature varies along the borehole depth, the heat flows per unit length can be replaced with first order derivatives of fluid temperature as a function of *z* multiplied by the fluid mass flow rate, $\dot{m}$, and the specific heat, *C*:

$$q_1 = \pm\dot{m}C\frac{dT_{f1}(z)}{dz}, q_2 = \pm\dot{m}C\frac{dT_{f2}(z)}{dz}, q_3 = \pm\dot{m}C\frac{dT_{f3}(z)}{dz}, q_4 = \pm\dot{m}C\frac{dT_{f4}(z)}{dz} \tag{3.5}$$

The z-coordinate direction is defined as downward (from the ground surface) and, as indicated in Figure 3-5, an outward heat flow is considered positive. Thus, a positive value of the ± signs in Eq. (3.5) indicates that the fluid is flowing in the upward direction. Conversely, a negative value implies downward flow. By substituting Eq. (3.5) into Eq. (3.4), a set of coupled linear differential equations are obtained:

$$\begin{aligned}
\pm\dot{m}C\frac{dT_{f1}(z)}{dz} &= \frac{T_{f1} - T_b}{R_1^{\Delta}} + \frac{T_{f1} - T_{f2}}{R_{12}^{\Delta}} + \frac{T_{f1} - T_{f3}}{R_{13}^{\Delta}} + \frac{T_{f1} - T_{f4}}{R_{12}^{\Delta}} \\
\pm\dot{m}C\frac{dT_{f2}(z)}{dz} &= \frac{T_{f2} - T_{f1}}{R_{12}^{\Delta}} + \frac{T_{f2} - T_b}{R_1^{\Delta}} + \frac{T_{f2} - T_{f3}}{R_{12}^{\Delta}} + \frac{T_{f2} - T_{f4}}{R_{13}^{\Delta}} \\
\pm\dot{m}C\frac{dT_{f3}(z)}{dz} &= \frac{T_{f3} - T_{f1}}{R_{13}^{\Delta}} + \frac{T_{f3} - T_{f2}}{R_{12}^{\Delta}} + \frac{T_{f3} - T_b}{R_1^{\Delta}} + \frac{T_{f3} - T_{f4}}{R_{12}^{\Delta}} \\
\pm\dot{m}C\frac{dT_{f4}(z)}{dz} &= \frac{T_{f4} - T_{f1}}{R_{12}^{\Delta}} + \frac{T_{f4} - T_{f2}}{R_{13}^{\Delta}} + \frac{T_{f4} - T_{f3}}{R_{12}^{\Delta}} + \frac{T_{f4} - T_b}{R_1^{\Delta}}
\end{aligned} \tag{3.6}$$

3.5 Dimensionless Governing Equations and Boundary Conditions

Equations (3.6) are non-dimensionalized using the following dimensionless variables:

$$\theta_{i=1,2,3,4} = \frac{\left(T_{fi}(z) - T_f'\right) + \left(T_{fi}(z) - T_f''\right)}{T_f' - T_f''}, \quad T_f' \neq T_f''$$

$$\theta_b = \frac{\left(T_b - T_f'\right) + \left(T_b - T_f''\right)}{T_f' - T_f''} \tag{3.7}$$

$$R_1^* = \frac{\dot{m}CR_1^\Delta}{H}, \; R_{12}^* = \frac{\dot{m}CR_{12}^\Delta}{H}, \; R_{13}^* = \frac{\dot{m}CR_{13}^\Delta}{H} \text{ and } Z = \frac{z}{H}$$

which leads to the following set of first order linear differential equations:

$$\begin{aligned}
\pm\frac{d\theta_1}{dZ} &= a\theta_1 + b\theta_2 + c\theta_3 + b\theta_4 + d \\
\pm\frac{d\theta_2}{dZ} &= b\theta_1 + a\theta_2 + b\theta_3 + c\theta_4 + d \\
\pm\frac{d\theta_3}{dZ} &= c\theta_1 + b\theta_2 + a\theta_3 + b\theta_4 + d \\
\pm\frac{d\theta_4}{dZ} &= b\theta_1 + c\theta_2 + b\theta_3 + a\theta_4 + d
\end{aligned} \tag{3.8}$$

where

$$a = \frac{1}{R_1^*} + \frac{2}{R_{12}^*} + \frac{1}{R_{13}^*}, \; b = -\frac{1}{R_{12}^*}, \; c = -\frac{1}{R_{13}^*}, \; d = -\frac{\theta_b}{R_1^*}$$

The boundary conditions are defined and summarized in Table 3-1.

Table 3-1: Boundary conditions

1-2,3-4		1-3,2-4		1-2,4-3	
	$\theta_1(0) = 1$		$\theta_1(0) = 1$		$\theta_1(0) = 1$
$T_f' = T_{f1}(0)$	$\theta_3(0) = -1$	$T_f' = T_{f1}(0)$	$\theta_2(0) = -1$	$T_f' = T_{f1}(0)$	$\theta_4(0) = -1$
$T_f'' = T_{f3}(0)$	$\theta_1(1) = \theta_2(1)$	$T_f'' = T_{f2}(0)$	$\theta_1(1) = \theta_3(1)$	$T_f'' = T_{f4}(0)$	$\theta_1(1) = \theta_2(1)$
	$\theta_3(1) = \theta_4(1)$		$\theta_2(1) = \theta_4(1)$		$\theta_3(1) = \theta_4(1)$

3.6 Laplace Transforms

Using Laplace transforms, the dimensionless heat flow balance equations are transformed to yield a set of linear algebraic equations as follows:

$$\begin{aligned}
(a \mp p)\bar{\theta}_1 + b\bar{\theta}_2 + c\bar{\theta}_3 + b\bar{\theta}_4 &= \mp\theta_1(0) - d/p \\
b\bar{\theta}_1 + (a \mp p)\bar{\theta}_2 + b\bar{\theta}_3 + c\bar{\theta}_4 &= \mp\theta_2(0) - d/p \\
c\bar{\theta}_1 + b\bar{\theta}_2 + (a \mp p)\bar{\theta}_3 + b\bar{\theta}_4 &= \mp\theta_3(0) - d/p \\
b\bar{\theta}_1 + c\bar{\theta}_2 + b\bar{\theta}_3 + (a \mp p)\bar{\theta}_4 &= \mp\theta_4(0) - d/p
\end{aligned} \tag{3.9}$$

where $\bar{\theta}(p)_i = \int_0^\infty e^{-pZ}\theta_i(Z)dZ$. Accordingly, the matrix form of Eq. (3.9) becomes:

$$\begin{bmatrix} a \mp p & b & c & b \\ b & a \mp p & b & c \\ c & b & a \mp p & b \\ b & c & b & a \mp p \end{bmatrix} \begin{bmatrix} \bar{\theta}_1 \\ \bar{\theta}_2 \\ \bar{\theta}_3 \\ \bar{\theta}_4 \end{bmatrix} = \begin{bmatrix} \mp\theta_1(0) - d/p \\ \mp\theta_2(0) - d/p \\ \mp\theta_3(0) - d/p \\ \mp\theta_4(0) - d/p \end{bmatrix} \tag{3.10}$$

This set of equations can be solved easily, using Gaussian elimination for example, to obtain $\bar{\theta}_1, \bar{\theta}_2, \bar{\theta}_3,$ and $\bar{\theta}_4$ as a function of *a, b, c, d, $\theta_1(0)$, $\theta_2(0)$, $\theta_3(0)$, $\theta_4(0)$, and p*. Then, the inverse Laplace transforms of $\bar{\theta}_1, \bar{\theta}_2, \bar{\theta}_3,$ and $\bar{\theta}_4$ are evaluated to obtain dimensionless temperature distributions. Boundary conditions are then applied to evaluate *$\theta_1(0)$, $\theta_2(0)$, $\theta_3(0)$,* and *$\theta_4(0)$*. The resulting dimensionless temperature distributions, $\theta_{i=1,2,3,4}(Z)$, are presented in appendix A for the three circuit configurations shown in Figure 3-6. As shown in appendix B, these equations for double U-tube boreholes with two independent circuits can be rearranged to obtain the relationships derived by Zeng et al. (2003) for a double U-tube but for single circuit configurations, thus confirming, indirectly, the exactness of the present derivation.

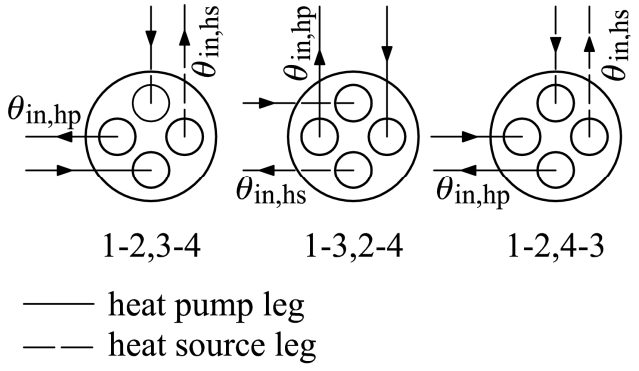

Figure 3-6: Borehole cross section for three different configurations

3.7 Applications

This section provides two applications where the model developed in this paper is used to understand and improve heat transfer in boreholes that use double U-tubes with two independent circuits. Both applications concern the geometries presented in Figure 3-6, where one circuit is linked to a heat pump and the other is linked to a heat source. In the first application, the performances of the three configurations are compared for a nondimensional borehole wall temperature, θ_b, of zero. This implies that the net amount of energy extracted from the ground is equal to zero since the borehole wall temperature is equal to the average of the two inlet temperatures. The inlet boundary conditions are $\theta_1(0) = 1$, $\theta_3(0) = -1$ for the 1-2,3-4 configuration, and $\theta_1(0) = 1$, $\theta_2(0) = -1$ for the 1-3,2-4 configuration, and $\theta_1(0) = 1$, $\theta_4(0) = -1$ for the 1-2,4-3 configuration.

Table 3-2: Borehole characteristics

r_b (m)	r_p (m)	H (m)	D (m)	k ($W \cdot m^{-1} \cdot K^{-1}$)	k_b ($W \cdot m^{-1} \cdot K^{-1}$)	$\dot{m}$ (kg s^{-1})	C (J kg^{-1} K^{-1})	θ_b	R_{pipe} ($m \cdot K.W^{-1}$)
0.055	0.016	100	0.03	1.5	1	0.2	4187	0	0.1

The borehole characteristics for this application are listed in Table 3-2. They are representative of typical geothermal boreholes used in practice. The thermal conductivity of the U-tubes is 0.4 $W \cdot m^{-1} \cdot K^{-1}$ (typical of high density polylethylene (HDPE) pipes) with a diameter to thickness ratio of 11. Turbulent flow prevails in the pipes for $\dot{m} = 0.2$ kg/s, and the corresponding convective heat transfer coefficient is 700 $W \cdot m^{-1} \cdot K^{-2}$. The value of R_{pipe} (Eq. (3.3)) is equal to 0.1 $m \cdot K \cdot W^{-1}$ with the convective thermal resistance accounting for about 15% of this value.

Results for this case are presented in Figure 3-7 where both dimensionless fluid temperature variations are presented as a function of the dimensionless borehole depth. For convenience, the outlet temperatures from the borehole to the heat source and the heat pump are denoted as $\theta_{in,hs}$ and $\theta_{in,hp}$, respectively. With reference to the nondimensional values presented earlier, they correspond to $\theta_2(0)$ and $\theta_4(0)$, $\theta_3(0)$ and $\theta_4(0)$, and $\theta_2(0)$ and $\theta_3(0)$ for the 1-2,3-4, 1-3,2-4, and 1-2,4-3 configurations, respectively. For a winter operation, the 1-3,2-4 configuration is the best as it provides the highest heat pump inlet temperature ($\theta_{in,hp}$= -0.29). The other two configurations show similar results with $\theta_{in,hp}$= -0.44 and -0.45 for the 1-2,3-4 and 1-2,4-3 configurations, respectively. As will be shown shortly, this close agreement is specific to this case and cannot be

generalized. Finally, it should be noted that calculated values of $\theta_{in,hs}$ are equal to $\theta_{in,hp}$ in all three cases, which was to be expected with equal $\dot{m}C$ in both circuits and $\theta_b = 0$.

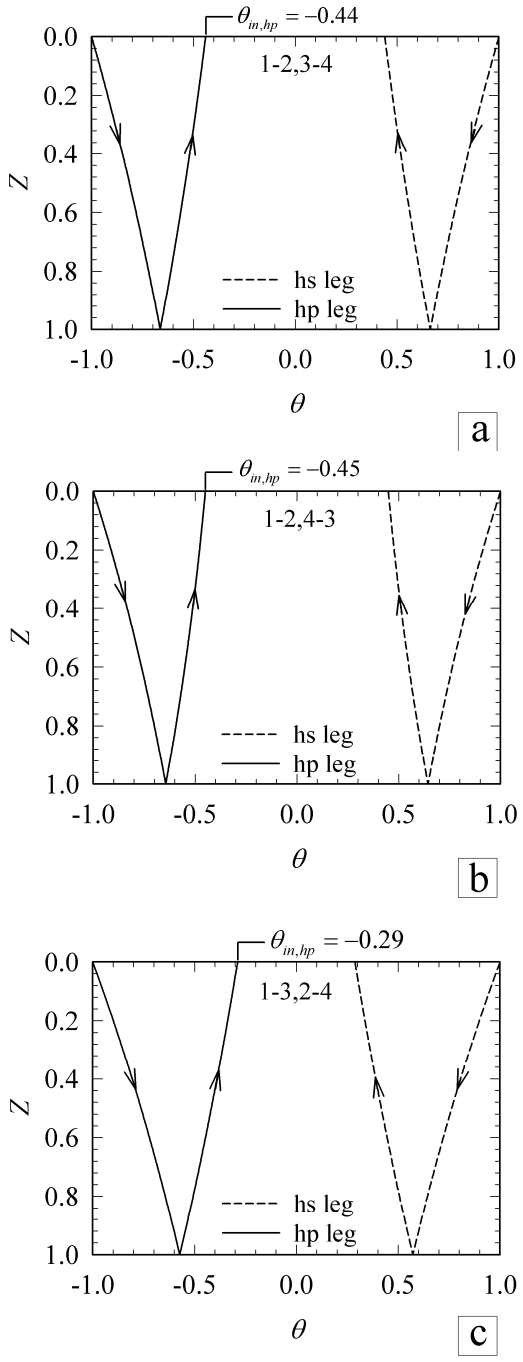

Figure 3-7: Dimensionless temperature profiles along the borehole depth

The superior performance of the 1-3,2-4 configuration compared with the other two is not surprising as pipes from the same circuit are further apart in the 1-3,2-4 configuration than in the

other two configurations. Thus, there is less thermal interference between pipes of the same circuit, and, consequently, more heat transfer takes place from the heat source legs to the heat pump legs. This can be seen in Figure 3-8 where local (Figure 3-8(*a*)) and cumulative (Figure 3-8(*b*)) heat exchanges are presented as a function of depth for ten equally distant pipe segments. For example, for the 1-3,2-4 configuration, q_2=0.652 kW, and q_4=0.304 kW at the top of the borehole (Z=0.05), while the corresponding values are 0.505/0.231 kW and 0.565/0.175 kW for the 1-2,3-4, and 1-2,4-3 configurations, respectively. Figure 3-8(*b*) shows that the cumulative heat addition is better for the 1-3,2-4 configuration with a total of 9 kW exchanged between the heat pump and heat source circuits, while the other two configurations exchange about 7 kW.

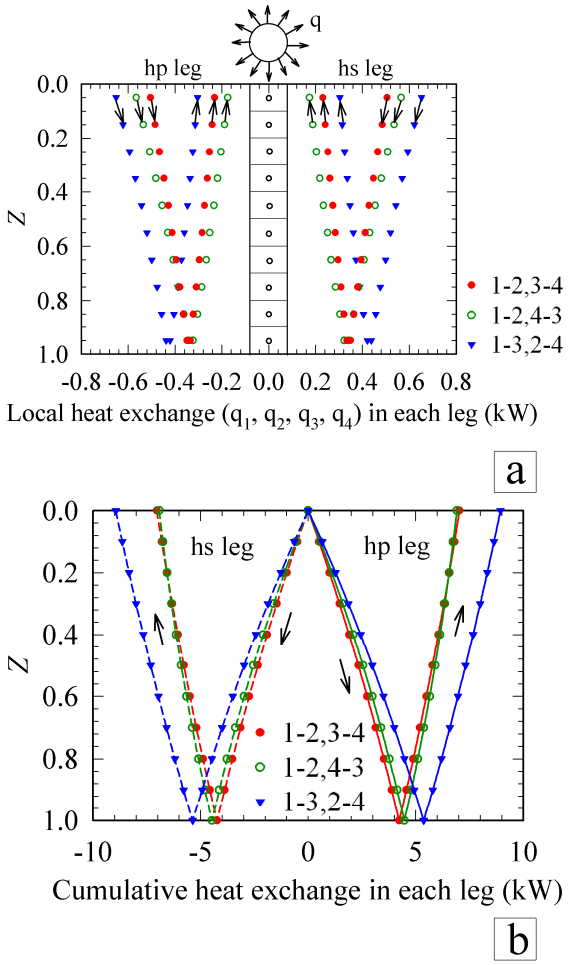

Figure 3-8: Local and cumulative heat exchanges for all three configurations

Figure 3-9 presents a sensitivity analysis performed on three parameters: dimensionless borehole temperature, θ_b; dimensionless pipe spacing, D/r_b; and grout thermal conductivity, k_b. In all cases, the parameter of interest is the inlet temperature to the heat pump, $\theta_{in,hp}$.

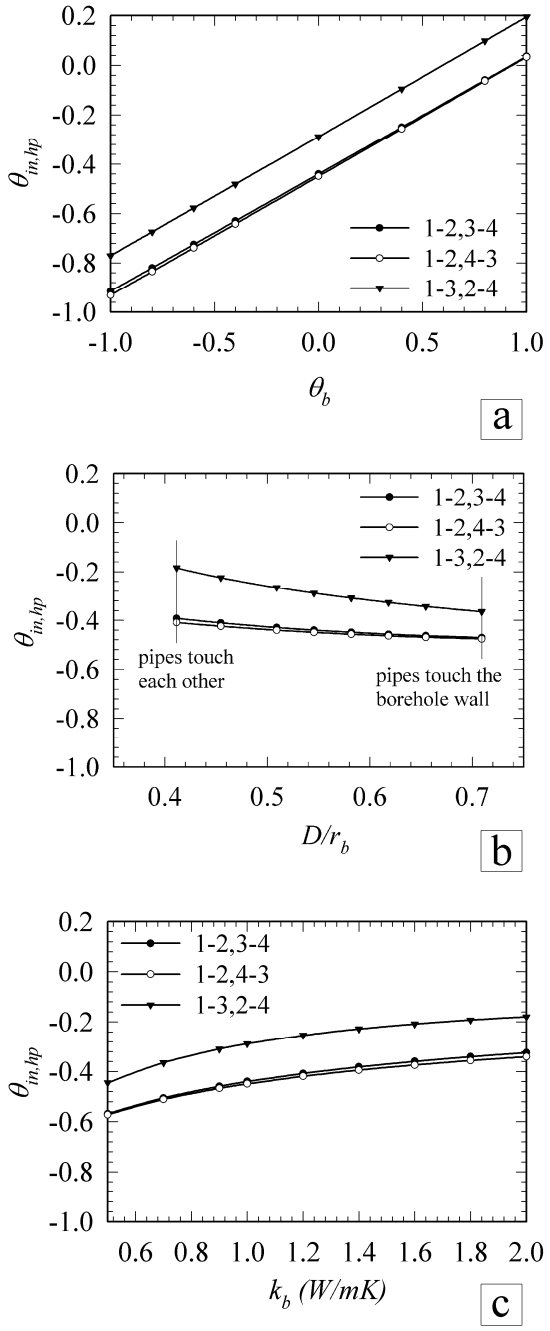

Figure 3-9: Impact of different parameters on borehole heat pump leg outlet temperature for different configurations

As shown in Figure 3-9(*a*), $\theta_{in,hp}$ varies linearly with θ_b for all three configurations. A value of θ_b>0 indicates that the borehole wall temperature is higher than the average of both inlet fluid temperatures and that there is a net heat transfer from the ground to the fluids in the borehole. Configuration 1-3,2-4 provides the highest $\theta_{in,hp}$, and the other two configurations show almost

identical behaviors. Reducing pipe spacing (Figure 3-9(*b*)) increases $\theta_{in,hp}$ for all three configurations. However, the rate of increase is greater for the 1-3,2-4 configuration. Thus, when θ_b =0 (no net heat exchange with the ground), it is advantageous to put the pipes as close as possible to each other to maximize heat transfer from the heat source leg to the heat pump leg.

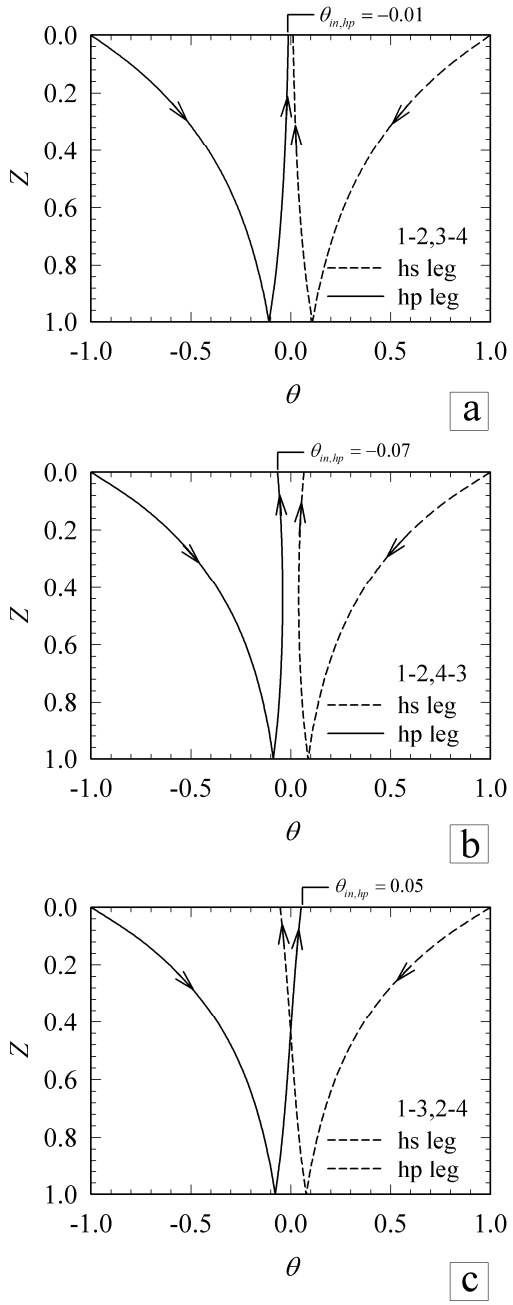

Figure 3-10: Dimensionless temperature profiles along the borehole depth for $\dot{m}$=0.05 kg/s and *H*=200 m

Similarly, increasing grout thermal conductivity (Figure 3-9(*c*)) increases the heat exchanged between both circuits, which results in an increase in the value of $\theta_{in,hp}$.

The effect of a change in flow rate (from 0.2 kg/s to 0.05 kg/s) and depth (from 100 m to 200 m) is illustrated in Figure 3-10. The other characteristics are the same as those presented earlier in Table 3-2 except that the flow is now laminar, which increases R_{pipe} to 0.24 m·K·W^{-1}. As shown in this figure, the 1-2,3-4 and 1-2,4-3 configurations do not give the same $\theta_{in,hp}$, as was the case earlier. There is also an interesting phenomenon occurring for the 1-2,4-3 configuration as the fluid in the hp leg gets cooled in its upward ascent up to $\theta_{in,hp}$ =-0.07 at the exit. Although this cooling is moderate, it is nonetheless the opposite of the desired effect. This is due to the fact that pipe 3 is closer to the "cold" pipe 4 than to the "hot" pipe 1. A similar but less severe effect can be seen with the 1-2,3-4 configuration where heat gains in the upward pipe (4) of the hp leg are small. The upward hp leg of the 1-3,2-4 configuration experiences a small heat gain with $\theta_{in,hp}$ =0.05. Aside from these differences with $\theta_{in,hp}$, all three configurations exhibit a similar behavior with an exponential-like fluid temperature variation in both downward legs and small temperature changes in the upward legs. Thus, geothermal borehole designers should be aware that most of the heat transfer takes place in the downward legs with deep boreholes fed with relatively small flow rates.

In this next application, the borehole length required for a given heat exchange is calculated for three configurations: (i) a single U-tube borehole, as shown in Figure 3-1(*a*), (ii) a double U-tube borehole in parallel, as shown in Figure 3-1(*b*) (corresponding to the 1-3,2-4 configuration, which provides the lowest borehole resistance according to Zeng et al. (2003)), and (iii) a double U-tube borehole with two independent circuits and heat injection in one of the circuits.

Aside from the borehole characteristics set in Table 3-2, the other important parameters are the return temperature from the heat pump, $T_{out,hp}$, and the borehole wall temperature, T_b, which are set here at -5°C and 10°C, respectively. In the case of heat injection, the first set of results will be presented with an inlet temperature to the heat source leg of 25°C. Finally, for the double U-tube parallel arrangement, the total mass flow rate given in Table 3-2 is divided into two to account for the parallel arrangement. In all three cases, the amount of power extracted from the heat pump leg is fixed at 7.2 kW. This represents approximately the heat extraction requirement of a 3 ton

(10.5 kW) heat pump operating in a heating mode. A simple heat balance shows that the outlet temperature from the heat pump leg is then 3.6°C.

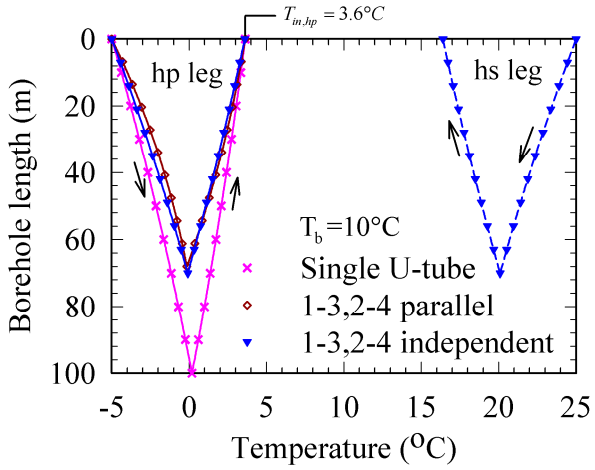

Figure 3-11: Fluid temperature profiles and borehole depth required to have $T_{in,hp}$=3.6°C for three configurations

Figure 3-11 shows the borehole length required in each of the three cases to obtain the required heat exchange. The single U-tube configuration requires 100 m, while the 1-3,2-4 parallel arrangement and the double U-tube 1-3,2-4 configuration (with heat injection) require 68 m and 70 m, respectively. This figure also shows the axial temperature variation for the three configurations. From a borehole depth point of view, there is essentially no difference between the double U-tube borehole with a 1-3,2-4 parallel arrangement and the double U-tube 1-3,2-4 configuration with two independent circuits and heat injection. However, one has to be careful in interpreting these results as the heat required by the 1-3,2-4 parallel arrangement is extracted from the ground, while the hp leg of the double U-tube with two independent circuits takes its heat from the hs leg and none from the ground. The impact of the inlet temperature of the hs leg ($T_{out,hs}$) is investigated in Figure 3-12, where comparisons are made with the single U-tube configuration and the parallel 1-3,2-4 double U-tube for different grout thermal conductivities and shank spacings. Results are presented in terms of borehole depth reduction. Generally, Figure 3-12(*a*)– Figure 3-12(*d*) indicate that the depth reduction of the double U-tube borehole with two independent circuit increases as the heat source inlet fluid temperature increases. Independent double U-tube boreholes charged with an entering fluid temperature above 10°C leads to a borehole depth reduction when compared with the single U-tube borehole configuration. However, in some cases, independent double U-tube boreholes present longer boreholes when

compared with the parallel double U-tube boreholes (negative percentage of borehole depth reduction).

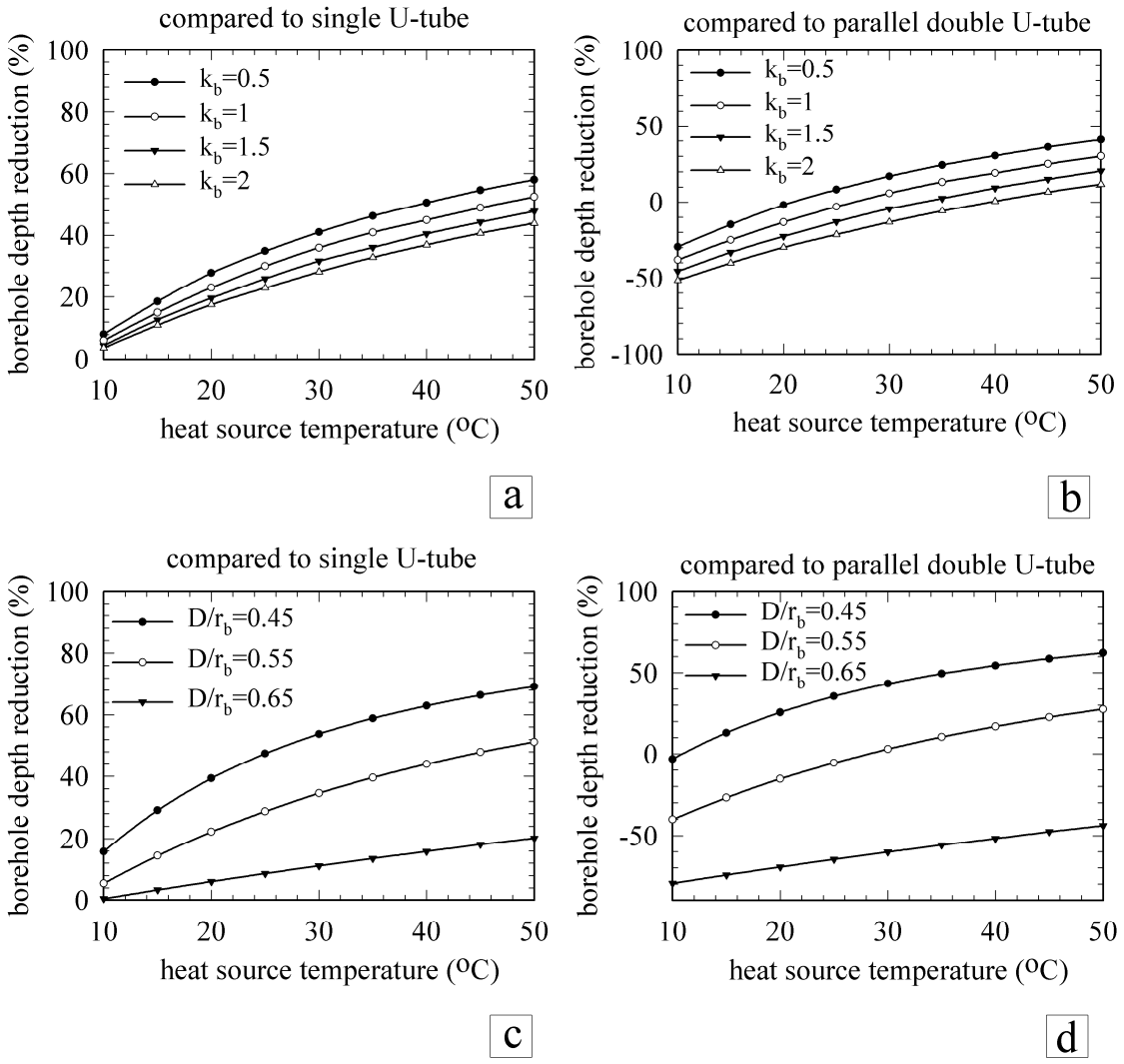

Figure 3-12: Comparison of the required depth of independent double U-tube boreholes with single and parallel double U-tube boreholes under different conditions

As shown in Figure 3-12(*b*), the independent double U-tube borehole depth for the reference case (k_b=1) with a 26.5°C heat source temperature is almost identical (0% borehole depth reduction) to that of a parallel double U-tube borehole. With higher heat source temperatures, the independent double U-tube borehole becomes superior. This advantage gets more significant if the grout thermal conductivity is low. Shank spacing significantly affects the differences between the required depth of independent double U-tube boreholes and single and parallel double U-tube

boreholes. For instance, in an extreme case ($T_{out,hs}$=50°C; D/r_b=0.45), the required depth of independent double U-tube boreholes is 68% lower than that of the single U-tube configuration (Figure 3-12(*c*)). Conversely, when the pipes are placed near the borehole wall, the parallel double U-tube borehole is superior as the hs leg in the independent double U-tube borehole gives heat to the adjacent ground instead of the hp leg (Figure 3-12(*d*)).

3.8 Conclusion

An analytical model to predict steady-state heat transfer in double U-tube geothermal boreholes equipped with two independent circuits is presented. Such boreholes can be used for simultaneous heat extraction in one circuit and heat recharging in the other. The model accounts for thermal interaction among pipes and predicts the fluid temperature profiles of both circuits along the borehole depth, including the exit fluid temperature. Using Laplace transforms, the governing dimensionless heat flow balance equations are transformed to yield a set of linear algebraic equations, which can easily be solved. Then, the inverse Laplace transforms are evaluated to obtain dimensionless temperature distributions. The model is successfully compared with the model of Zeng et al. (2003) for the 1-2,3-4 parallel arrangement.

The model is then used in two applications where one circuit is linked to a heat pump and the other to a heat source. Typical borehole characteristics are used. In the first application, the performances of three U-tube configurations are compared for a nondimensional borehole wall temperature of zero (i.e., the net amount of energy extracted from the ground is equal to zero). Results show that heat transfer between the hot and cold legs is superior for the 1-3,2-4 configuration when compared with the 1-2,3-4 and 1-2,4-3 configurations. A sensitivity analysis is then performed on three parameters: dimensionless borehole wall temperature, θ_b; dimensionless pipe spacing, D/r_b; and grout thermal conductivity, k_b. It is shown that the outlet temperature from the heat pump leg (i.e., the inlet temperature to the heat pump) varies linearly with θ_b for all three configurations. The 1-3,2-4 configuration provides the highest inlet temperature to the heat pump, and the other two configurations show almost identical behaviors. Reducing pipe spacing increases the inlet temperature to the heat pump for all three configurations. Increasing grout thermal conductivity increases the heat exchanged between both circuits, which results in an increase in the heat pump inlet temperature.

For the typical borehole characteristics used in this paper, double U-tube boreholes with two independent circuits connected to a relatively low temperature heat source are shallower than single U-tube boreholes and regular (one circuit) double U-tube boreholes. The axial variation in fluid temperature and heat exchange among pipes show that most of the heat transfer occurs in the downward legs. Furthermore, in some cases, the fluid in the heat extraction leg gets cooled as it flows upward, which is contrary to the desired effect. This work opens new possibilities into the use of geothermal boreholes by enabling a better understanding of heat transfer for a novel borehole geometry.

3.9 Nomenclature

a, b, c, d	dimensionless parameters, defined in Eq. (3.8)
C	fluid specific heat ($J \cdot kg^{-1} \cdot K^{-1}$)
D	half of the shank spacing between U-tube (m)
H	active borehole depth (m)
k	ground thermal conductivity ($W \cdot m^{-1} \cdot K^{-1}$)
k_b	grout thermal conductivity ($W \cdot m^{-1} \cdot K^{-1}$)
$\dot{m}$	mass flow rate of circulating fluid ($kg \cdot s^{-1}$)
p	Laplace transform operator
q	heat flow per unit length of pipe ($W \cdot m^{-1}$)
r_b	borehole radius (m)
r_p	pipe outer radius (m)
R	thermal resistance, defined in Eq. (3.1) ($m \cdot K \cdot W^{-1}$)
R^{Δ}	thermal resistance, defined in Eq. (3.4) ($m \cdot K \cdot W^{-1}$)
R^{*}	dimensionless thermal resistance
R_{pipe}	combined thermal resistance of the fluid and pipe wall ($m \cdot K \cdot W^{-1}$)
S	dimensionless thermal resistance, defined in Eq. (3.A.1)-(3.A.3)
T_b	borehole wall temperature (^{o}C)
T_f	fluid temperature (^{o}C)
T_f', T_f''	inlet fluid temperatures (^{o}C)
z	axial coordinate along the borehole depth (m)
Z	dimensionless z coordinate

Greek symbols

$\beta, \varepsilon, \gamma, \eta$	dimensionless parameters in Eq. (3.A.1)-(3.A.3)
θ	dimensionless fluid temperature
$\bar{\theta}$	Laplace transform of θ

Subscripts

1,2,3,4	pipe sequence in the borehole
in,hp	heat pump inlet
in,hs	heat source inlet
out,hp	heat pump outlet
out,hs	heat source outlet

3.10 Appendix A

The dimensionless fluid temperature profiles as a function of borehole depth are derived in this appendix for the three possible configurations.

Configuration 1-2,3-4:

$$\theta_1(Z) = \theta_b - \theta_b \cosh(\beta Z) + \frac{2\theta_b S_{12} + S_1\left[\theta_2(0) + \theta_4(0)\right]}{2\beta S_1 S_{12}} \sinh(\beta Z) + e^{-\varepsilon Z}$$

$$\theta_2(Z) = \theta_b - \theta_b \cosh(\beta Z) + \frac{\theta_2(0) + \theta_4(0)}{2} \cosh(\beta Z) + \frac{(S_{12} + S_1)\left[\theta_2(0) + \theta_4(0)\right] - 2\theta_b S_{12}}{2\beta S_1 S_{12}} \sinh(\beta Z) + \frac{\theta_2(0) - \theta_4(0)}{2} e^{\varepsilon Z}$$

$$\theta_3(Z) = \theta_b - \theta_b \cosh(\beta Z) + \frac{2\theta_b S_{12} + S_1\left[\theta_2(0) + \theta_4(0)\right]}{2\beta S_1 S_{12}} \sinh(\beta Z) - e^{-\varepsilon Z}$$

$$\theta_4(Z) = \theta_b - \theta_b \cosh(\beta Z) + \frac{\theta_2(0) + \theta_4(0)}{2} \cosh(\beta Z) + \frac{(S_{12} + S_1)\left[\theta_2(0) + \theta_4(0)\right] - 2\theta_b S_{12}}{2\beta S_1 S_{12}} \sinh(\beta Z) - \frac{\theta_2(0) - \theta_4(0)}{2} e^{\varepsilon Z} \qquad (3.A.1)$$

Where

$$S_1 = R_1^*,\ S_{12} = \frac{R_{12}^*}{2},\ S_{13} = \frac{R_{13}^*}{2}$$

$$\beta = \sqrt{\frac{1}{S_1^2} + \frac{2}{S_1 S_{12}}},\ \varepsilon = \frac{1}{S_1} + \frac{1}{S_{12}} + \frac{1}{S_{13}}$$

$$\theta_2(0) = e^{-2\varepsilon} + \frac{\dfrac{2\theta_b \sinh(\beta)}{S_1\beta}}{\cosh(\beta) + \dfrac{\sinh(\beta)}{S_1\beta}}$$

$$\theta_4(0) = -e^{-2\varepsilon} + \frac{\dfrac{2\theta_b \sinh(\beta)}{S_1\beta}}{\cosh(\beta) + \dfrac{\sinh(\beta)}{S_1\beta}}$$

Configuration 1-3,2-4:

$$\theta_1(Z)=\theta_b-\theta_b\cosh(\gamma Z)+\frac{2S_{12}S_{13}\theta_b+\frac{S_1}{2}\left(S_{12}+S_{13}\right)\left[\theta_3(0)+\theta_4(0)\right]}{2S_1S_{12}S_{13}\gamma}\sinh(\gamma Z)+\cosh(\eta Z)$$
$$-\frac{\left[2S_{12}S_{13}+3S_1S_{13}+S_{12}S_1\right]+\frac{S_1}{2}\left(S_{13}-S_{12}\right)\left[\theta_3(0)-\theta_4(0)\right]}{2S_1S_{12}S_{13}\eta}\sinh(\eta Z)$$

$$\theta_2(Z)=\theta_b-\theta_b\cosh(\gamma Z)+\frac{2S_{12}S_{13}\theta_b+\frac{S_1}{2}\left(S_{12}+S_{13}\right)\left[\theta_3(0)+\theta_4(0)\right]}{2S_1S_{12}S_{13}\gamma}\sinh(\gamma Z)-\cosh(\eta Z)$$
$$+\frac{\left[2S_{12}S_{13}+3S_1S_{13}+S_{12}S_1\right]+\frac{S_1}{2}\left(S_{13}-S_{12}\right)\left[\theta_3(0)-\theta_4(0)\right]}{2S_1S_{12}S_{13}\eta}\sinh(\eta Z)$$

$$\theta_3(Z)=\theta_b+\left[\frac{\theta_3(0)+\theta_4(0)}{2}-\theta_b\right]\cosh(\gamma Z)+\frac{\left(S_{12}S_{13}+\frac{1}{2}S_1S_{13}+\frac{1}{2}S_1S_{12}\right)\left[\theta_3(0)+\theta_4(0)\right]}{2S_1S_{12}S_{13}\gamma}\sinh(\gamma Z)$$
$$-\frac{2S_{12}S_{13}\theta_b}{2S_1S_{12}S_{13}\gamma}\sinh(\gamma Z)+\frac{\theta_3(0)-\theta_4(0)}{2}\cosh(\eta Z)$$
$$+\frac{\left(S_{12}S_{13}+\frac{3}{2}S_1S_{13}+\frac{1}{2}S_{12}S_1\right)\left[\theta_3(0)-\theta_4(0)\right]+S_1\left(S_{13}-S_{12}\right)}{2S_1S_{12}S_{13}\eta}\sinh(\eta Z)$$

$$\theta_4(Z)=\theta_b+\left[\frac{\theta_3(0)+\theta_4(0)}{2}-\theta_b\right]\cosh(\gamma Z)+\frac{\left(S_{12}S_{13}+\frac{1}{2}S_1S_{13}+\frac{1}{2}S_1S_{12}\right)\left[\theta_3(0)+\theta_4(0)\right]}{2S_1S_{12}S_{13}\gamma}\sinh(\gamma Z)$$
$$-\frac{2S_{12}S_{13}\theta_b}{2S_1S_{12}S_{13}\gamma}\sinh(\gamma Z)-\frac{\theta_3(0)-\theta_4(0)}{2}\cosh(\eta Z)$$
$$-\frac{\left(S_{12}S_{13}+\frac{3}{2}S_1S_{13}+\frac{1}{2}S_{12}S_1\right)\left[\theta_3(0)-\theta_4(0)\right]+S_1\left(S_{13}-S_{12}\right)}{2S_1S_{12}S_{13}\eta}\sinh(\eta Z)$$

(3.A.2)

Where

$$S_1=R_1^*,\ S_{12}=\frac{R_{12}^*}{2},\ S_{13}=\frac{R_{13}^*}{2}$$

$$\gamma = \sqrt{\frac{1}{S_1^2} + \frac{1}{S_1 S_{12}} + \frac{1}{S_1 S_{13}}},\ \eta = \sqrt{\frac{1}{S_1^2} + \frac{3}{S_1 S_{12}} + \frac{2}{S_{12}^2} + \frac{1}{S_1 S_{13}} + \frac{2}{S_{12} S_{13}}}$$

$$\theta_3(0) = \frac{\frac{2\theta_b \sinh(\gamma)}{S_1\gamma}}{\cosh(\gamma) + \frac{\sinh(\gamma)}{S_1\gamma}} + \frac{\cosh(\eta) - \frac{2S_1 + S_{12}}{S_1 S_{12}\eta}\sinh(\eta)}{\cosh(\eta) + \frac{2S_1 + S_{12}}{S_1 S_{12}\eta}\sinh(\eta)}$$

$$\theta_4(0) = \frac{\frac{2\theta_b \sinh(\gamma)}{S_1\gamma}}{\cosh(\gamma) + \frac{\sinh(\gamma)}{S_1\gamma}} - \frac{\cosh(\eta) - \frac{2S_1 + S_{12}}{S_1 S_{12}\eta}\sinh(\eta)}{\cosh(\eta) + \frac{2S_1 + S_{12}}{S_1 S_{12}\eta}\sinh(\eta)}$$

Configuration 1-2,4-3:

$$\theta_1(Z) = \theta_b - \theta_b \cosh(\gamma Z) + \frac{2S_{12}S_{13}\theta_b + \frac{S_1}{2}(S_{12} + S_{13})\left[\theta_3(0) + \theta_2(0)\right]}{2S_1 S_{12} S_{13}\gamma}\sinh(\gamma Z) + \cosh(\eta Z)$$
$$- \frac{\left[2S_{12}S_{13} + 3S_1 S_{13} + S_{12}S_1\right] + \frac{S_1}{2}(S_{12} - S_{13})\left[\theta_2(0) - \theta_3(0)\right]}{2S_1 S_{12} S_{13}\eta}\sinh(\eta Z)$$

$$\theta_2(Z) = \theta_b + \left[\frac{\theta_3(0) + \theta_2(0)}{2} - \theta_b\right]\cosh(\gamma Z) + \frac{\left(S_{12}S_{13} + \frac{1}{2}S_1 S_{13} + \frac{1}{2}S_1 S_{12}\right)\left[\theta_3(0) + \theta_2(0)\right]}{2S_1 S_{12} S_{13}\gamma}\sinh(\gamma Z)$$
$$- \frac{2S_{12}S_{13}\theta_b}{2S_1 S_{12} S_{13}\gamma}\sinh(\gamma Z) + \frac{\theta_2(0) - \theta_3(0)}{2}\cosh(\eta Z)$$
$$+ \frac{\left(S_{12}S_{13} + \frac{3}{2}S_1 S_{13} + \frac{1}{2}S_{12}S_1\right)\left[\theta_2(0) - \theta_3(0)\right] + S_1(S_{12} - S_{13})}{2S_1 S_{12} S_{13}\eta}\sinh(\eta Z)$$

$$\theta_3(Z) = \theta_b + \left[\frac{\theta_3(0) + \theta_2(0)}{2} - \theta_b\right]\cosh(\gamma Z) + \frac{\left(S_{12}S_{13} + \frac{1}{2}S_1 S_{13} + \frac{1}{2}S_1 S_{12}\right)\left[\theta_3(0) + \theta_2(0)\right]}{2S_1 S_{12} S_{13}\gamma}\sinh(\gamma Z)$$
$$- \frac{2S_{12}S_{13}\theta_b}{2S_1 S_{12} S_{13}\gamma}\sinh(\gamma Z) - \frac{\theta_2(0) - \theta_3(0)}{2}\cosh(\eta Z)$$
$$- \frac{\left(S_{12}S_{13} + \frac{3}{2}S_1 S_{13} + \frac{1}{2}S_{12}S_1\right)\left[\theta_2(0) - \theta_3(0)\right] + S_1(S_{12} - S_{13})}{2S_1 S_{12} S_{13}\eta}\sinh(\eta Z)$$

$$\theta_4(Z)=\theta_b-\theta_b\cosh(\gamma Z)+\frac{2S_{12}S_{13}\theta_b+\frac{S_1}{2}\left(S_{12}+S_{13}\right)\left[\theta_3(0)+\theta_2(0)\right]}{2S_1S_{12}S_{13}\gamma}\sinh(\gamma Z)-\cosh(\eta Z)$$
$$+\frac{\left[2S_{12}S_{13}+3S_1S_{13}+S_{12}S_1\right]+\frac{S_1}{2}\left(S_{12}-S_{13}\right)\left[\theta_2(0)-\theta_3(0)\right]}{2S_1S_{12}S_{13}\eta}\sinh(\eta Z) \quad (3.A.3)$$

Where

$$S_1=R_1^*,\ S_{12}=\frac{R_{12}^*}{2},\ S_{13}=\frac{R_{13}^*}{2}$$

$$\gamma=\sqrt{\frac{1}{S_1^2}+\frac{1}{S_1S_{12}}+\frac{1}{S_1S_{13}}},\ \eta=\sqrt{\frac{1}{S_1^2}+\frac{3}{S_1S_{12}}+\frac{2}{S_{12}^2}+\frac{1}{S_1S_{13}}+\frac{2}{S_{12}S_{13}}}$$

$$\theta_2(0)=\frac{\frac{2\theta_b\sinh(\gamma)}{S_1\gamma}}{\cosh\left(\gamma\right)+\frac{\sinh\left(\gamma\right)}{S_1\gamma}}+\frac{\cosh\left(\eta\right)-\frac{S_1S_{13}+S_1S_{12}+S_{12}S_{13}}{S_1S_{12}S_{13}\eta}\sinh\left(\eta\right)}{\cosh\left(\eta\right)+\frac{S_1S_{13}+S_1S_{12}+S_{12}S_{13}}{S_1S_{12}S_{13}\eta}\sinh\left(\eta\right)}$$

$$\theta_4(0)=\frac{\frac{2\theta_b\sinh(\gamma)}{S_1\gamma}}{\cosh\left(\gamma\right)+\frac{\sinh\left(\gamma\right)}{S_1\gamma}}-\frac{\cosh\left(\eta\right)-\frac{S_1S_{13}+S_1S_{12}+S_{12}S_{13}}{S_1S_{12}S_{13}\eta}\sinh\left(\eta\right)}{\cosh\left(\eta\right)+\frac{S_1S_{13}+S_1S_{12}+S_{12}S_{13}}{S_1S_{12}S_{13}\eta}\sinh\left(\eta\right)}$$

3.11 Appendix B

In this appendix, the relationships derived by Zeng et al. (2003) for double U-tube boreholes in a parallel arrangement are derived from the equations developed in this study for a double U-tube borehole with two independent circuits. The analysis focuses on pipe 1 of the 1-2,3-4 configuration (Eq. (3.A.3) in Appendix A),

$$\theta_1(Z) = \theta_b - \theta_b \cosh(\beta Z) + \frac{2\theta_b S_{12} + S_1\left[\theta_2(0) + \theta_4(0)\right]}{2\beta S_1 S_{12}} \sinh(\beta Z) + e^{-\varepsilon Z} \tag{3.B.1}$$

For a parallel arrangement, $T_f' = T_f''$. This is inconvenient here as the definition of the dimensionless temperature is based on the difference of these two quantities in the denominator. Thus, it is not possible to substitute them directly in Eq.(3.B.1). Instead, both sides of Eq. (3.B.1) are first multiplied by $\left(T_f' - T_f''\right)$,

$$\theta_1(Z) \times \left(T_f' - T_f''\right) = \left(T_f' - T_f''\right) \times \left[\theta_b - \theta_b \cosh(\beta Z) + \frac{2\theta_b S_{12} + S_1\left[\theta_2(0) + \theta_4(0)\right]}{2\beta S_1 S_{12}} \sinh(\beta Z) + e^{-\varepsilon Z} \right] \tag{3.B.2}$$

Using the definition of the dimensionless temperature, Eq. (3.7),

$$\begin{aligned} 2T_{f1}(Z) - T_f' - T_f'' = {} & \left[2T_b - T_f' - T_f''\right] \times \left[1 - \cosh(\beta Z)\right] \\ & + \left[\frac{2\left[2T_b - T_f' - T_f''\right] S_{12} + S_1\left[2T_2(0) - 2T_4(0) - 2T_f' - 2T_f''\right]}{2\beta S_1 S_{12}} \right] \sinh(\beta Z) \\ & + \left(T_f' - T_f''\right) e^{-\varepsilon Z} \end{aligned} \tag{3.B.3}$$

Due to symmetry, the four equations for double U-tube boreholes with two independent circuits are reduced to two equations for the parallel arrangement,

$$\begin{aligned} &T_{f1}(z) = T_{f3}(z) = T_d(z) && \text{or} && \theta_1(Z) = \theta_3(Z) = \theta_d(Z) \\ &T_{f2}(z) = T_{f4}(z) = T_u(z) && \text{or} && \theta_2(Z) = \theta_4(Z) = \theta_u(Z) \\ &T_2(0) = T_4(0) = T_u(0) && \text{or} && \theta_2(0) = \theta_4(0) = \theta'' \end{aligned}$$

Then, Eq. (3.B.3) can be written as

$$2\left[T_d(Z) - T_f'\right] = 2\left(T_b - T_f'\right) - 2\left(T_b - T_f'\right)\cosh(\beta Z) + \frac{2\left[T_b - T_f'\right] S_{12} + 2S_1\left[T_u(0) - T_f'\right]}{\beta S_1 S_{12}} \sinh(\beta Z) \tag{3.B.4}$$

The dimensionless temperature parameter defined by Zeng et al. (2003) is

$$\theta = \frac{T - T_b}{T_f' - T_b} \tag{3.B.5}$$

In order to compare Eq. (3.B.4) with the corresponding equation in Zeng et al. (2003), the dimensionless form is required. Thus, the first term in the right hand side of Eq. (3.B.4) is brought to the left, and both sides are divided by $2\left(T_f' - T_b\right)$ to get the dimensionless temperature distribution of the 1-2,3-4 parallel configuration (Zeng et al., 2003) Eq. (3.B.5),

$$\theta_d(Z) = \cosh(\beta Z) - \frac{1}{\beta S_{12}}\left[\frac{S_{12}}{S_1} + 1 - \theta''\right]\sinh(\beta Z)$$

where θ'' is the dimensionless outlet temperature and

$$S_1 = R_1^*,\ S_{12} = \frac{R_{12}^*}{2},\ \beta = \sqrt{\frac{1}{S_1^2} + \frac{2}{S_1 S_{12}}}$$

The same procedure can be used to obtain the $\theta_u(Z)$ value of Zeng et al. (2003) using $\theta_2(Z)$ and $\theta_4(Z)$. This appendix has shown that it is possible to derive the equations for the 1-2,3-4 parallel arrangement of Zeng et al. (2003) from the relationships developed in this study for the 1-2,3-4 double U-tube with two independent circuits.

3.12 References

Al-Khoury, R., and Bonnier, P. G. (2006). Efficient finite element formulation for geothermal heating systems. Part II: Transient. *International Journal of Numerical Methods in Engineering*, 67 (5), 725-745.

Anonymity A, site consulted on Nov. 9, 2009, http://en.ivt.se/products.asp?lngID=489&lngLangID=1

Bernier, M. (2000). A Review of the Cylindrical Heat Source Method for the Design and Analysis of Vertical Ground-Coupled Heat Pump Systems. 4th International Conference of Heat Pumps in Cold Climates, 14 pages.

Bernier, M., and Salim Shirazi, A. (2007). Solar heat injection into boreholes: a preliminary analysis. Proceeding of 2nd Canadian Solar Building Conference, T1-1-1, 8 pages.

Carslaw, H. S., and Jaeger, J. C. (1947). *Conduction of heat in solids* (1st ed). Oxford, U.K.: Claremore Press.

Chapuis, S., and Bernier, M. (2008). Étude préliminaire sur le stockage solaire saisonnier par puits géothermique. Proceeding of 3rd Canadian Solar Building Conference, 14-23.

Chapuis, S., and Bernier, M. (2009). Seasonal storage of solar energy in borehole heat exchangers. Proceeding of 11th International IBPSA Conference, 599-606.

Chiasson, A. D., and Yavuzturk, C. (2003). Assessment of the viability of hybrid geothermal heat pump systems with solar thermal collectors. *ASHRAE Transactions*, 109 (2), 487-500.

Diao, N. R., Zeng, H. Y., and Fang, Z. H. (2004). Improvement in modeling of heat transfer in vertical ground heat exchangers. *HVAC&R Research*, 10 (4), 459-470.

Eslami nejad, P., Langlois, A., Chapuis, S., Bernier, M., and Faraj, W. (2009). Solar heat injection into boreholes. Proceeding of 4th Canadian Solar Building Conference, 237-246.

He, M., Rees, S., and Shao, L. (2009). Simulation of a domestic ground source heat pump system using a transient numerical borehole heat exchanger model. Proceeding of 11th International IBPSA Conference, 607-614.

Hellström, G. (1991). Ground heat storage, thermal analysis of duct storage system. Doctorial Thesis, University of Lund, Sweden.

Hellström, G. (1989). Duct ground heat storage model. Manual for Computer Code, Department of Mathematical Physics, University of Lund, Sweden.

Kjellsson, E., Hellström, G., and Perers, B. (2010). Optimization of systems with the combination of ground-source heat pump and solar collectors in dwellings. *Energy*, 35 (6), 2667-2673.

Kummert, M., and Bernier, M. (2008). Analysis of a combined photovoltaic-geothermal gas-fired absorption heat pump system in a Canadian climate. *Journal of Building Performance Simulation*, 1 (4), 245-256.

Lamarche, L., and Beauchamp, B. (2007). New solutions for the short-time analysis of geothermal vertical boreholes. *International Journal of Heat and Mass Transfer*, 50(7-8), 1408-1419.

Lamarche, L., Kajl, S., and Beauchamp, B. (2010). A review of methods to evaluate borehole thermal resistances in geothermal heat-pump systems. *Journal of Geothermics*, 39 (1), 187-200.

Man, Y., Yang, H., Diao, N., Liu, J., and Fang, Z. (2010). A new model and analytical solutions for borehole and pile ground heat exchangers. *International Journal of Heat and Mass Transfer*, 53 (13-14), 2593-2601.

Marcotte, D., and Pasquier, P. (2008). On the estimation of thermal resistance in borehole thermal conductivity test. *Renewable Energy*, 33 (11), 2407-2415.

Penrod, E. B., and Prasanna, D. V. (1962). Design of flat-plate collector for solar earth heat pump. *Solar Energy*, 6 (1), 9-22.

Penrod, E. B., and Prasanna, D. V. (1969). Procedure for designing solar-earth heat pumps. *Heating, Piping and Air Conditioning*, 41 (6), 97-100.

Philippacopoulos, A. J., and Berndt, M. L. (2001). Influence of debonding in ground heat exchangers used with geothermal heat pumps. *Journal of Geothermics*, 30 (5), 527-545.

Remund, C. P. (1999). Borehole thermal resistance: laboratory and field studies. *ASHRAE Transactions*, 105 (1), 439-445.

Stojanovic, B., and Akander, J. (2010). Build-up and long-term performance test of a full-scale solar-assisted heat pump system for residential heating in Nordic climatic conditions. *Applied Thermal Engineering*, 30 (2-3), 188-195.

Sibbitt, B., Onno, T., McClenahan, D., Thornton, J., Brunger, A., Kokko, J., and Wong, B. (2007). The Drake Landing Solar Community Project – Early Results. Proceeding of 2nd Canadian Solar Building Conference, M2-1-3, 11 pages.

Wang, X., Zheng, M., Zhang, W., Zhang, S., and Yang, T. (2010). Experimental study of a solar-assisted ground-coupled heat pump system with solar seasonal thermal storage in severe cold areas. *Energy and Buildings*, 42 (11), 2104-2110.

Wetter, M., and Huber, A. (1997). TRNSYS Type 451: Vertical Borehole Heat Exchanger (3.1 ed).

Yang, W., Shi, M. H., and Dong, H. (2006). Numerical simulation of the performance of a solar-earth source heat pump system. *Applied Thermal Engineering*, 26 (17-18), 2367-2376.

Yang, W., Shi, M., Liu, G., and Chen, Z. (2009). A two-region simulation model of vertical U-tube ground heat exchanger and its experimental verification. *Applied Energy*, 86 (10), 2005-2012.

Young, T. R. (2004). Development, verification, and design analysis of the borehole fluid thermal mass model for approximating short-term borehole thermal response. Master of Science Thesis, Oklahoma State University, United States.

Zeng, H., Diao, N., and Fang, Z. (2003). Heat transfer analysis of boreholes in vertical ground heat exchangers. *International Journal of Heat and Mass Transfer*, 46 (23), 4467-4481.

CHAPITRE 4 SCIENTIFIC ARTICLE 2: COUPLING OF GEOTHERMAL HEAT PUMPS WITH THERMAL SOLAR COLLECTORS USING DOUBLE U-TUBE BOREHOLES WITH TWO INDEPENDENT CIRCUITS

Abstract

This study presents an analytical model to predict steady-state heat transfer in double U-tube boreholes with two independent circuits operating with unequal mass flow rates and inlet temperatures. The model predicts the fluid temperature profiles in both circuits along the borehole depth. It accounts for fluid and pipe thermal resistance and thermal interaction among U-tube circuits. The proposed model is used to study a novel double U-tube borehole configuration with one circuit linked to a ground-source heat pump operating in heating mode and the other to thermal solar collectors. The performance of this configuration is compared to a conventional ground-source heat pump system (without thermal recharge of the borehole) and to a single-circuit solar assisted ground-source heat pump system. All three systems are simulated over a 20-year period for a residential-type single borehole configuration. Results indicate that winter solar recharging, either for the proposed configuration or the solar assisted ground-source heat pump system, reduces by 168 and 194% the amount of energy extracted from the ground by the heat pump. It is also shown that, for a ground thermal conductivity of 1.5 W·m-1·K-1, the borehole length can be reduced by up to 17.6%, and 33.1% when the proposed configuration or the solar assisted ground-source heat pump system are used. The impact on the annual heat pump energy consumption is less dramatic with corresponding reductions of 3.5% and 6.5%.

4.1 Introduction

Systems that link heat pumps to vertical borehole ground heat exchangers are proving to be energy-efficient systems to heat and cool buildings. However, the cost associated with the borehole remains relatively high which handicaps the widespread application of this technology. Furthermore, when the heat pump operates in heating mode, it collects heat from the ground which reduces the ground temperature near the borehole. In turn, the lower ground temperature decreases the Coefficient of Performance (COP) of the heat pump. Thus, it might be

advantageous to inject heat into the borehole to increase the ground temperature and heat pump performance. One possible way is to inject solar energy by using the novel borehole configuration presented schematically in Figure 4-1.

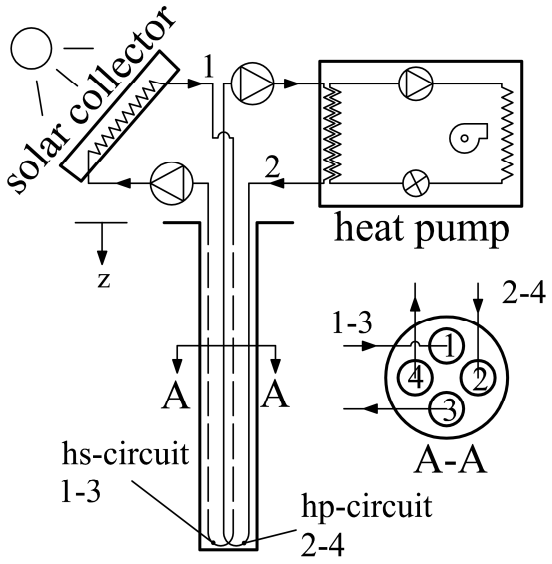

Figure 4-1: Schematic representation of the system under study

It consists of a 4 pipe (2 U-tubes) vertical borehole with two independent circuits. One U-tube is linked to a heat pump and the other to a thermal solar collector. As shown in Figure 4-1, these circuits are referred to as the heat pump circuit (hp-circuit) and the heat source circuit (hs-circuit), respectively. In effect, this configuration with two independent circuits acts as a heat exchanger between the heat source and the heat pump. The system can operate in three different modes: heat pump only; solar charging only, or simultaneous heat pump and solar charging operation. This latter case is the main subject of the present investigation. A new model for such a configuration is elaborated in this paper to accurately assess its performance. The proposed model predicts steady-state heat transfer in double U-tube boreholes with two independent circuits operating with unequal mass flow rates and inlet temperatures. The model predicts the fluid temperature profiles in both circuits along the borehole depth. It accounts for fluid and pipe thermal resistance and thermal interaction among U-tube pipes.

4.2 Literature Review

Several numerical and analytical models have been developed to simulate heat transfer in single U-tube boreholes. He et al. (2009) developed a finite-volume based three-dimensional model to

simulate the dynamic response of the circulating fluid as well as transient heat transfer in and around boreholes. Young (2004) evaluated analytically the short time response of boreholes based on the “buried cable” solution given by Carslaw and Jaeger (1947) which accounts for the grout and fluid thermal capacities. Lamarche and Beauchamp (2007) approximated the short-time response of single U-tube boreholes using an analytical solution to the unsteady one-dimensional heat conduction problem of concentric cylinders. Man et al. (2010) developed an analytical model which accounts for the heat capacity of boreholes by assuming a homogenous medium for the whole calculation domain including the ground in the vicinity of the borehole. Remund (1999) proposed a set of relationships for different single U-tube borehole configurations to calculate the steady-state borehole thermal resistances based on conduction shape factors obtained from empirical data. Equal fluid temperatures in both circuits are assumed in his approach. Marcotte and Pasquier (b2008) proposed a so-called “p-linear” average temperature using a 3-D numerical simulation to evaluate the borehole thermal resistance from experimental data. A review paper by Lamarche et al. (2010) compared different existing approaches to calculate borehole thermal resistance including thermal short-circuit between pipes. They also performed an unsteady 3-D numerical simulation of a standard single U-tube borehole.

A few studies have also modeled conventional single-circuit double U-tube boreholes. Al-Khoury and Bonnier (2006) applied the three-dimensional finite element method to analyze transient heat transfer in a double U-tube parallel arrangement. Hellström (1991) derived steady-state two-dimensional analytical solutions for borehole thermal resistances with an arbitrary number of pipes. Zeng et al. (2003) used this work to establish an analytical quasi-three-dimensional model for single and double U-tube configured either in parallel or in series. Diao et al. (2004) used this latter approach to simulate heat transfer inside boreholes, including thermal interactions among tubes, along with the finite-line source solution to predict heat transfer in the ground. Wetter and Huber (1997) modeled the transient behavior of a double U-tube borehole with a single equivalent pipe diameter which does not allow modeling of two independent circuits in one borehole. Even though these last five studies examined double U-tubes none of them investigated the use of two independent circuits.

Despite the fact that ground source heat pump (GSHP) systems constitute attractive options for heating and cooling applications, it has been shown that in heating dominated climates, the performance of conventional GSHP system decreases gradually over time. This is due to the fact

that more heat is extracted from the ground than the amount rejected during the cooling season. Thus, the ground temperature in the vicinity of the borehole decreases over the years with a resulting decrease in the inlet temperature to the heat pumps which translates into a reduction in the coefficient of performance (COP). Bernier (2000) indicated that for a typical constant heat extraction of 37.5 W/m, the borehole wall temperature decreases by approximately 5ºC over a 24 hour period. Trillat-Berdal et al. (2007) also reported a reduction of 2ºC of the soil temperature in the vicinity of double U-tube borehole over twenty years of heat pump operation.

One possibility to let the ground temperature recover from heat extraction is to use, alternatively, the ground and another source for the heat pump. This idea was first introduced by Penrod and Prasanna (1962,1969) who proposed such a dual-source (solar collector and ground) system. Yang et al. (2006) recently recommended using solar-source heat pump (SSHP) and ground-source heat pump (GSHP) systems alternately for a period of 10-14 hours a day to achieve a 30-60% recovery-rate for the ground temperature in the vicinity of the borehole.

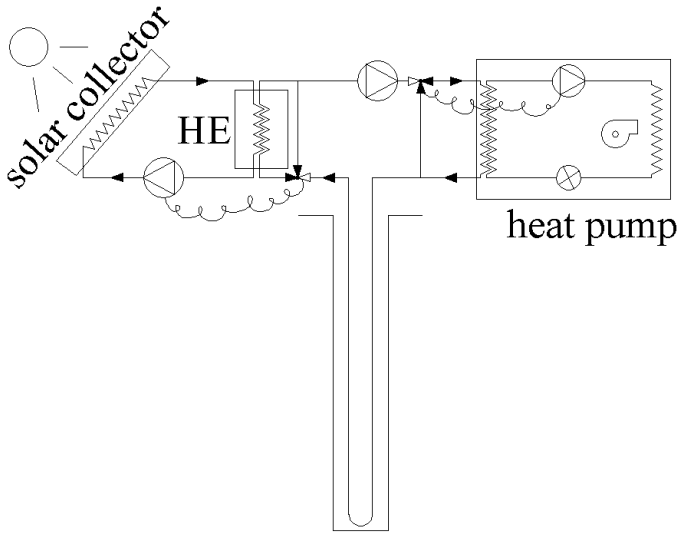

Figure 4-2: Schematic representation of conventional solar-assisted ground source heat pump system

Another possibility which can be used for ground temperature recovery is to inject heat into the boreholes. In this configuration a GSHP is combined with thermal solar collectors using an additional heat exchanger as shown in Figure 4-2. Although adding an additional heat exchanger may add to the complexity of the system (Sibbitt et al., 2007), several studies indicated that it is a viable option for heating-dominated climates. Yang et al. (2010) reviewed various GSHP systems

assisted by supplemental heat rejecters or heat supply devices such as solar collectors. They concluded that in general, the use of a supplemental source such as solar energy can make GSHP systems economically attractive. Wang et al. (2010) performed an experimental study of a GSHP system coupled with seasonal borehole storage. Solar energy is stored in the summer in 12 single U-tube boreholes. They indicated that the operation of such a system improves significantly the heat pump heating COP. Chiasson and Yavuzturk (2003) performed a 20-year life-cycle cost analysis to evaluate the economics of ground heat pump systems coupled to thermal solar collectors for six different climates in the U.S. They concluded that GSHP systems combined with solar collectors are economically viable for heating dominated climates. Stojanovic and Akander (2010) conducted a two year performance test on a full-scale solar-assisted heat pump system for a residential building in a nordic climatic. They indicated that despite unfavourable building conditions, the proposed system succeeded in fulfilling the heating requirements. Han et al. (2008) investigated different operational modes of a solar assisted GSHP system in the presence of latent heat energy storage tanks in a heating dominated climate. They indicated that using storage tanks increases system performance by 12.3%. Kjellsson et al. (2010) analyzed five alternatives to supply solar energy to a ground source heat pump (GSHP) system and compared them against a base case without solar collectors. They concluded that the option with the highest electrical consumption savings is a hybrid system with solar heat injection into the borehole in winter and solar domestic hot water production during the summer. Solar heat is first directed to the heat pump and then to the borehole. Double U-tube boreholes with two independent circuits were not considered. Based on a series of experiments, Georgiev et al. (2006) indicated that only a small portion of solar energy injected into the ground can be extracted after a month from the first injection. They injected solar energy to a shallow single U-tube borehole for a period of 700 hours and afterwards they started to extract heat out of the borehole for 300 hours. Only 32% of the total accumulated energy could eventually be extracted due to the heat dissipation into the ground and heat losses to the surface.

In order to reduce the relative complexity of the system presented in Figure 4-2 and to make simultaneous heat injection and heat extraction possible, double U-tube boreholes with two independent circuits can be used (Figure 4-1). Chapuis and Bernier (2008, 2009) are at the origin of two studies which attempted to model double U-tubes with two independent circuits. In the first study, Chapuis and Bernier (2008) used an external heat exchanger combined to the duct

ground heat storage (DST) model (Hellström, 1989) to mimic simultaneous charging and discharging in the ground heat exchanger. Later, they modified the DST model to handle double U-tube boreholes with two independent circuits (Chapuis and Bernier, 2009). However, thermal interaction between the U-tubes in the borehole was not taken into account nor was the axial temperature variation in the fluid in both legs. Kummert and Bernier (2008) proposed a new system for space conditioning and domestic hot water heating in a cold climate using a gas-fired absorption heat pump coupled to a vertical geothermal borehole with two independent circuits linked, respectively, to the evaporator and condenser of the heat pump. They considered three modes of operations including heating only, cooling only, and simultaneous heating/cooling. The ground heat exchanger was modeled using the DST model but simultaneous flows in the two circuits could not be evaluated. Bernier and Salim Shirazy (2007) and Eslami nejad et al. (2009) evaluated the impact of solar heat injection on borehole length and heat pump energy consumption. However, they approximated the double U-tube configuration with a single U-tube based on a simple approach which assumed that heat collected/rejected into the ground is the sum of the solar energy injected and heat pump energy extraction/rejection. Furthermore, both outlet fluid temperatures were assumed equal.

4.3 Model Development

Figure 4-3 presents a cross-section of a four-pipe borehole. The space between the pipes and the borehole wall is assumed to be filled with a solid material (grout). There are three possible ways of connecting these four pipes to form two independent circuits: As suggested by Zeng et al. (2003), each configuration can be identified with a four digit notation.

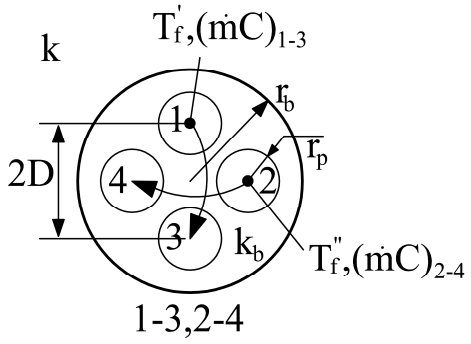

Figure 4-3: Borehole cross-section showing the 1-3,2-4 configuration

For example, in the 1-3, 2-4 configuration, the fluid from the first circuit enters pipe #1 goes to the bottom of the borehole and then up pipe #3. Similarly, the fluid from the second circuit enters pipe #2 goes to the bottom of the borehole and then up pipe #4. The other possible configurations are: 1-2, 3-4, 1-2,4-3.

Zeng et al. (2003) examined the performance of all three configurations for the single-circuit case with pipes arranged in series or parallel. They concluded that the 1-3, 2-4 configuration presents the lowest borehole thermal resistance. Based on this result it was decided to restrict the model development to the 1-3, 2-4 configuration.

As shown in Figure 4-3, the model assumes that the pipes are placed symmetrically in the borehole with identical center-to-center distance (2D) between two opposing pipes. Both circuits are independent and have different inlet temperatures $T_f' \neq T_f''$ and heat capacities $(\dot{m}C)_{1-3} \neq (\dot{m}C)_{2-4}$ .Other modeling assumptions include: (i) the heat capacities of the grout and pipe inside the borehole are neglected; (ii) the ground and the grout are homogeneous and their thermal properties are constant; (iii) the borehole wall temperature (T_b in Figure 4-4) is uniform over the borehole depth; (iv) heat conduction in the axial direction is neglected; (iv) the combined fluid convective resistance, pipe wall thickness conduction resistances are assumed to be equal in both circuits. These assumptions have been used in the past by a number of researchers (e.g. Zeng et al., 2003; Hellström, 1991). More recently, Lamarche et al. (2010) compared borehole thermal resistance calculation methods against an unsteady three-dimensional borehole model. A good agreement for the axial fluid temperature distribution of a single U-tube borehole was reported between the approach proposed by Zeng et al. (2003), which uses the assumptions mentioned above, and the three-dimensional simulation results. Yang et al. (2009) coupled a steady-state single U-tube borehole model, assuming a uniform T_b, to a unsteady one-dimensional ground heat transfer model based on the cylindrical heat source approach. This two-region model was validated experimentally. Results indicated that the calculated fluid outlet temperatures are in very good agreement with experimental data in the steady-state regime.

4.4 Heat Flow Balance Equations

The difference between the borehole wall temperature and the fluid temperatures in each circuit is the result of net heat flows per unit length, q_1, q_2, q_3, and q_4 in and out of the four pipes. Based

on the approach presented by other authors (Hellström, 1991; Zeng et al., 2003) and using the nomenclature presented in Figure 4-4, the following heat flow balances are obtained:

$$\begin{aligned} T_{f1}(z) - T_b &= R_{11}q_1 + R_{12}q_2 + R_{13}q_3 + R_{14}q_4 \\ T_{f2}(z) - T_b &= R_{21}q_1 + R_{22}q_2 + R_{23}q_3 + R_{24}q_4 \\ T_{f3}(z) - T_b &= R_{31}q_1 + R_{32}q_2 + R_{33}q_3 + R_{34}q_4 \\ T_{f4}(z) - T_b &= R_{41}q_1 + R_{42}q_2 + R_{43}q_3 + R_{44}q_4 \end{aligned} \tag{4.1}$$

In Eq. (4.1), $T_{fi}(z)$ ($i=1, 2, 3, 4$) represents the fluid temperature at a certain borehole depth z, R_{ii} ($i=1, 2, 3, 4$) is the thermal resistance between the fluid in pipe i and the borehole wall, and R_{ij} ($i=1, 2, 3, 4$) is the thermal resistance between pipes i and j.

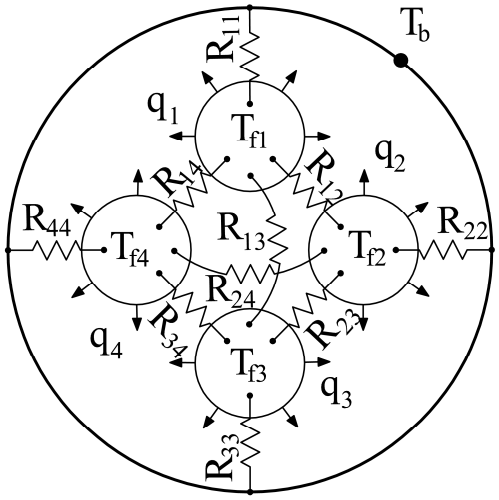

Figure 4-4: Nomenclature used in Eq. (4.1)

Since the pipes are assumed to be positioned symmetrically in the borehole, $R_{ij}=R_{ji}$, $R_{ii}=R_{jj}$, $R_{24}=R_{13}$ and $R_{23}=R_{14}=R_{34}=R_{12}$. Thus, only three thermal resistances, R_{11}, R_{12}, R_{13}, need to be evaluated. Hellström (1991) presented a technique to evaluate and R_{ii} and R_{ij} based on the line source solutions for each pipe which are then superimposed. This leads to:

$$R_{11} = \frac{1}{2\pi k_b}\left[\ln\left(\frac{r_b}{r_p}\right) - \frac{k_b - k}{k_b + k}\ln\left(\frac{r_b^2 - D^2}{r_b^2}\right)\right] + R_{pipe}$$
$$R_{12} = \frac{1}{2\pi k_b}\left[\ln\left(\frac{r_b}{\sqrt{2}D}\right) - \frac{k_b - k}{2(k_b + k)}\ln\left(\frac{r_b^4 + D^4}{r_b^4}\right)\right] \qquad (4.2)$$
$$R_{13} = \frac{1}{2\pi k_b}\left[\ln\left(\frac{r_b}{2D}\right) - \frac{k_b - k}{k_b + k}\ln\left(\frac{r_b^2 + D^2}{r_b^2}\right)\right]$$

Where k and k_b are the ground and grout thermal conductivities, respectively, r_p is the outer radius of the pipe, R_{pipe}, which is assumed constant over the borehole depth, is the combined fluid convective resistance, pipe wall thickness conduction resistance, and contact resistance associated with gaps between the pipes and the grout. It is defined as follow:

$$R_{pipe} = \frac{1}{2\pi h_i r_{i,p}} + \frac{\ln\left(r_p / r_{i,p}\right)}{2\pi k_p} + R_{air} \qquad (4.3)$$

where $r_{i,p}$ is the inner pipe radius, k_p is the pipe thermal conductivity, and h_i is fluid convective heat transfer coefficient. The second term on the right hand side is the conductive thermal resistance of the pipe. The third term, R_{air}, is a contact resistance at the grout/pipe interface. This last resistance was set to zero in this work. However, it could easily be included in the value of R_{pipe} if required. The reader is referred to the work of Philippacopoulos and Berndt (2001) for a discussion on the effect of air-filled gaps at the grout/pipe interface. Finally, the value of h_i is assumed to be the same in both circuits and constant along the depth of the borehole.

The fluid temperature varies along the borehole depth so each heat flow per unit length in Eq. (4.1) can be replaced with the first order derivative of the corresponding fluid temperature as a function of z multiplied by the corresponding fluid thermal capacity, i.e. the product of fluid mass flow rate, $\dot{m}$, and specific heat, C. For configuration 1-3,2-4 the net heat flows per unit length, q_1, q_2, q_3, and q_4 are then:

$$q_1 = -\left(\dot{m}C\right)_{1-3} dT_{f1}(z)/dz \,, q_2 = -\left(\dot{m}C\right)_{2-4} dT_{f2}(z)/dz$$
$$q_3 = +\left(\dot{m}C\right)_{1-3} dT_{f3}(z)/dz \,, q_4 = +\left(\dot{m}C\right)_{2-4} dT_{f4}(z)/dz \qquad (4.4)$$

The z-coordinate direction is defined as downward (from the ground surface) and, as indicated in Figure 4-4, an outward heat flow is considered positive. Thus, a negative sign in Eq. (4.4)

indicates that the fluid is flowing in the downward direction. Conversely, a positive signs implies an upward flow. It is to be noted that the model can handle different thermal capacities in both circuits, i.e. $(\dot{m}C)_{1-3} \neq (\dot{m}C)_{2-4}$.

Equation (4.1) can be rearranged in terms of the net heat flows in each pipe and afterwards by substituting Eq. (4.4) into Eq. (4.1), a set of coupled linear differential equations are obtained:

$$\begin{aligned}
-(\dot{m}C)_{1-3}\, dT_{f1}(z)/dz &= \frac{T_{f1}-T_b}{R_1^{\Delta}} + \frac{T_{f1}-T_{f2}}{R_{12}^{\Delta}} + \frac{T_{f1}-T_{f3}}{R_{13}^{\Delta}} + \frac{T_{f1}-T_{f4}}{R_{12}^{\Delta}} \\
-(\dot{m}C)_{2-4}\, dT_{f2}(z)/dz &= \frac{T_{f2}-T_{f1}}{R_{12}^{\Delta}} + \frac{T_{f2}-T_b}{R_1^{\Delta}} + \frac{T_{f2}-T_{f3}}{R_{12}^{\Delta}} + \frac{T_{f2}-T_{f4}}{R_{13}^{\Delta}} \\
(\dot{m}C)_{1-3}\, dT_{f3}(z)/dz &= \frac{T_{f3}-T_{f1}}{R_{13}^{\Delta}} + \frac{T_{f3}-T_{f2}}{R_{12}^{\Delta}} + \frac{T_{f3}-T_b}{R_1^{\Delta}} + \frac{T_{f3}-T_{f4}}{R_{12}^{\Delta}} \\
(\dot{m}C)_{2-4}\, dT_{f4}(z)/dz &= \frac{T_{f4}-T_{f1}}{R_{12}^{\Delta}} + \frac{T_{f4}-T_{f2}}{R_{13}^{\Delta}} + \frac{T_{f4}-T_{f3}}{R_{12}^{\Delta}} + \frac{T_{f4}-T_b}{R_1^{\Delta}}
\end{aligned} \tag{4.5}$$

where

$$\begin{aligned}
R_1^{\Delta} &= R_{11} + R_{13} + 2R_{12} \\
R_{12}^{\Delta} &= \left(R_{11}^2 + R_{13}^2 + 2R_{11}R_{13} - 4R_{12}^2\right)/R_{12} \\
R_{13}^{\Delta} &= \left[(R_{11}-R_{13})(R_{11}^2 + R_{13}^2 + 2R_{11}R_{13} - 4R_{12}^2)\right]/\left(R_{13}^2 + R_{11}R_{13} - 2R_{12}^2\right)
\end{aligned}$$

4.5 Dimensionless Governing Equations and Boundary Conditions

Equations (4.6) are non-dimensionalised using the following dimensionless variables:

$$\begin{aligned}
\theta_{i=1,2,3,4} &= \left[\left(T_{fi}(z) - T_f'\right) + \left(T_{fi}(z) - T_f''\right)\right]/\left(T_f' - T_f''\right), \;\; T_f' \neq T_f'' \\
\theta_b &= \left[\left(T_b - T_f'\right) + \left(T_b - T_f''\right)\right]/\left(T_f' - T_f''\right) \\
R_1^* &= (\dot{m}C)_{1-3}\, R_1^{\Delta}/H \;\; , R_{12}^* = (\dot{m}C)_{1-3}\, R_{12}^{\Delta}/H \;\; , R_{13}^* = (\dot{m}C)_{1-3}\, R_{13}^{\Delta}/H \;\; \text{and} \;\; Z = z/H
\end{aligned} \tag{4.6}$$

where, as indicated in Figure 4-3, T_f' and T_f'' are the inlet temperatures to the 1-3 and 2-4 circuits, respectively. The dimensionless thermal resistances, $R_1^*, R_{12}^*, R_{13}^*$, are all defined based on the thermal capacitance of circuit 1-3, $(\dot{m}C)_{1-3}$. Then, the heat flow balance equations are simplified as follows:

$$
\begin{aligned}
-d\theta_1/dZ &= a\theta_1 + b\theta_2 + c\theta_3 + b\theta_4 + d \\
-d\theta_2/dZ &= \alpha\left(b\theta_1 + a\theta_2 + b\theta_3 + c\theta_4 + d\right) \\
d\theta_3/dZ &= c\theta_1 + b\theta_2 + a\theta_3 + b\theta_4 + d \\
d\theta_4/dZ &= \alpha\left(b\theta_1 + c\theta_2 + b\theta_3 + a\theta_4 + d\right)
\end{aligned}
\qquad (4.7)
$$

where

$a = 1/R_1^* + 2/R_{12}^* + 1/R_{13}^*$, $b = -1/R_{12}^*$, $c = -1/R_{13}^*$, $d = -\theta_b/R_1^*$

and

$\alpha = (\dot{m}C)_{1-3}/(\dot{m}C)_{2-4}$

Considering that $T_f' = T_{f1}(0)$ and $T_f'' = T_{f2}(0)$, the dimensionless boundary conditions are:

$$\theta_1(0) = 1 \quad \theta_2(0) = -1 \quad \theta_1(1) = \theta_3(1) \quad \theta_2(1) = \theta_4(1) \qquad (4.8)$$

Finally, the dimensional and dimensionless outlet temperatures of both circuits will be denoted by $T_{f3}(0)$, $T_{f4}(0)$, $\theta_3(0)$, $\theta_4(0)$, respectively.

4.6 Laplace Transforms

Using Laplace transforms the dimensionless heat flow balance equations are transformed to yield a set of linear algebraic equations as follows:

$$
\begin{aligned}
(a+p)\bar{\theta}_1 + b\bar{\theta}_2 + c\bar{\theta}_3 + b\bar{\theta}_4 &= 1 - d/p \\
\alpha b\bar{\theta}_1 + (\alpha a + p)\bar{\theta}_2 + \alpha b\bar{\theta}_3 + \alpha c\bar{\theta}_4 &= -1 - \alpha\, d/p \\
c\bar{\theta}_1 + b\bar{\theta}_2 + (a-p)\bar{\theta}_3 + b\bar{\theta}_4 &= -\theta_3(0) - d/p \\
\alpha b\bar{\theta}_1 + \alpha c\bar{\theta}_2 + \alpha b\bar{\theta}_3 + (\alpha a - p)\bar{\theta}_4 &= -\theta_4(0) - \alpha\, d/p
\end{aligned}
\qquad (4.9)
$$

where $\bar{\theta}(p)_i = \int_0^\infty e^{-pZ}\theta_i(Z)dZ$.

This set of equations can be solved, using Gaussian elimination for example, to obtain $\bar{\theta}_1, \bar{\theta}_2, \bar{\theta}_3,$ and $\bar{\theta}_4$ a function of *a, b, c, d,* α, $\theta_3(0)$, $\theta_4(0)$, and *p*. Then, the inverse Laplace transforms of $\bar{\theta}_1, \bar{\theta}_2, \bar{\theta}_3,$ and $\bar{\theta}_4$ are evaluated to obtain dimensionless temperature distributions. Boundary conditions are then applied to evaluate the dimensionless outlet temperature, $\theta_3(0)$ and

$\theta_4(0)$. The resulting dimensionless temperature distributions, $\theta_{i=1,2,3,4}(Z)$ are presented in the appendix. These results were validated against the equations developed by Zeng et al. (2003) for the simpler case of equal mass flow rates in a parallel single-circuit arrangement. It can be shown that the resulting temperature distributions are identical for both approaches indicating that the proposed model has been correctly implemented.

4.7 Applications

In this section, the proposed model for double U-tube boreholes with two independent circuits is used in two applications. The first application evaluates the effect of unequal mass flow rates on heat transfer between each circuit for constant (but different) inlet temperatures in both circuits. In the second application, hourly simulations over a twenty year period are performed to quantify the impact of solar recharging a borehole on heat pump energy consumption, borehole length, and net ground heat extraction. Results are compared with the solar assisted GSHP system presented in Figure 4-2 and typical a GSHP system without solar recharging. Typical geothermal borehole characteristics are used and are presented in Table 4-1. The specific heats of both fluids are set to the same value (4.00 kJ/kg-K) but the mass flow rates are different.

Table 4-1: Borehole characteristics

r_b (cm)	R_{op} (cm)	D (cm)	k ($W \cdot m^{-1} \cdot K^{-1}$)	$\dot{m}_{ref}$ ($kg.s^{-1}$)	k_b ($W \cdot m^{-1} \cdot K^{-1}$)
7.5	1.67	3.06	1.5	0.44	1

4.8 Constant Inlet Conditions

For this first application, the borehole length (H) is set to 100m and $T_{f1}(0)$=25°C, $T_{f2}(0)$=-5°C , T_b=10°C leading to a dimensionless borehole wall temperature θ_b (Eq. (4.6)) equal to zero. The mass flow rate of the hp-circuit is equal to $\dot{m}_{ref}$ and is kept constant. The thermal capacity ratio, α, is varied by changing the mass flow rate in the hs-circuit. The flow regime is assumed to be turbulent over the range of variation of α which lead to a value of R_{pipe} equal to 0.1 [$m.K.W^{-1}$] for all four pipes.

Figure 4-5 shows the temperature difference between the inlet and outlet of each circuit as a function of α, the thermal capacity ratio. The left axis presents the results in dimensionless form and the dimensional values are given on the right axis. It is shown that the hs-circuit experiences large temperature difference changes while the corresponding hp-circuit changes are not as large.

This is due to the fact that the flow rate increases in the hs-circuit while it is constant in the hp-circuit. Thus, the hs-circuit sees its inlet-outlet temperature difference decrease with an increase in the value of α. As will be shown shortly this does not imply that the hs-circuit rejects less heat when α is increased. The observed temperature difference increase in the hp-circuit with increasing values of α is due to the fact that the average temperature in the hs-circuit is larger leading to higher heat transfer from the hs-circuit to the hp-circuit.

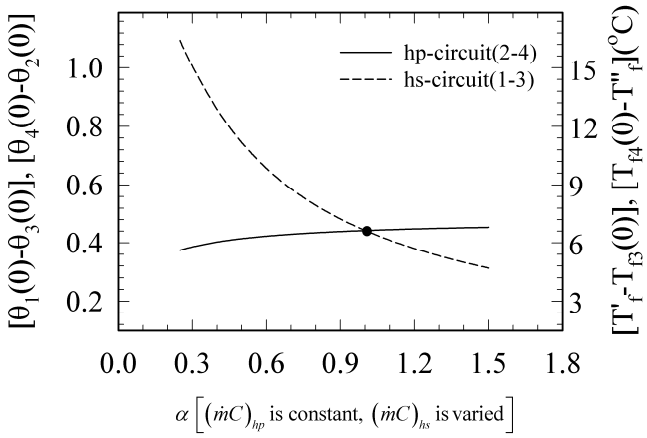

Figure 4-5: Temperature difference between the inlet and outlet of both circuits as a function of α ($\dot{m}_{hp}$ is kept constant).

The black dot represents the case where α=1 with equal thermal capacities in both circuits. For this case, the resulting temperature difference is the same in both circuits and since the mass flow rates and specific heats are equal, the amount of energy extracted from the hp-circuit and rejected by the hs-circuit is the same and there is no heat exchange with the neighboring ground.

Figure 4-6 presents the fluid temperatures (Figure 4-6(a)) as well as local and cumulative heat exchanges (Figure 4-6(b) and (c)) as a function of the non-dimensional depth for ten equally distant pipe segments and four different thermal capacity ratios. As shown in Figure 4-6(a), the fluid temperature evolution for α=0.8, 1, and 1.2 exhibit the same behavior with a quasi linear profile in both the upward and downward legs of both circuits. The exit temperature from the hp-circuit is approximately the same for these three cases (approximately +1.5°C) resulting in cumulative heat exchanges of 11.48, 11.68, and 11.82 kW, respectively (Figure 4-6(c)). The heat exchange is not split equally between the downward and upward legs of the hp-circuit. For example, for α=1, the amount of heat exchanged in the downward and upward legs are 6.40 kW and 5.28 kW, respectively. This is clearly seen in the local heat exchanges (Figure 4-6(b)) where

the local heat exchange in the first segment of the downward leg is 0.70 kW while it is 0.49 kW in the last segment of the upward leg.

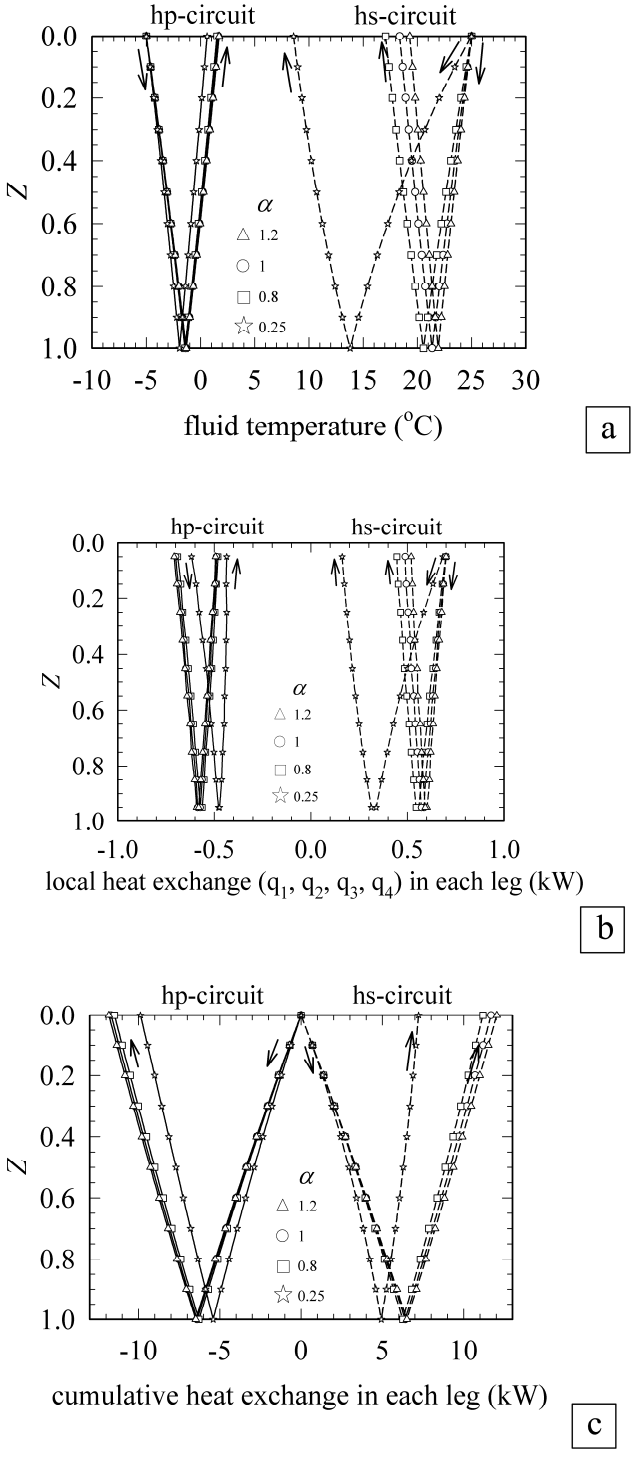

Figure 4-6: Temperature profile and local and cumulative heat exchange along the borehole depth for different flow rate ratios

The hs-circuit for α=0.8, 1, and 1.2 shows a similar behavior except that there are larger differences among these cases simply due to the fact that $(\dot{m}C)_{hs}$ is varied while $(\dot{m}C)_{hp}$ is kept constant.

It is worth noting that the cumulative amounts of heat exchanged in the hs-circuit are 11.18, 11.68, 12.03 kW for α=0.8, 1, and 1.2, respectively. Comparing these values with the ones presented above for the hp-circuit, it can be observed that there is a net amount of heat exchanged between both circuits and the ground. For α=0.8, 0.3 kW is transferred to the borehole from the adjoining ground. For α = 1.2, the heat transfer is in the opposite direction and the borehole transfers 0.21 kW to the ground. For α = 1.0, there is no net heat exchanged between the borehole and the ground.

The differences are more significant, when α=0.25. As shown in Figure 4-6(a), the temperature in the hs-circuit drops from 25°C to 13.80°C in the downward leg and from 13.80°C to 8.59°C in the upward leg. This translates into relatively small local heat exchanges in the upward leg as shown in Figure 4-6(b). Overall, the hs-circuit rejects 7.22 kW in the borehole. This relatively poor performance has repercussions on the hp-circuit which collects 9.88 kW, less than the other three cases. The net heat exchanged with the ground is 2.66 kW.

4.9 Thermal Recharging over a Heating Season

In this section, simulations are carried out over twenty years to examine the impact of thermal recharging of a single-borehole residential system. The hourly heating load of this building is presented in Figure 4-7. It corresponds to a well-insulated building located in Montréal, Canada. As shown in Figure 4-7, the building experiences a peak space heating load of 5.2 kW. The annual space heating requirement is 11945 kWh over the heating season (mid-September to mid-May). During the summer, the building heating load is zero and the cooling load is negligible. Thus, the heat pump does not operate during that period.

This building is heated with a single-capacity GSHP. The heating capacity and compressor power requirements of the GSHP are given in Figure 4-8 as a function of the inlet temperature to the heat pump, i.e. the outlet temperature from the hp-circuit of the borehole. These characteristics are based on a commercially available 3-ton (10.5 kW) water-to-water GSHP with a mass flow rate on the evaporator side, $\dot{m}_{ref}$, equal to 0.44 kg/s.

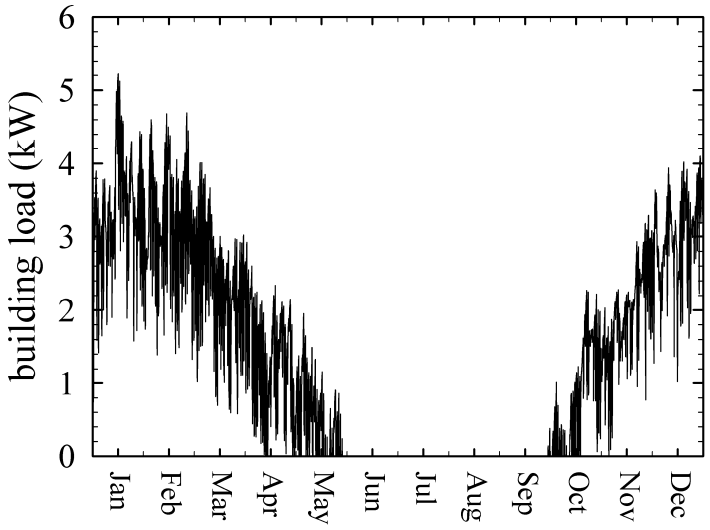

Figure 4-7: Building heating load during the heating season

As shown in Figure 4-8, the operation of this heat pump is not recommended when the inlet temperature is below -6°C. System simulations are performed using a 6 minute time step with the GSHP cycling on and off to meet the building load.

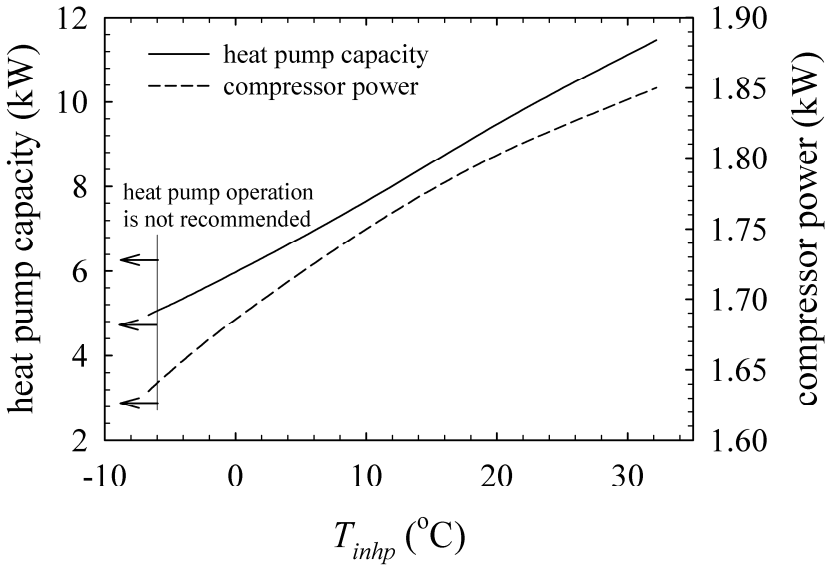

Figure 4-8: Heat pump capacity and corresponding compressor power requirement as a function of the inlet temperature.

Three alternatives to provide space heating for this building are compared; cases 1, 2, and 3 (Figure 4-9). In all three cases, the double U-tube borehole with characteristics presented in Table 4-1 is used.

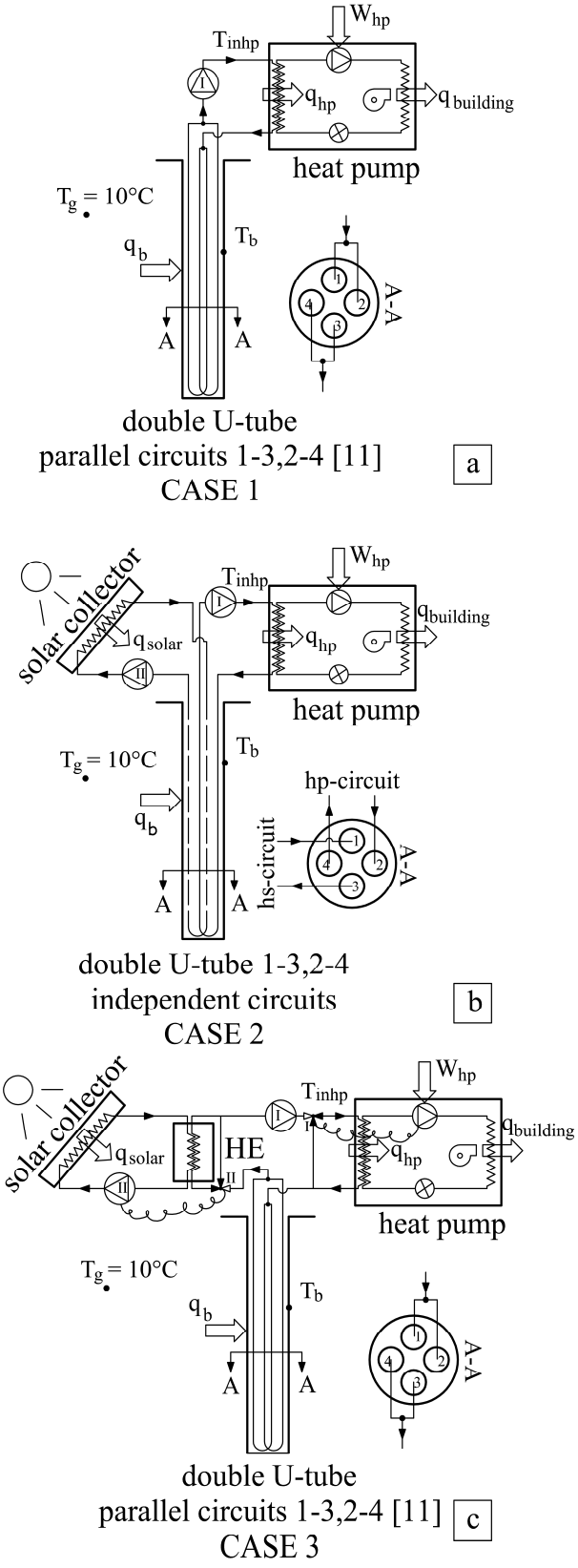

Figure 4-9: Schematic representation of three cases

Case 1 represents a conventional GSHP system with a standard parallel double U-tube borehole. In this case, the mass flow rate of the fluid circulating in each U-tube of the borehole is equal to $\dot{m}_{ref}/2$. The circulating pump (I) is used to circulate the working fluid with the total mass flow rate of *ref m* through the heat pump evaporator and borehole as shown in Figure 4-9(a).

Cases 2 and 3 involve solar recharging during the heating season (mid-September to mid-May). In Case 2 (Figure 4-9(b)) the newly proposed borehole configuration, is used. It consists of a solar collector and a heat pump, connected to the hs-circuit and hp-circuit, respectively. Two separate pumps, I and II, are used to circulate fluids in these two loops. When the heat pump is not working or/and solar energy is unavailable, pump I or/and II are turned off. The mass flow rate circulating in the hp-circuit is equal to $\dot{m}_{ref}$. The solar collector is a standard single-glazed flat plate collector whose efficiency can be described by a second order curve relating the efficiency to $(T_{mean}-T_a)/G$ .The intercept of this curve is 0.78, and first and second order slope coefficients are 3.20 $W \cdot m^{-2} \cdot K^{-1}$ and 0.015 $W \cdot m^{-2} \cdot K^{-2}$, respectively. The collector area is set at 10 m^2 and the mass flow rate circulating in the hs-circuit is equal to 0.11 kg/s resulting in a thermal capacity ratio, α, of 0.25.

Case 3 (Figure 4-9(c)) shows a more conventional solar assisted GSHP system. It consists of solar and heat pump loops which are linked using a heat exchanger. The mass flow rate of the fluid circulating in the solar loop is equal to 0.11 kg/s and the mass flow rate of the fluid circulating in each U-tube of the borehole is equal to $\dot{m}_{ref}/2$. The efficiency of the heat exchanger is assumed equal to 70%. In this case, the borehole is modeled using the analytical model of Zeng (2003) for the parallel 1-3,2-4 configuration.

As shown in Figure 4-9(c), two pumps circulate the fluids through the two loops. When solar energy is not available, pump (II) stops working and a three-way valve (II) directs the fluid to the borehole bypassing the heat exchanger. Pump (I) is turned off when solar energy is unavailable and the heat pump is off. When the heat pump is off and solar energy is available both circulating pumps are working and the three-way valve (I) directs the fluid away from the heat pump loop while valve (II) lets the flow go through the heat exchanger. The solar collector is the same as the one used in case 2.

In all three cases, transient ground heat transfer from the borehole wall to the far-field is evaluated using the multiple load aggregation algorithm (MLAA) developed by Bernier et al. (2004). This ground model is coupled to a borehole model. In Cases 1 and 3, the borehole model provided by Zeng (2003) is used while Case 2 uses the model proposed here. An iterative solution is required at each time step in order to match the heat transfer rate at the borehole wall given by both the borehole and ground models. This results in a variation of the borehole wall temperature at each time step. Finally, for this case, the ground thermal conductivity and diffusivity are 1.5 $W \cdot m^{-1} \cdot K^{-1}$and 0.06 $m^2 \cdot day^{-1}$, respectively and the undisturbed far-field ground temperature is set at 10 °C.

Simulation results, including cumulative heat pump energy consumption (W_{hp}), extracted energy from the ground (q_b), and injected solar energy to the borehole (q_{solar}) for the first and the last year and the average over 20 years, are presented in Table 4-2 for all three cases.

Table 4-2: Simulation results for the first and the last years and the average over 20 years

		equal W_{hp}									**equal H**					
		1st year			20th year			20 y average			1st year		20th year		20 y average	
CASE		1	2	3	1	2	3	1	2	3	2	3	2	3	2	3
H (m)		142	117	95	142	117	95	142	117	95	142		142		142	
q_{build}	MWh	11.94			11.94			11.94			11.94		11.94		11.94	
W_{hp}	MWh	3.27	3.32	3.31	3.34	3.33	3.32	3.32	3.32	3.32	3.21	3.11	3.22	3.12	3.21	3.11
q_b	MWh	8.67	2.84	3.05	8.60	2.83	3.03	8.62	2.85	3.04	2.93	3.22	2.92	3.21	2.93	3.22
q_{solar}	MWh	-	5.78	5.58	-	5.78	5.59	-	5.77	5.58	5.80	5.61	5.80	5.61	5.80	5.61

Table 4-2 has two separate sections referred to as "equal W_{hp}" and "equal H". The results in the left portion, for equal W_{hp}, are obtained by varying the borehole length so that the total heat pump energy consumptions over the 20-year period are equal (within less than 0.5%) for all three cases without allowing T_{inhp} to fall below -4ºC (thus 2ºC above the recommended limit). The resulting borehole lengths are 142, 117, and 95 m for Cases 1, 2, and 3, respectively. The right portion of Table 4-2, for equal H, represents the results obtained by setting an equal length of 142 m in Cases 2 and 3. These two results can be readily compared to the results for Case 1, also for 142 m, presented in the left portion of Table 4-2.

As shown for the reference case (Case 1), the heat pump extracts, on average over 20 years, 8.62 MWh/year from the ground (q_b) and uses 3.32 MWh/year for the compressor (W_{hp}) to provide the required building load of 11.94 MWh/year (q_{build}). Heat extraction from the ground in Case 1

decreases slightly over the years (from 8.67 MWh in the first year to 8.60 MWh in the last year). In turn, heat pump energy consumption increases by approximately 2% from the first year to the 20^{th} year (3.27 MWh to 3.34 MWh) due to the ground temperature decrease after 20 years of heat extraction from the ground.

In Case 2, an average of 5.77 MWh/year of solar energy is injected into the borehole, thereby reducing the energy extracted from the ground by 67% compared to case 1 (8.62 MWh/year in Case 1 to 2.85 MWh/year in Case 2). As explained earlier, a good heat exchange between the two borehole circuits reduces significantly the energy required from the ground for the heat pump operation. When using the configuration of Case 2, the borehole length can be reduced to 117 m (a 17.6% reduction compared to Case 1) while keeping the same average heat pump energy consumption of 3.32 MWh/year over 20 years. This reduction is essentially due to solar energy injected and stored into the ground over the heating season which increases ground temperature in the vicinity of the borehole. Due to the solar heat injection into the borehole, the heat pump energy consumption remains almost constant over 20 years of operation as *Whp* varies from 3.32 MWh to 3.33 MWh over 20 years.

In Case 3, the GSHP system requires a shorter borehole, 95 m (a 33.1% reduction compared to Case1), since the solar heat is transferred directly to the heat pump during heat pump operation. As shown in the left portion of Table 4-2, more heat is extracted from the ground for Case 3 when compared to Case 2 (3.04 MWh/year for Case 3 and 2.85 MWh/year for Case 2) since less solar energy is injected into the ground due to the system configuration (5.58 MWh/year in Case 3 compared to 5.77 MWh/year in Case 2). As was the case for Case 2, the heat pump energy consumption remains almost constant over the 20-year simulation due to solar heat injection.

Even though the average heat pump energy consumption over 20 years is equal for the three cases, Case 1 consumes the least amount of energy during the first year due to the longer borehole and thus higher inlet temperature to the heat pump. However, heat pump energy consumption for Case 1 increases gradually over the years and it surpasses the corresponding value for Cases 2 and 3 after 20 years. This is due to the relatively large amount of heat extraction which induces a ground temperature reduction and a corresponding reduction in the inlet heat pump temperature. In contrast, the heat pump energy consumption remains constant for Cases 2 and 3 because of solar energy injection.

In the right portion of Table 4-2 the results for Cases 2 and 3 with the same length as Case 1 in the left portion, i.e. 142 m, are presented to compare W_{hp}, q_b, and q_{solar} for the three cases. For Case 2, the heat pump receives an average of 5.80 MWh/year and 2.93 MWh/year from the solar and the ground, respectively, and uses 3.21 MWh/year for the compressor to provide the required building load of 11.94 MWh/year. When compared to Case 2, Case 3 receives about 3% less energy from solar, extracts 10% more energy from the ground and consumes 3% less energy for the heat pump. The amount of energy extracted from the ground in Case 1 is, respectively, 194% and 168% higher than in Cases 2 and 3. The heat pump energy consumption improves only marginally over Cases 2 and 3 by 3.5% and 6.5%, respectively.

Consequently, Case 3, with the borehole length of 142 m, has the lowest heat pump energy consumption among all three cases. As will now be shown, this is due to higher inlet fluid temperature to the heat pump.

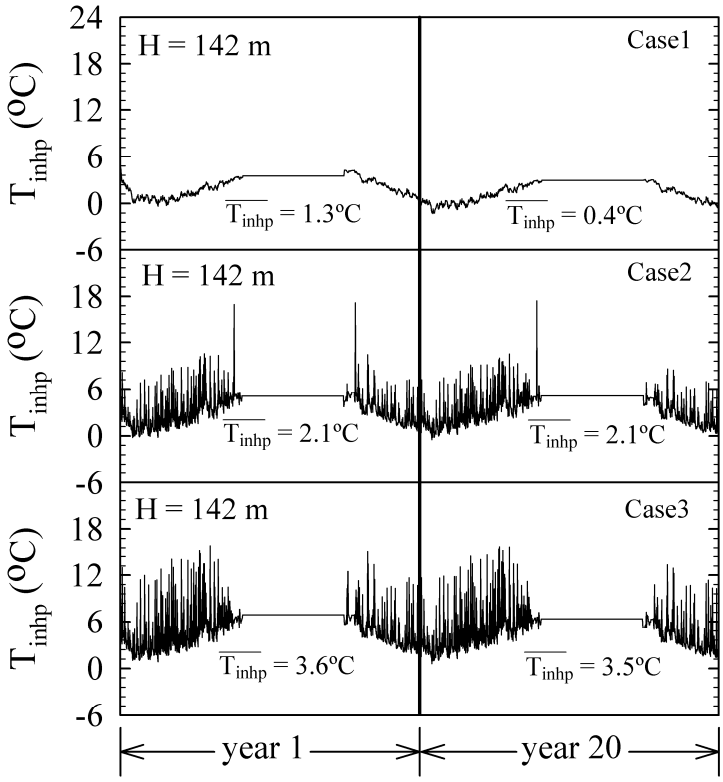

Figure 4-10: Heat pump inlet temperature (i.e. borehole outlet temperature) for all three cases for the first and last year of simulation

The evolution of the fluid temperature into the borehole, T_{inhp}, for the first and the last years of simulation are given in Figure 4-10. As shown in this figure, the average fluid temperature to the heat pump, T_{inhp}, for Case 1 with the borehole length of 142 m is equal to 1.3ºC for the first year and it decreases to 0.4 ºC for the 20th year due to a relatively large amount of heat extraction. With the same borehole length, the average of T_{inhp} for the first year for Cases 2 and 3 is slightly higher than for Case 1, 2.2 ºC and 3.6 ºC, respectively. The average value of T_{inhp} drops only by 0.1ºC over 20 years of operation because of solar heat injection. As shown in Figure 4-10, the peaks for Case 3 are slightly higher as solar heat is transferred directly to the heat pump when it is operating.

Figure 4-11 provides finer details over a 24 hour period (January 17th, 20th year) when solar energy is available for almost 8 hours with a peak of about 6 kW. The top two figures present T_b and T_{inhp} for all three cases. The bottom three figures show the instantaneous net heat transfer from the ground for all three cases, solar energy injection for Cases 2 and 3 and the building load. The top two figures show that solar injection has a significant impact on T_{inhp} and T_b. For example, at the peak of solar injection, T_{inhp} reaches 10.6ºC and 6.0ºC and T_b reaches 7.3 ºC and 7.7 ºC for Cases 3 and 2, respectively while T_{inhp} is -0.9ºC and Tb is 2.1ºC in Case 1. As shown in the second figure from the top, T_{inhp} is higher for Case 3 than for Case 2 when solar heat is available. As mentioned earlier, this is due to the fact that solar heat is transferred directly to the heat pump in Case 3. As shown in the first figure from the top, T_b in Case 2 is slightly higher than in Case 3 due to the fact that more solar energy is injected into the ground. When solar injection stops, at around 16h, T_{inhp} and T_b are higher for Cases 2 and 3 than for Case 1 indicating that previous solar heat injection into the ground, is still present in the vicinity of the borehole and it contributes to the warming of the ground and the observed higher values of T_{inhp} and T_b. It is also worth examining the values of q_b. Positive and negative values of q_b represent, respectively, heat extraction from the ground and heat injection into the ground. As shown in the bottom three figures, the values of q_b are cyclic indicating the on-off nature of the heat pump operation. Usually, a value of $q_b = 0$ indicates that the heat pump is not operating. There are some rare cases, including one presented below, where solar heat injection is exactly equal to the amount of solar injection. The heat pump does not cycle at the same frequency in all three cases even though the building load is the same. Since T_{inhp} is higher for Cases 2 and 3, the heat pump capacity is higher and the operating time of the heat pump is reduced when compared to Case 1.

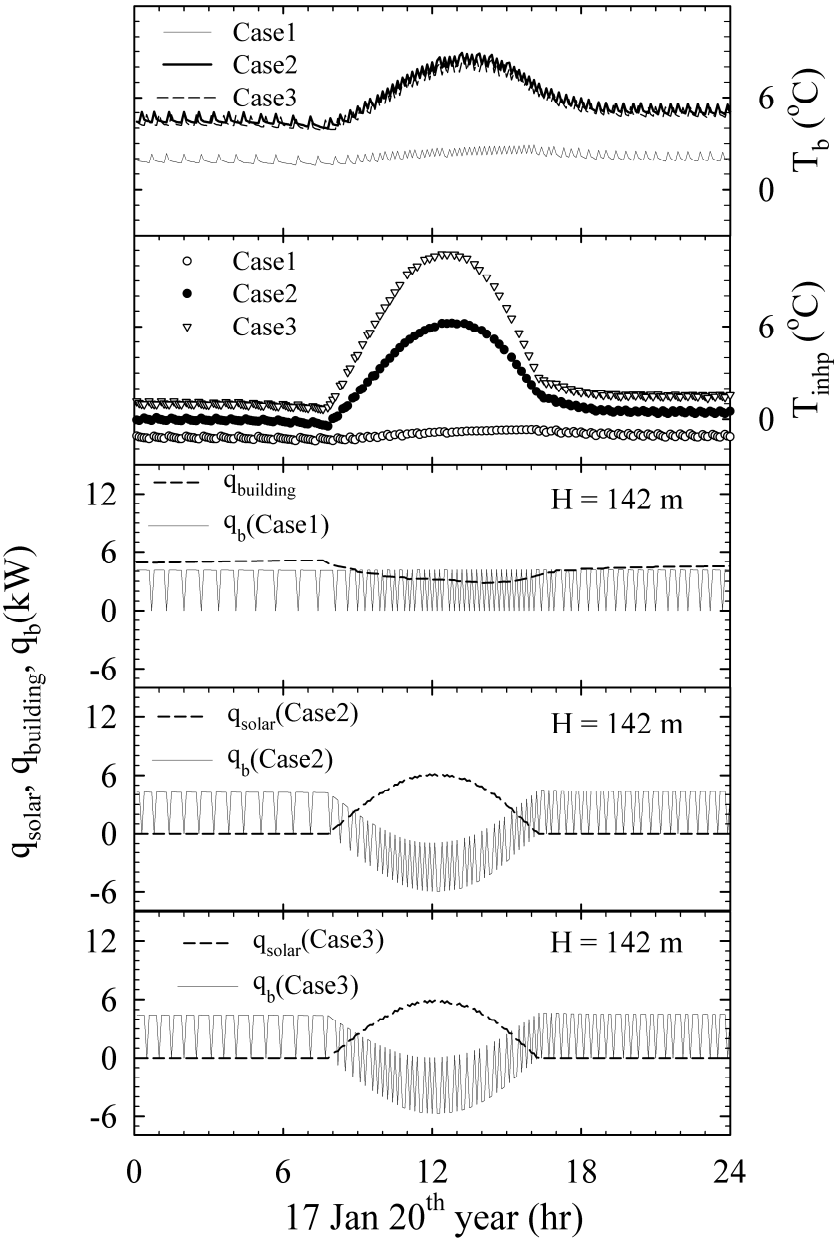

Figure 4-11: Comparison between three cases over 24 hour period in winter

As shown in the bottom two figures, when solar energy is available (from 8 to 16h) and the heat pump is not operating, q_b is negative and equal to q_{solar}. When the heat pump is operating, q_b is simply equal to q_{solar} minus the heat extraction from the heat pump. For example, for Case 3 at 12h, q_{solar} is equal to 6 kW and the heat extraction is also 6 kW (i.e. the heat pump capacity is 7.76 kW and the compressor power is 1.76 kW for a T_{inhp} of 10.5°C) resulting in a value of q_b=0.

Finally, it is interesting to evaluate the changes on H, q_b, W_{hp}, and q_{solar} when the ground thermal conductivity is doubled from 1.5 to 3 $W \cdot m^{-1} \cdot K^{-1}$ (with other parameters remaining the same). The results of this analysis are presented in Table 4-3 for a 20 year averaging period. Also included in this table are results obtained earlier for k=1.5 $W \cdot m^{-1} \cdot K^{-1}$.

Table 4-3: Simulation results for ground thermal conductivity of 1.5 and 3.0 $W \cdot m^{-1} \cdot K^{-1}$

		k=1.5 $W \cdot m^{-1} \cdot K^{-1}$			k= 3.0 $W \cdot m^{-1} \cdot K^{-1}$		
CASE		1	2	3	1	2	3
H (m)		142			103		
q_{build}	MWh	11.94			11.94		
W_{hp}	MWh	3.32	3.21	3.11	3.32	3.29	3.16
q_b	MWh	8.62	2.93	3.22	8.62	2.94	3.24
q_{solar}	MWh	-	5.80	5.61	-	5.71	5.54

As shown in Table 4-3, the borehole length can be reduced from 142 m to 103 m (27% reduction) with the same heat pump consumption for Case 1 when k increases from 1.5 to 3 $W \cdot m^{-1} \cdot K^{-1}$. High ground thermal conductivities reduce the required borehole length; however they have somewhat of a detrimental effect on solar heat injection. For example, the results for Case 2 in Table 4-3, indicates that the heat pump energy consumption is 3.29 MWh/year on average. This represents a modest decrease (1%) from 3.32 MWh/year when compared to Case 1. The corresponding decrease for k = 1.5 $W \cdot m^{-1} \cdot K^{-1}$ is 3.5% (from 3.32 to 3.21 MWh/year). This indicates that despite the fact that solar energy is injected over a shorter length, good heat diffusion distributes solar heat injection away from the borehole so that it does not contribute to an increase in the ground temperature in the vicinity of the borehole.

4.10 Conclusion

This study presents an analytical model to predict steady-state heat transfer in double U-tube boreholes with two independent circuits operating with unequal mass flow rates and inlet temperatures. The model predicts the fluid temperature profiles in both circuits along the borehole depth. It accounts for fluid and pipe thermal resistance and thermal interaction among U-tube circuits.

The proposed model is used for two applications which could not be previously examined. Both applications can be represented schematically by Figure 4-1 where one circuit is linked to a heat pump operating in heating mode and the other to a heat source. The first application evaluates the

effect of unequal mass flow rates on heat transfer between each circuit for constant inlet temperatures in both circuits. Results show that the flow rate variation of one circuit has a small effect on heat transfer and temperature profile of the other circuit due to the thermal interaction among pipes in the borehole.

In the second application, simulations over 20 years are performed to examine the impact of thermal recharging of a single-borehole residential system. A conventional solar assisted heat pump system (Case 3) and the novel system proposed in this study (Case 2) are compared against a reference case (ground source heat pump system without thermal recharging, Case 1). The results indicate that despite a relatively large amount of solar energy injected into the system in Cases 2 and 3, the annual heat pump energy consumption is not reduced significantly. For example, for an average ground thermal conductivity of 1.5 $W \cdot m^{-1} \cdot K^{-1}$ and identical borehole length in all three cases, Cases 2 and 3 consume, respectively, 3.5% and 6.5% less energy than Case 1. When the heat pump energy consumption is the same in all three cases, Borehole length reductions of 17.6% and 33.1% for Cases 2 and 3 is reported. Based on these results, it can be concluded that solar recharging alternatives do not improve the annual heat pump energy consumption of single boreholes. However they might contribute to reduce installation costs as they lead to shorter boreholes.

4.11 Nomenclature

a, b, c, d	dimensionless parameters, defined in Eq. (4.7)
C	fluid specific heat ($J \cdot kg^{-1} \cdot K^{-1}$)
D	half of the shank spacing between U-tube (m)
h_i	fluid convective heat transfer coefficient, inside surface of the pipes ($W \cdot m^{-2} \cdot K^{-1}$)
H	active borehole depth (m)
k	ground thermal conductivity ($W \cdot m^{-1} \cdot K^{-1}$)
k_b	grout thermal conductivity ($W \cdot m^{-1} \cdot K^{-1}$)
$\dot{m}$	mass flow rate of the circulating fluid ($kg \cdot s^{-1}$)
p	Laplace transform operator
q	heat flow per unit length of pipe ($W \cdot m^{-1}$)
r_b	borehole radius (m)
r_p	pipe outer radius (m)

R	thermal resistance, defined in Eq. (4.1) ($m \cdot K \cdot W^{-1}$)
R^{Δ}	thermal resistance, defined in Eq. (4.5) ($m \cdot K \cdot W^{-1}$)
R^{*}	dimensionless thermal resistance
R_{pipe}	combined thermal resistance of the fluid and pipe wall ($m \cdot K \cdot W^{-1}$)
$G_{ij}, G'_{ij}, G''_{ij}$	dimensionless parameters, defined in Eq. (4.A.1)
T_b	borehole wall temperature (^{o}C)
T_f	fluid temperature (^{o}C)
T_m	solar collector mean fluid temperature (^{o}C)
T_a	ambient temperature (^{o}C)
G	solar radiation ($W \cdot m^{-2}$)
T'_f, T''_f	inlet fluid temperatures (^{o}C)
z	axial coordinate along the borehole depth (m)
Z	dimensionless z coordinate

Greek symbols

α	ratio of thermal capacities (defined in Eq. (4.9))
γ, η	dimensionless parameters in Eq. (4.A.1)
θ	dimensionless fluid temperature
$\bar{\theta}$	Laplace transform of θ

Subscripts

1,2,3,4	pipe sequence in the borehole
1-3	1-3 circuit in 1-3,2-4 configuration
2-4	2-4 circuit in 1-3,2-4 configuration
inhp	heat pump inlet
ouths	heat source outlet

4.12 Appendix

The dimensionless fluid temperature profiles as a function of borehole depth are derived in this appendix for the configuration 1-3,2-4 with different thermal capacitances.

Configuration 1-3,2-4

$$\theta_{i=1,2,3,4}(Z) = G_{i1} + \left[\frac{G_{i2} + G'_{i2}\theta_3(0) + G''_{i2}\theta_4(0)}{\gamma^2 - \eta^2}\right]\cosh(\gamma Z) + \left[\frac{G_{i3} + G'_{i3}\theta_3(0) + G''_{i3}\theta_4(0)}{(\gamma^2 - \eta^2)\gamma}\right]\sinh(\gamma Z)$$
$$+ \left[\frac{G_{i4} + G'_{i4}\theta_3(0) + G''_{i4}\theta_4(0)}{\gamma^2 - \eta^2}\right]\cosh(\eta Z) + \left[\frac{G_{i5} + G'_{i5}\theta_3(0) + G''_{i5}\theta_4(0)}{(\gamma^2 - \eta^2)\eta}\right]\sinh(\eta Z)$$

$G_{i1}\big|_{i=1,2,3,4} = \theta_b$

$G_{12} = \gamma^2 + \eta^2\theta_b + d(a-c) - \alpha^2(a^2-c^2) - b(a-c)(\alpha+1), G'_{12} = 0, G''_{12} = b(a-c)(1-\alpha)$

$G_{13} = \alpha^2(a-c)\left[-2bd + d(a+c) - 2b^2 + a(a+c)\right] + \alpha b(a-c)^2 + \gamma^2\left[b - a - d\right]$

$G'_{13} = \alpha^2 c(a^2-c^2) - 2\alpha^2 b^2(a-c) - c\gamma^2, G''_{13} = \alpha b(a-c)^2 - b\gamma^2$

$G_{14} = -\left[\eta^2 + \gamma^2\theta_b + d(a-c) - \alpha^2(a^2-c^2) - b(a-c)(\alpha+1)\right], G'_{14} = 0, G''_{14} = -G''_{12}$

$G_{15} = -\left\{\alpha^2(a-c)\left[-2bd + d(a+c) - 2b^2 + a(a+c)\right] + \alpha b(a-c)^2 + \eta^2\left[b - a - d\right]\right\}$

$G'_{15} = -\left[\alpha^2 c(a^2-c^2) - 2\alpha^2 b^2(a-c) - c\eta^2\right], G''_{15} = -\left[\alpha b(a-c)^2 - b\eta^2\right]$

$G_{22} = -\gamma^2 + \eta^2\theta_b + d\alpha^2(a-c) + a^2 - c^2 + b\alpha(a-c)(\alpha+1), G'_{22} = -\alpha G''_{12}, G''_{22} = 0$

$G_{23} = \alpha(a-c)\left[-2bd + d(a+c) + 2b^2 - a(a+c)\right] - \alpha^2 b(a-c)^2 + \gamma^2\alpha\left[-b + a - d\right]$

$G'_{23} = \alpha G''_{13}, G''_{23} = \alpha c(a^2-c^2) - 2\alpha b^2(a-c) - c\alpha\gamma^2$

$G_{24} = -\left[-\eta^2 + \gamma^2\theta_b + d\alpha^2(a-c) + a^2 - c^2 + b\alpha(a-c)(\alpha+1)\right], G'_{24} = \alpha G''_{12}, G''_{22} = 0$

$G_{25} = -\left\{\alpha(a-c)\left[-2bd + d(a+c) + 2b^2 - a(a+c)\right] - \alpha^2 b(a-c)^2 + \eta^2\alpha\left[-b + a - d\right]\right\}$

$G'_{25} = \alpha G''_{15}, G''_{25} = -\left[\alpha c(a^2-c^2) - 2\alpha b^2(a-c) - c\alpha\eta^2\right]$

$G_{32} = \eta^2\theta_b + d(a-c) + b(a-c)(\alpha-1), G'_{32} = \gamma^2 - \alpha^2(a^2-c^2), G''_{32} = b(a-c)(1+\alpha)$

$G_{33} = \alpha^2(a-c)\left[2bd - d(a+c) + 2b^2 - c(a+c)\right] + \alpha b(a-c)^2 + \gamma^2\left[-b + c + d\right]$

$G'_{33} = -\alpha^2 a(a^2-c^2) + 2\alpha^2 b^2(a-c) + a\gamma^2, G''_{33} = \alpha b(a-c)^2 + b\gamma^2$

$G_{34} = -\left[\gamma^2\theta_b + d(a-c) + b(a-c)(\alpha-1)\right], G'_{42} = \eta^2 - \alpha^2(a^2-c^2), G''_{42} = b(a-c)(1+\alpha)$

$G_{35} = -\left\{\alpha^2(a-c)\left[2bd - d(a+c) + 2b^2 - c(a+c)\right] + \alpha b(a-c)^2 + \eta^2\left[-b + c + d\right]\right\}$

$G'_{35} = -\left[-\alpha^2 a(a^2-c^2) + 2\alpha^2 b^2(a-c) + a\eta^2\right] G''_{35} = -\left[\alpha b(a-c)^2 + b\eta^2\right]$

$G_{42} = \eta^2\theta_b + d\alpha^2(a-c) + b\alpha(a-c)(\alpha-1), G'_{42} = \alpha G''_{32}, G''_{42} = \gamma^2 - a^2 + c^2$

$$G_{43} = \alpha(a-c)\left[2bd - d(a+c) - 2b^2 + c(a+c)\right] - \alpha^2 b(a-c)^2 + \gamma^2\alpha\left[b-c+d\right]$$
$$G'_{43} = \alpha G''_{33}, G''_{43} = -\alpha a(a^2-c^2) + 2\alpha b^2(a-c) + \alpha a\gamma^2$$
$$G_{44} = -\left[\gamma^2\theta_b + d\alpha^2(a-c) + b\alpha(a-c)(\alpha-1)\right], G'_{44} = -\alpha G''_{32}, G''_{44} = -\eta^2 + a^2 - c^2$$
$$G_{45} = -\left\{\alpha(a-c)\left[2bd - d(a+c) - 2b^2 + c(a+c)\right] - \alpha^2 b(a-c)^2 + \eta^2\alpha\left[b-c+d\right]\right\}$$
$$G'_{45} = \alpha G''_{35}, G''_{45} = -\left[-\alpha a(a^2-c^2) + 2\alpha b^2(a-c) + \alpha a\eta^2\right] \qquad (4.A.1)$$

Where

$$\gamma^2 = \left\{(a^2-c^2)(1+\alpha^2) + \sqrt{(a^2-c^2)^2(\alpha^2-1)^2 + 16b^2\alpha^2(a-c)^2}\right\}\Big/2$$
$$\eta^2 = \left\{(a^2-c^2)(1+\alpha^2) - \sqrt{(a^2-c^2)^2(\alpha^2-1)^2 + 16b^2\alpha^2(a-c)^2}\right\}\Big/2$$

$$a = \frac{1}{R_1^*} + \frac{2}{R_{12}^*} + \frac{1}{R_{13}^*}, b = -\frac{1}{R_{12}^*}, c = -\frac{1}{R_{13}^*}, d = -\frac{\theta_b}{R_1^*}$$

$$\alpha = \left(\dot{m}C\right)_{1-3}\Big/\left(\dot{m}C\right)_{2-4}$$

$$\begin{bmatrix}\theta_3(0)\\ \theta_4(0)\end{bmatrix} = \begin{bmatrix}A_{11} & A_{12}\\ A_{21} & A_{22}\end{bmatrix}^{-1}\begin{bmatrix}C_1\\ C_2\end{bmatrix}$$

$$\theta_3(0) = \frac{A_{22}C_1}{A_{11}A_{22} - A_{12}A_{21}} - \frac{A_{12}C_2}{A_{11}A_{22} - A_{12}A_{21}}$$
$$\theta_4(0) = -\frac{A_{21}C_1}{A_{11}A_{22} - A_{12}A_{21}} - \frac{A_{11}C_2}{A_{11}A_{22} - A_{12}A_{21}}$$

$$A_{11} = (G'_{12} - G'_{32})\cosh(\gamma) + (G'_{13} - G'_{33})\sinh(\gamma) + (G'_{14} - G'_{34})\cosh(\eta) + (G'_{15} - G'_{35})\sinh(\eta);$$
$$A_{12} = (G''_{12} - G''_{32})\cosh(\gamma) + (G''_{13} - G''_{33})\sinh(\gamma) + (G''_{14} - G''_{34})\cosh(\eta) + (G''_{15} - G''_{35})\sinh(\eta);$$
$$A_{21} = (G'_{22} - G'_{42})\cosh(\gamma) + (G'_{23} - G'_{43})\sinh(\gamma) + (G'_{24} - G'_{44})\cosh(\eta) + (G'_{25} - G'_{45})\sinh(\eta);$$
$$A_{22} = (G''_{22} - G''_{42})\cosh(\gamma) + (G''_{23} - G''_{43})\sinh(\gamma) + (G''_{24} - G''_{44})\cosh(\eta) + (G''_{25} - G''_{45})\sinh(\eta);$$
$$C_1 = G_{31} - G_{11} + (G_{32} - G_{12})\cosh(\gamma) + (G_{33} - G_{13})\sinh(\gamma) + (G_{34} - G_{14})\cosh(\eta) + (G_{35} - G_{15})\sinh(\eta);$$
$$C_2 = G_{41} - G_{21} + (G_{42} - G_{22})\cosh(\gamma) + (G_{43} - G_{23})\sinh(\gamma) + (G_{44} - G_{24})\cosh(\eta) + (G_{45} - G_{25})\sinh(\eta);$$

4.13 References

Al-Khoury, R., and Bonnier, P. G. (2006). Efficient finite element formulation for geothermal heating systems. Part II: Transient. *International Journal of Numerical Methods in Engineering*, 67 (5), 725-745.

Bernier, M. (2000). A Review of the Cylindrical Heat Source Method for the Design and Analysis of Vertical Ground-Coupled Heat Pump Systems. 4th International Conference of Heat Pumps in Cold Climates, 14 pages.

Bernier, M., Labib, R., Pinel, P., and Paillot, R. (2004). A multiple load aggregation algorithm for annual hourly simulations of GCHP systems. *HVAC&R Research*, 10 (4), 471-487.

Bernier, M., and Salim Shirazi, A. (2007). Solar heat injection into boreholes: a preliminary analysis. Proceeding of 2nd Canadian Solar Building Conference, T1-1-1, 8 pages.

Carslaw, H. S., and Jaeger, J. C. (1947). *Conduction of heat in solids* (1st ed). Oxford, U.K.: Claremore Press.

Chapuis, S., and Bernier, M. (2008). Étude préliminaire sur le stockage solaire saisonnier par puits géothermique. Proceeding of 3rd Canadian Solar Building Conference, 14-23.

Chapuis, S., and Bernier, M. (2009). Seasonal storage of solar energy in borehole heat exchangers. Proceeding of 11th International IBPSA Conference, 599-606.

Chiasson, A. D., and Yavuzturk, C. (2003). Assessment of the viability of hybrid geothermal heat pump systems with solar thermal collectors. *ASHRAE Transactions*, 109 (2), 487-500.

Diao, N. R., Zeng, H. Y., and Fang, Z. H. (2004). Improvement in modeling of heat transfer in vertical ground heat exchangers. *HVAC&R Research*, 10 (4), 459-470.

Eslami nejad, P., Langlois, A., Chapuis, S., Bernier, M., and Faraj, W. (2009). Solar heat injection into boreholes. Proceeding of 4th Canadian Solar Building Conference, 237-246.

Georgiev, A., Busso, A., and Roth, P. (2006). Shallow borehole heat exchanger: Response test and charging-discharging test with solar collectors. *Renewable Energy*, 31 (7), 971-985.

Han, Z., Zheng, M., Kong, F., Wang, F., Li, Z., and Bai, T. (2008). Numerical simulation of solar assisted ground-source heat pump heating system with latent heat energy storage in severely cold area. *Applied Thermal Engineering*, 28 (11-12), 1427-1436.

He, M., Rees, S., and Shao, L. (2009). Simulation of a domestic ground source heat pump system using a transient numerical borehole heat exchanger model. Proceeding of 11th International IBPSA Conference, 607-614.

Hellström, G. (1989). Duct ground heat storage model. Manual for Computer Code, Department of Mathematical Physics, University of Lund, Sweden.

Hellström, G. (1991). Ground heat storage, thermal analysis of duct storage system. Doctorial Thesis, University of Lund, Sweden.

Kjellsson, E., Hellström, G., and Perers, B. (2010). Optimization of systems with the combination of ground-source heat pump and solar collectors in dwellings. *Energy*, 35 (6), 2667-2673.

Kummert, M., and Bernier, M. (2008). Analysis of a combined photovoltaic-geothermal gas-fired absorption heat pump system in a Canadian climate. *Journal of Building Performance Simulation*, 1 (4), 245-256.

Lamarche, L., and Beauchamp, B. (2007). New solutions for the short-time analysis of geothermal vertical boreholes. *International Journal of Heat and Mass Transfer*, 50(7-8), 1408-1419.

Lamarche, L., Kajl, S., and Beauchamp, B. (2010). A review of methods to evaluate borehole thermal resistances in geothermal heat-pump systems. *Journal of Geothermics*, 39 (1), 187-200.

Man, Y., Yang, H., Diao, N., Liu, J., and Fang, Z. (2010). A new model and analytical solutions for borehole and pile ground heat exchangers. *International Journal of Heat and Mass Transfer*, 53 (13-14), 2593-2601.

Marcotte, D., and Pasquier, P. (2008). On the estimation of thermal resistance in borehole thermal conductivity test. *Renewable Energy*, 33 (11), 2407-2415.

Penrod, E. B., and Prasanna, D. V. (1962). Design of flat-plate collector for solar earth heat pump. *Solar Energy*, 6 (1), 9-22.

Penrod, E. B., and Prasanna, D. V. (1969). Procedure for designing solar-earth heat pumps. *Heating, Piping and Air Conditioning*, 41 (6), 97-100.

Philippacopoulos, A. J., and Berndt, M. L. (2001). Influence of debonding in ground heat exchangers used with geothermal heat pumps. *Journal of Geothermics*, 30 (5), 527-545.

Remund, C. P. (1999). Borehole thermal resistance: laboratory and field studies. ASHRAE Transaction, 105 (1), 439-445.

Sibbitt, B., Onno, T., McClenahan, D., Thornton, J., Brunger, A., Kokko, J., and Wong, B. (2007). The Drake Landing Solar Community Project – Early Results. Proceeding of 2nd Canadian Solar Building Conference, M2-1-3, 11 pages.

Stojanovic, B., and Akander, J. (2010). Build-up and long-term performance test of a full-scale solar-assisted heat pump system for residential heating in Nordic climatic conditions. *Applied Thermal Engineering*, 30 (2-3), 188-195.

Trillat-Berdal, V., Souyri, B., and Achard, G. (2007). Coupling of geothermal heat pumps with thermal solar collectors. *Applied Thermal Engineering*, 27 (10), 1750-1755.

Wang, X., Zheng, M., Zhang, W., Zhang, S., and Yang, T. (2010). Experimental study of a solar-assisted ground-coupled heat pump system with solar seasonal thermal storage in severe cold areas. *Energy and Building*, 42 (11), 2104-2110.

Wetter, M., and Huber, A. (1997). TRNSYS Type 451: Vertical Borehole Heat Exchanger (3.1 ed).

Yang, H., Cui, P., and Fang, Z. (2010). Vertical- borehole ground-coupled heat pumps: A review of models and systems. *Applied Energy*, 87 (1), 16-27.

Yang, W., Shi, M. H., and Dong, H. (2006). Numerical simulation of the performance of a solar-earth source heat pump system. *Applied Thermal Engineering*, 26 (17-18), 2367-2376.

Yang, W., Shi, M., Liu, G., and Chen, Z. (2009). A two-region simulation model of vertical U-tube ground heat exchanger and its experimental verification. *Applied Energy*, 86 (10), 2005-2012.

Young, T. R. (2004). Development, verification, and design analysis of the borehole fluid thermal mass model for approximating short-term borehole thermal response. Master of Science Thesis, Oklahoma State University, United States.

Zeng, H., Diao, N., and Fang, Z. (2003). Heat transfer analysis of boreholes in vertical ground heat exchangers. *International Journal of Heat and Mass Transfer*, 46 (23), 4467-4481.

CHAPITRE 5 SCIENTIFIC ARTICLE 3: FREEZING OF GEOTHERMAL BOREHOLE SURROUNDINGS: A NUMERICAL AND EXPERIMENTAL ASSESSMENT WITH APPLICATIONS

Abstract

This study examines the thermal consequences of freezing the ground in the immediate vicinity of geothermal boreholes. First, a one-dimensional radial numerical heat transfer model is developed to evaluate heat transfer from the borehole wall to the ground. The model can account for multiple ground layers and phase change is handled using the effective capacity method. The results of the model are in excellent agreement with the results given by analytical solutions for simple cases. A small-scale experimental set-up has also been built to validate the numerical model. The apparatus mimics the behaviour of a geothermal borehole and uses a homogeneous saturated laboratory-grade sand to reproduce unsaturated and saturated conditions. Based on temperature measurements, it is shown that the results of the numerical model are in good agreement with the experimental results.

In the application section of the paper, the numerical ground model is combined with a borehole model to examine various scenarios involving typical heat pump operation. Results show that the borehole wall temperature remains around 0ºC for several days when the ground freezes while it would drop to much lower values in non-freezing conditions. Freezing is restricted to a few centimetres around the borehole. If solar energy is available, and a 4-pipe borehole with two independent circuits is used, then it is possible to melt the ice and recharge the ground for the next freezing cycle. Using this approach, borehole depth can be reduced by as much as 38% in some cases.

5.1 Introduction

Ground coupled heat pump (GCHP) systems with vertical ground heat exchangers (GHX) have become very attractive for air conditioning and domestic hot water production due to their high efficiency. However, the relatively high initial cost of the ground loop portion handicaps the widespread application of this technology. In most single borehole cases (typically for residential buildings), the length of the GHX is driven by peak ground load conditions. For these conditions,

the return fluid temperature to the heat pump is usually near the minimum value tolerated by the heat pump. To mitigate the peak heat removal from the ground, it has been suggested to recharge the ground using solar energy. However, in single borehole installations, it has been shown that solar heat injection does not reduce the borehole length significantly since solar energy injection is not necessarily coincident with the peak building load (Eslami nejad and Bernier, b2011).

An alternative solar heat injection method is proposed here and is presented schematically in Figure 5-1. It consists of a double U-tube borehole with two independent circuits surrounded by a saturated (with water) sand ring. One circuit is linked to a heat pump and the other is connected to thermal solar collectors. During peak building loads, usually at night when solar energy is unavailable, the heat pump extracts energy from the ground and in some cases the saturated sand freezes. This slows down the decrease in the return temperature to the heat pump and takes advantage of the relatively high energy content associated with the latent heat of fusion of water in the sand. When solar energy is available, solar heat is injected in the second U-tube to melt the frozen saturated ring. The objective of the present study is to examine the impact of this approach on borehole length reduction and heat pump energy consumption for single borehole installations.

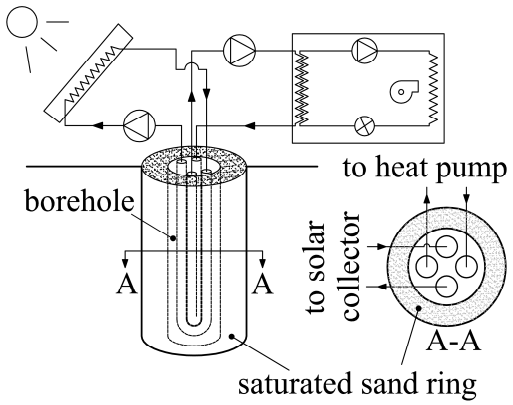

Figure 5-1: System configuration for the proposed system

This paper is subdivided in two main parts. First, a 1-D radial numerical heat transfer model is developed to account for freezing and thawing of the saturated ring region. This model is compared to simple analytical solutions and validated using a laboratory-scale experiment. The ground numerical model is then coupled to an elaborate borehole model which accounts for the double U-tube with two independent circuit configuration. In the second part of the paper, the resulting coupled model is used to examine the merits of the proposed configuration.

5.2 Literature review

One way to balance the ground load and reduce the borehole length is to combine a supplementary source of energy such as solar energy with conventional GCHP systems. They are usually known as solar assisted GCHP systems or hybrid GCHP systems. This idea was first introduced by Penrod and Prasanna (1962, 1969) who proposed a system that uses, alternatively, the ground and solar collectors as the heat source of the heat pump. Kjellsson et al. (2010) analyzed five alternatives to supply solar energy to GCHP systems and compared them against a base case without solar collectors. They concluded that the option with the highest electrical consumption savings is a hybrid system with solar heat injection into the borehole in winter and solar domestic hot water production during the summer. Solar heat is first directed to the heat pump and then to the borehole. Hongxing Yang et al. (2010) and Xi et al. (2011) recently indicated that using a supplementary heat source such as thermal solar collectors to charge the heat pump evaporator is a feasible way to make GCHP systems attractive for space heating and domestic hot water (DHW) production in cold climates. Yang et al. (2006) found the optimum operating time of GCHP and solar source heat pump (SSHP) systems. They recommended operating the SSHP system for 10-14 hours per day to achieve a 30-60% recovery-rate for the ground temperature in the vicinity of the borehole. Han et al. (2008) investigated different operation modes of a solar assisted GCHP system in the presence of a latent heat energy storage tank in a heating dominated climate; a 12.3% increase in system performance is reported. Wang et al. (2009) simulated a solar assisted GCHP system linked to a storage tank for residential buildings. The results indicated that the performance of the system depends strongly on the solar collector area and tank volume. Chiasson and Yavuzturk (2003) performed a 20-year life-cycle cost analysis to evaluate the economics of GCHP systems coupled to solar thermal collectors. They indicated that solar heat injection into multiple boreholes can reduce the borehole length.

Some researchers also conducted laboratory or real scale tests to evaluate system performance of solar assisted ground source heat pump. For example, Ozgener and Hepbasli (2005) performed an experimental study to investigate the performance of a solar assisted GCHP system for greenhouse heating, based on the exergy analysis method. They used solar energy to supply the heat pump prior to charging the ground. The authors reported the exergy efficiency values of each of the system components and the potential for improvements. Trillat-Berdal et al. (2007) performed an experimentally validated simulation to investigate a solar assisted GCHP used year

round for air conditioning and DHW production. Bakirci et al. (2011) and Stojanovic and Akander (2010) recently conducted a long-term experimental investigation of a solar assisted GCHP system for a cold climate condition to find the seasonal performance. Wang et al. (2010) performed an experimental study of a solar assisted GCHP with solar energy storage in the ground during the summer in severe cold climates. The authors indicated that the energy extracted from the ground represents 75.5% of the heat stored in the summer.

Double U-tube boreholes with two independent circuits have been proposed by Eslami nejad and Bernier (a2011, b2011). In this configuration, one circuit is simply connected to solar collectors and the other is linked to heat pump(s). However, the authors indicated that ground recharging of single residential boreholes does not reduce the borehole length significantly since solar energy is not necessarily coincident with the peak building load.

Artificial ground freezing, which is commonly used for construction and mining purposes, has been reported in several studies. They mainly evaluated frost expansion, soil temperature distribution and required refrigeration capacity. For example, in an early study, Hashemi and Sliepcevich (1973) developed a 2-D numerical model to evaluate the effect of ground water flow on artificial soil freezing. The authors indicated that small ground water flows perpendicular to the pipe axis have no significant effect on the ice interface growth. Giudice et al. (1978) developed a finite-element ground freezing model to study freezing under roads in cold weather. Newman and Wilson (1997) developed an experimentally validated 1-D model to calculate the temperature evolution as well as unfrozen water content in unsaturated soils. Frivik and Comini (1982) developed an experimentally validated 2-D finite element model of ground freezing in the presence of ground water flows. Small convection contribution to total energy transfer was reported due to a very low permeability. Mikkola and Hartikainen (2001) studied the heat and mass transfer in freezing of saturated soils including frost expansion. Sres et al. (2006) and Sres and Anagnostou (2007) developed a 3-D thermo-hydraulic numerical model based on a finite element scheme for the case of ground deformation and ground water flow. Lu and Wang (2008) developed a 2-D flow and heat transfer model for buried crude oil pipelines in saturated soils.

Relatively few studies have developed models to account for ground freezing in geothermal energy system. However, ground freezing effects on system performance were not addressed. For example, Mei and Emerson (1985) developed a numerical 1-D flow and heat transfer model for

buried horizontal single coil connected to a heat pump. The model accounted for heat pump cyclic operation and ground freezing around the coil. Results indicated that when the fluid inlet temperature is much lower than the ground freezing point, the total energy extracted from the ground comes mainly from the latent heat of fusion of the water in the ground. Fukusako and Seki (1987) investigated the heat transfer characteristics of a combined system made of a concentric-tube thermosyphon and a heat pump. They accounted for ground freezing in the vicinity of the tube. Fan et al. (2007) investigated the impact of coupled heat conduction and groundwater advection on the heat transfer between a vertical borehole and its surrounding soil. The phase change of the ground water content was accounted for using the solid-phase increment method. Nordell and Alström (2006) reported that, in certain unusual cases, water-filled borehole freezing causes a high pressure that deforms the pipes in the borehole thus perturbing the working fluid circulation. They also suggested some solutions such as replacing the water with a grout. Marcotte et al. (2010) examined the effects of axial heat conduction by comparing the results obtained using the finite and infinite line source methods. In one of their test cases they evaluated the effect of axial heat conduction on the energy required to freeze the ground for environmental purposes. Weibo Yang et al. (2010) recently investigated the effect of different alternate operating modes of a solar GCHP system on soil temperature recovery in the vicinity of geothermal boreholes. A 2-D numerical model with phase change capabilities was developed. Solar injection when the heat pump is not operating was recommended in order to achieve faster ground temperature recovery. The effect of ground freezing on system design and performance was, however, not evaluated.

5.3 Model development

5.3.1 Ground model

Heat transfer to and from the ground in the vicinity of geothermal boreholes is rather complex. Several thermo-physical processes are involved such as multidimensional heat and moisture transfer, ground water movement, possible freezing and thawing, and frost expansion. In order to facilitate the analysis, particularly in geothermal engineering applications, different assumptions have been considered. For example, Ingersoll (1954) reduced the problem to a 1-D pure conduction case and provided an analytical solution. Others have developed multidimensional

heat conduction models with (Diao et al., 2004; Raymond et al., 2011) or without (Eskilson, 1987; Hellström, 1991; Lee, 2011) the effects of ground water movement in geothermal applications. Relatively few studies have been performed to model heat transfer in the ground under freezing and thawing conditions for geothermal applications (Fukusako et al., 1987; Fan et al., 2007; Weibo Yang et al., 2010). Finally, various models have also been developed for porous materials to handle solidification and melting under pure conduction or combined conduction and natural convection conditions (Weaver and Viskanta, 1985; Wang et al., 1990; Rattanadecho and Wongwises, 2008).

In the present study, a 1-D radial pure conduction numerical model which accounts for freezing and thawing is used. The model can handle different properties in multiple unsaturated and saturated ground rings around the boreholes. The following assumptions are considered.

5.3.1.1 Assumptions

- The ground (sand in the present case) is a homogeneous porous medium which consists of soil particles and void spaces filled with water in the saturated region(s).
- The sand is fully saturated in the saturated region(s).
- The ground has a uniform initial temperature.
- The temperature at an infinite radial distance from the borehole remains constant.
- The volumetric change due to water freezing in the saturated region is ignored and thus the density of the water is constant.
- Natural convection and moisture transfer effects in the saturated region are ignored and thus heat conduction is the only mode of heat transfer in the ground.
- The freezing or thawing process is assumed to take place over a small temperature range.
- Bulk average values of thermal conductivity for the frozen and unfrozen regions are considered.

Heat conduction problems under phase change conditions have been first studied by Stefan in 1889.Two types of numerical techniques are commonly used to handle this class of problems: the moving grid (time dependent grid) and the fixed grid approaches. The latter is used more frequently due to its conceptual simplicity and ease of implementation. Fixed mesh approaches

account for the latent heat evolution in the energy equation using either the enthalpy (Voller, 1990), or an effective heat capacity (Bonacina et al., 1973).

In this study the effective heat capacity with fixed meshes is used. Consequently, the latent heat effect is approximated by a large effective specific heat over a small temperature range. Many researchers have used this approach to solve numerically heat conduction problems under phase change conditions (Hashemi and Sliepcevich, 1973; Guidice et al., 1978; Sres et al., 2006; Sres and Anagnostou, 2007). Due to abrupt changes of the specific heat at the liquid/solid interface, non-convergence problems have been reported by some authors (Gong and Mujumdar, 1997). Civan and Sliepcevich (1987) evaluated the error introduced by assuming a finite temperature range for the phase change in the effective heat capacity method. Some researchers have proposed improvements for both the finite-element and finite-difference methods (Gong and Mujumdar, 1997; Hsiao 1985).

5.3.1.2 Mathematical formulation

A one-dimensional heat conduction model including phase change is developed in the ground, i.e. from the borehole wall to the far-field. Three phases are considered: ice-soil mixture (solid), water-soil mixture (liquid), and a transition phase. The governing equation is the energy equation in cylindrical coordinates:

$$\rho c \frac{\partial T}{\partial t} = \frac{1}{r} \frac{\partial}{\partial r} \left(kr \frac{\partial T}{\partial r} \right) \tag{5.1}$$

where ρc is the heat capacity, and k is thermal conductivity. These physical properties are constant for a given phase and are given as follows:

if $T \geq T_m + \delta$

$k = k_{ws}$

$\rho c = \rho_{sp} c_s \left(1 - \phi\right) + \rho_w c_w \phi$

if $T \leq T_m - \delta$

$k = k_{is}$

$\rho c = \rho_{sp} c_s \left(1 - \phi\right) + \rho_w c_i \phi$

if $T_m - \delta \leq T \geq T_m + \delta$

$$k = k_{is} + \frac{k_{ws} - k_{is}}{2\delta}\left[T - \left(T_m - \delta\right)\right]$$

$$\rho c = \rho_{sp} c_s \left(1 - \phi\right) + \rho_w \left(\frac{c_w + c_i}{2} + \frac{L}{2\delta}\right)\phi$$

where T_m is the melting temperature, 2δ is the phase change temperature range, L is the latent heat per unit mass, and ϕ is the soil porosity. Subscripts *is* and *ws* refer to the bulk average values for the frozen and unfrozen regions, respectively. For example, k_{is} is the bulk average thermal conductivity for the ice-soil mixture (solid phase). The remaining parameters are: ρ_{sp} and ρ_w, the densities of soil particles and water, respectively and c_s, c_i, and c_w, the soil, ice and water specific heats, respectively. The density of water is assumed to remain constant in each phase, thus ρ_w is used for both water and ice.

5.3.1.3 Boundary conditions

The model can handle the three standard boundary conditions (given temperature, heat flux and convection coefficient). A calculation domain corresponding to the experimental set-up of this study, to be described below, is shown in Figure 5-2.

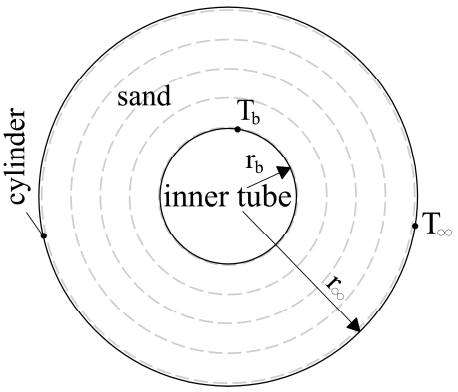

Figure 5-2: Illustration of the calculation domain and boundary conditions

As shown in Figure 5-2, the geometry consists of an inner tube surrounded by sand contained in an outer cylinder. In the present case, the temperatures of the inner tube, T_b, at r_b and the far-field temperature, T_∞, at r_∞ vary with time. Experimentally, they are measured every 5 seconds and recorded in a file which can be read by the model as boundary conditions.

5.3.1.4 Numerical approach

Equation (5.1) is discretized using the classic fully-implicit finite-volume approach of Patankar (1980) with Type-B grids. The dependent variable is the temperature *T*. A typical arrangement of the control volumes is shown in Figure 5-3 where the control volume *P* is represented by the node *P* at its centre. This control volume is surrounded by two adjacent neighbours *N* and *S* with connecting control volume faces *n* and *s*.

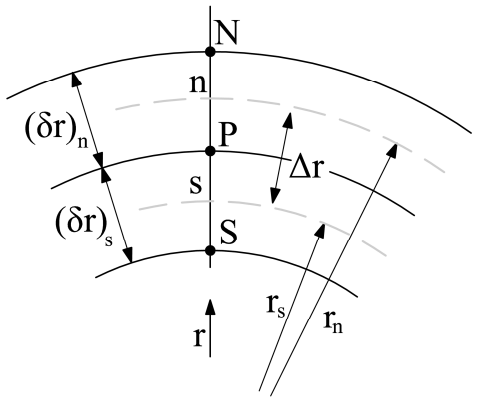

Figure 5-3: Finite control volumes

Equation (5.1) is integrated over control volumes using piecewise linear interpolation and over time intervals, Δt, using the fully-implicit scheme.

$$\int_{r_s}^{r_n}\int_{t}^{t+\Delta t} \rho c \frac{\partial T}{\partial t}\, dt dr = \int_{r_s}^{r_n}\int_{t}^{t+\Delta t} \frac{1}{r}\frac{\partial}{\partial r}\left(kr \frac{\partial T}{\partial r}\right) \tag{5.2}$$

$$\underbrace{\left[\left(\rho c\right)_P \frac{\Delta r}{2\Delta t}\left(r_n + r_s\right) + \frac{k_n r_n}{\delta r_n} + \frac{k_s r_s}{\delta r_s}\right]}_{a_P} T_p = \underbrace{\frac{k_n r_n}{\delta r_n}}_{a_N} T_N + \underbrace{\frac{k_s r_s}{\delta r_s}}_{a_S} T_S + \underbrace{\left(\rho c\right)_P \frac{\Delta r}{2\Delta t}\left(r_n + r_s\right)}_{a_P^0} T_P^0 \tag{5.3}$$

$$a_P T_P = a_N T_N + a_S T_S + b \tag{5.4}$$

where

$$b = a_P^0 T_P^0$$

The interface thermal conductivity in equation (5.3) is approximated at the control volume interface as follows:

$$\frac{1}{k_n} = \frac{1}{\ln\left(r_N/r_P\right)}\left[\frac{\ln\left(r_n/r_P\right)}{k_P} + \frac{\ln\left(r_N/r_n\right)}{k_N}\right]$$
$$\frac{1}{k_s} = \frac{1}{\ln\left(r_P/r_S\right)}\left[\frac{\ln\left(r_P/r_s\right)}{k_P} + \frac{\ln\left(r_s/r_S\right)}{k_S}\right] \quad (5.5)$$

The resulting coupled nonlinear (properties are temperature dependent) set of algebraic equations (Equation (5.4)) are solved over the whole domain using the tridiagonal matrix algorithm (Patankar, 1980). Nodes on the boundaries have no control volumes thereby no discretized integral balance equations are associated with them. Therefore, the temperature at the boundary nodes is either assumed to be known (given temperature at the boundaries) or calculated using quadratic interpolation as proposed by Baliga and Atabaki (2006).

The effective heat capacity approach is simple in its implementation. However, problems regarding grid independence and convergence have been reported. First, in order to make the solution insensitive to the phase change temperature range, 2δ, the specific heat of different phases is determined based on a linear interpolation of temperatures of neighbouring nodes as suggested by Hsiao (1985). This technique is described in more details in the Appendix. Convergence issues can be attributable to abrupt changes in specific heat and/or small time steps; the under-relaxation approach of Patankar (1980) is used to solve these problems.

Spatial and temporal grid independence checks have been performed. In the saturated region, where freezing occurs, very fine grids, of the order of 0.15 mm, are required. In the dry region, 20 mm grids are used. Since the first order fully-implicit approach is used, the model is relatively stable for time steps in the 1 to 60 seconds range. For that interval, small differences are observed in the results.

5.3.2 Borehole model

The ground model described above is coupled to a borehole model of a double U-tube borehole with two independent circuits operating with unequal mass flow rates and inlet temperatures. This model has been described by Eslami nejad and Bernier (a2011, b2011). It accounts for fluid and pipe thermal resistance and thermal interaction among U-tube circuits and predicts the fluid temperature profiles in both circuits along the borehole depth.

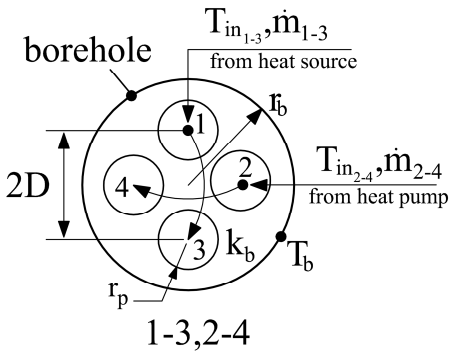

Figure 5-4: Four-pipe borehole cross section

Figure 5-4 presents a cross-section of a four-pipe borehole where the space between the pipes and the borehole wall is filled with a grout having a thermal conductivity k_b. The pipes, with an external radius r_p, are placed symmetrically in the borehole with identical center-to-center distance ($2D$) between two opposing pipes. In the present work, the 1-3,2-4 configuration is used (Zeng et al., 2003): the fluids from the heat source and the heat pump flow inside circuit 1-3 and 2-4, respectively. In effect, this configuration with two independent circuits acts as a heat exchanger between the heat source and the heat pump. For a given borehole wall temperature, T_b, and inlet conditions from both circuits, the model predicts the outlet temperatures of both circuits.

The ground model is coupled to the borehole model at the connecting boundary, i.e. at the borehole wall. An iterative solution is required at each time step in order to match the heat transfer rate, q_b, at the borehole wall given by both the borehole and ground models. This technique was previously used by Yang et al. (2009) who coupled a steady-state single U-tube borehole model to an unsteady one-dimensional ground heat transfer model without freezing.

5.4 Experimental set-up

An experimental set-up has been built to validate the ground model. A schematic of the apparatus is illustrated in Figure 5-5. It consists of a data acquisition system, a constant temperature bath, and a sand-filled cylinder. The cylinder is made of PVC and is 500 mm high with a 430 mm internal diameter and a 12 mm wall thickness. The bottom plate is also made of PVC while the top cap and inner rack are made of Plexiglas. The cylinder and all connecting pipes are insulated using closed-cell foam insulation with thicknesses of 25 mm and 13 mm, respectively. An inner copper tube with an external diameter of 22 mm is placed at the geometric center of the cylinder. Both ends of the pipe are connected to the constant temperature bath so as to form a closed

circuit. A solution of water/Ethylene-glycol (50%) is pumped through the inner tube from the bottom.

Temperature measurements are all made with T-type calibrated thermocouples. The temperature in the sand is measured using 16 probes. These stainless-steel probes are 30 cm long with a diameter of 1.6 mm. They are carefully inserted through the top cap and inner rack (shown in the photo insert in Figure 5-5) so as to be parallel to the cylinder wall.

Table 5-1: Positions of the thermocouples inside the sand-filled cylinder

Thermocouples		Radial position (mm)	Azimuth position (°)	Axial position (mm)
TCP1		25	0	0
TCP2		30	90	0
TCP3		35	180	0
TCP4		40	270	0
TCP5		45	0	0
TCP6		50	90	0
TCP7		55	180	0
TCP8		65	270	0
TCP9		75	0	0
TCP10		85	90	0
TCP11		95	180	0
TCP12		115	270	0
TCP13		135	0	0
TCP14		155	90	0
TCP15		175	180	0
TCP16		205	270	0
Profile Probe	PP1	104	0	-152
	PP2	104	0	-89
	PP3	104	0	-25
	PP4	104	0	+25
	PP5	104	0	+89
	PP6	104	0	+152

The tips of the probes are located at the mid-height of the cylinder. As show in Table 5-1 and in Figure 5-5, the thermocouples are staggered radialy and placed along four azimuthal positions. Furthermore, a six-point temperature profile probe is placed midway between the geometric center and the cylinder wall to measure axial temperatures along the cylinder height (axial positions are also given in Table 5-1). It is estimated that the position uncertainty of all the

temperature measurements in the sand is ±1mm. Two T-type thermocouple probes are immersed in the fluid at the inlet and outlet of the inner tube to measure the fluid temperature.

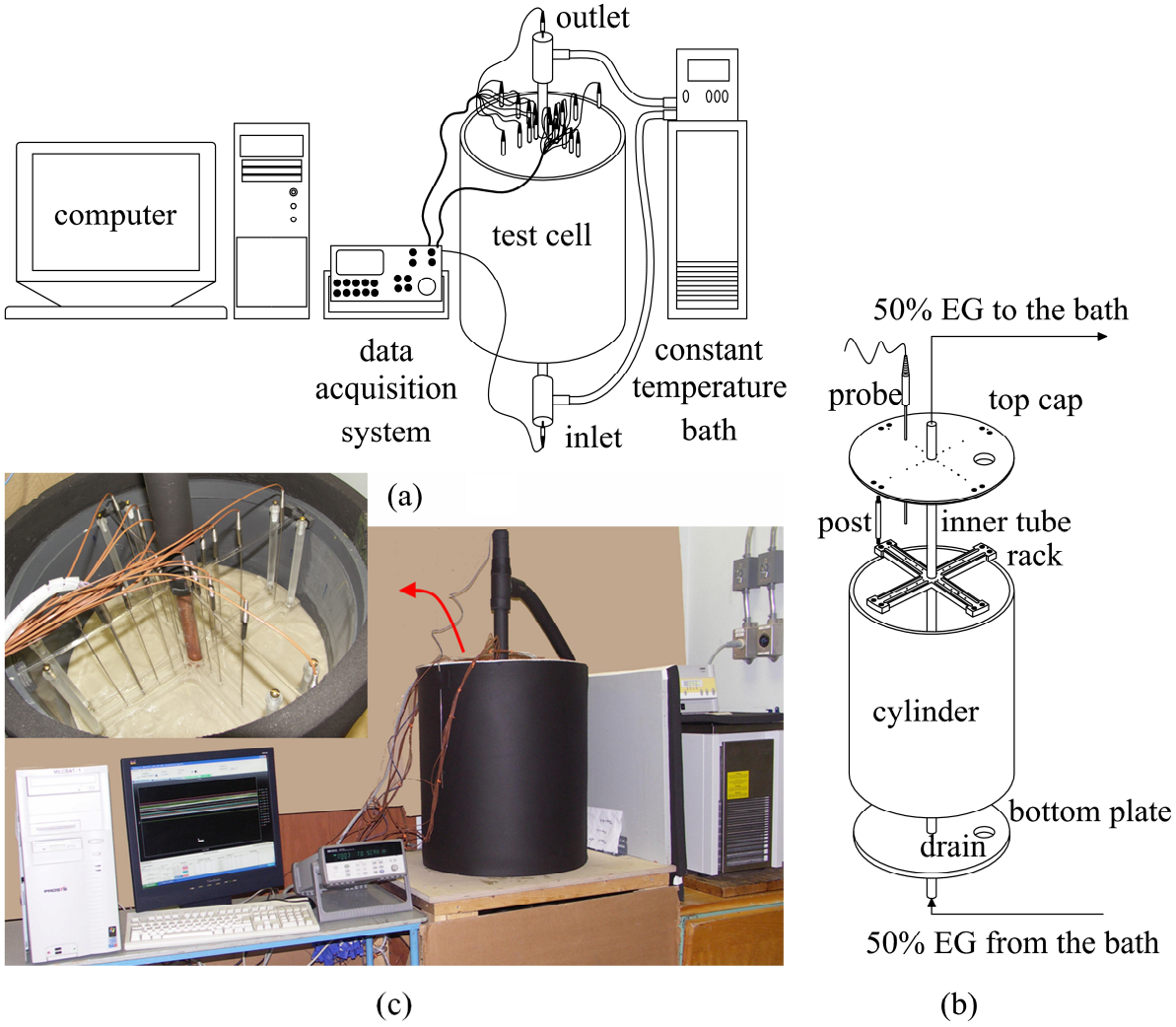

Figure 5-5: Experimental set-up

The temperatures of the outer surface of the inner tube and the inner surface of the cylinder at the measuring height are measured as well as the ambient temperature at two different locations.

The cylinder is filled with so-called "Ottawa sand (C-109)". This laboratory grade sand is frequently used as a test sample. It is made of sub-rounded quartz grains composed almost entirely of natural silica (SiO_2). The physical characteristics and thermal properties of the Ottawa sand have recently been measured and documented by Tarnawski et al. (2009, 2011). Most physical characteristics and thermal properties such as density and thermal conductivity depend on the porosity (volume of voids over the total volume) of the sand. According to Tarnawski et

al. (2009), porosity can vary from 0.4 to 0.32. The porosity of the sample used in this study was determined to be 0.36. All required sand properties are concisely listed in Table 5-2.

Table 5-2: Properties of the Ottawa sand (C-109) with a porosity of 0.36

	Thermal conductivity ($W \cdot m^{-1} \cdot K^{-1}$)	Thermal diffusivity ($m^2.day^{-1}$)
Dry sand	0.29	0.0198
Fully saturated and frozen sand	3.0	0.0934

Tests were performed with dry and fully saturated sand. Preparing a fully saturated sand is difficult and has to be accomplished with care. In this study, fully saturated sand is prepared by adding small amounts of dry sand to purified water. Sand and water are then well-mixed and the water which does not percolate down is vacuumed out of the cylinder. The water amount which is vacuumed out of the cylinder is replaced with fresh water. In this way, the dry sand is "rinsed" by the water.

5.4.1 Axial symmetry

As mentioned above, one T-type temperature profile probe is used to measure sand temperature at six positions along the cylinder height to verify the axial temperature uniformity.

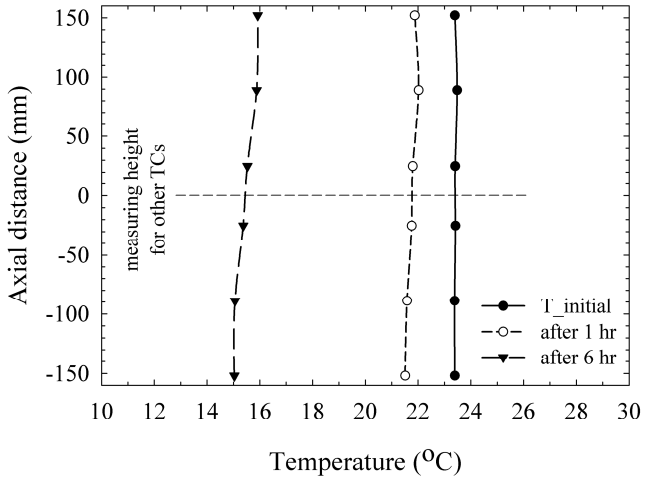

Figure 5-6: Example of axial temperature uniformity

Figure 5-6 presents temperatures measured by this probe for a somewhat extreme case which corresponds to the last test case reported below where saturated sand is used and the inner tube temperature varies from -20 to 55 ºC. As shown in Figure 5-6, at the beginning of the test the

temperature differences between points on this vertical axis are negligible. However, as the test progresses, the temperature uniformity degrades. After 6 hours, the temperature difference between the bottom and the top points on the profile probe reaches 0.9ºC.

5.4.2 Uncertainty analysis

In this study, the uncertainty in the temperature measurement in the sand can result from two sources: the uncertainty of the temperature measurement itself, $(U_T)_c$, and the uncertainty resulting from the accuracy of the probe locations, $(U_T)_r$.

The value of $(U_T)_c$ is determined based on a calibration in a constant temperature bath in the range from -20 to 60ºC. The resulting temperatures were checked against a reference platinum resistance thermometer which has an uncertainty of ± 0.21ºC. The value of $(U_T)_c$ is the result of the uncertainty of the reference thermometer and the uncertainty associated with the linear regressions associated with each thermocouple. In this study, in the worst case, the value of $(U_T)_c$ is ±0.3ºC. This value is used for all thermocouples.

The uncertainty resulting from the accuracy of the probe location is calculated numerically using a method presented by Moffat (1982).

$$\left(U_T\right)_r = \frac{T(r+\Delta r) - T(r)}{\Delta r} U_r \tag{5.6}$$

where U_r is the uncertainty of thermocouple tip location which is equal to ±1mm.

The fraction on the right hand side of Equation 6 is the temperature gradient (dT/dr) where $T(r+\Delta r)$ and $T(r)$ are the temperatures of two locations located before and after the probe and Δr is the radial distance between these two locations.

$(U_T)_r$ is combined with the thermocouple calibration uncertainty, $(U_T)_c$, based on the method described in ASHRAE/ANSI 1986 (1986). The global temperature uncertainty, U_T, is calculated as follows:

$$U_T = \sqrt{\left(U_T\right)_r^{\,2} + \left(U_T\right)_c^{\,2}} \tag{5.7}$$

For each experimental data, the global uncertainties are calculated and presented on the experimental data using error bars.

As will be shown in the results section, the impact of imprecise probe position on the global uncertainty is significantly larger for the thermocouples closer to inner tube because the temperature gradient, *dT/dr*, is higher for those smaller radius.

A series of experiments were performed to validate the ground model. Typically, a test would proceed as follows. First, the sand temperature was allowed to stabilized in order to become uniform everywhere. Then, the fluid flow rate is set to a high value so as to have constant temperatures at the inner tube wall. Then, the test proceeds with measurements recorded every 5 seconds by the data acquisition system.

5.5 Ground model validation

A comparison and two validation cases are presented below. In the first case, the ground model is compared with an analytical solution to the Stefan problem in cylindrical coordinates. Experimental results are used in the next two cases to validate the numerical ground model. Dry sand is used for the second case while saturated sand is used for the third case to test freezing conditions.

5.5.1 First test case

In this first case, the ground model is compared to a one-dimensional analytical solution, derived by Carslaw and Jaeger (1993), of an infinite line source (sink in the present case) immersed in a medium experiencing a solid-liquid phase change.

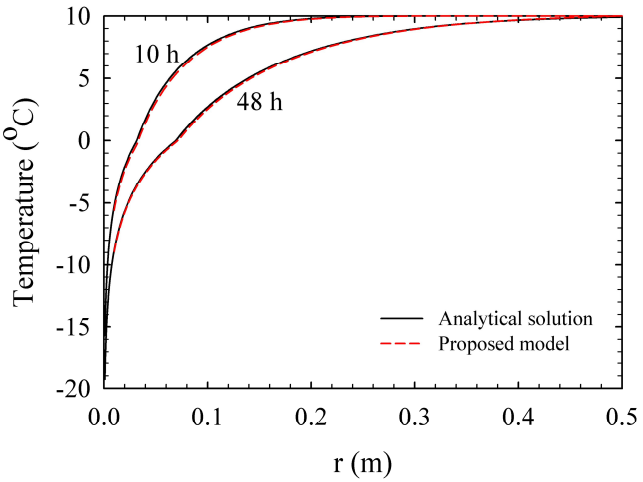

Figure 5-7: Temperature profile for the first test case

The results of this comparison are shown in Figure 5-7. In this case, 60 W/m are removed from a line sink. Numerically, the diameter of the line sink has been set to a small value of 1 mm. The medium is pure water and it is assumed that the problem is governed only by heat conduction in the radial direction. The temperature profiles after 10 and 48 hours for both the proposed numerical model and the analytical solution are in excellent agreement including the prediction of the freezing region. One such region can be seen after 48 hours for r=0.07 m at 0ºC.

5.5.2 Second test case: Dry sand

For this test case, the inlet temperature of the circulating fluid to the inner pipe is varied randomly in the range from -15ºC to 60ºC. The initial temperature of the sand was 18.3 ºC and the test lasted about seven hours.

The temperature evolutions of TC1, TC3, and TC9 are presented in Figure 5-8. As shown in Figure 5-8, the numerical ground model is in good agreement with the experiments and calculated values are all within the uncertainty bands of the experimental data. The sharp increases and decreases of temperatures are also well predicted. High heat flow rates, caused by steep changes of the inlet fluid temperature, results in relatively large temperature uncertainties. For example, at t = 1.67 hr, the control volume containing the node for TC1 (at 25 mm) receives relatively high heat flow rates at its south boundary which results in a temperature uncertainty of ± 2.37ºC. Also, as expected, the thermal mass of the sand tends to reduce the amplitude of the oscillations and shift them in time as *r* increases.

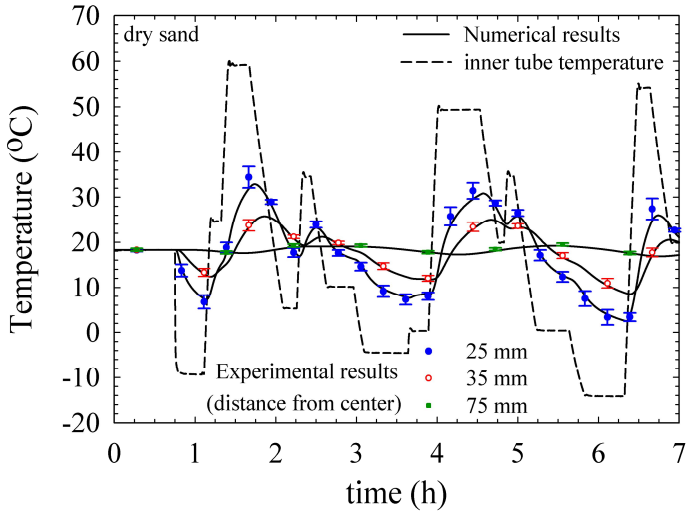

Figure 5-8: Temperature evolution for the second test case (dry sand)

Temperature profiles in the cylinder after 1, 5, and 7 hours are given in Figure 5-9. Due to the low thermal diffusivity of the dry sand, the temperature of almost half of the cylinder remains unchanged even the seven hour test. Again, very good agreement is observed between experimental and calculated results and almost all calculated temperatures are within the uncertainty range of measured values.

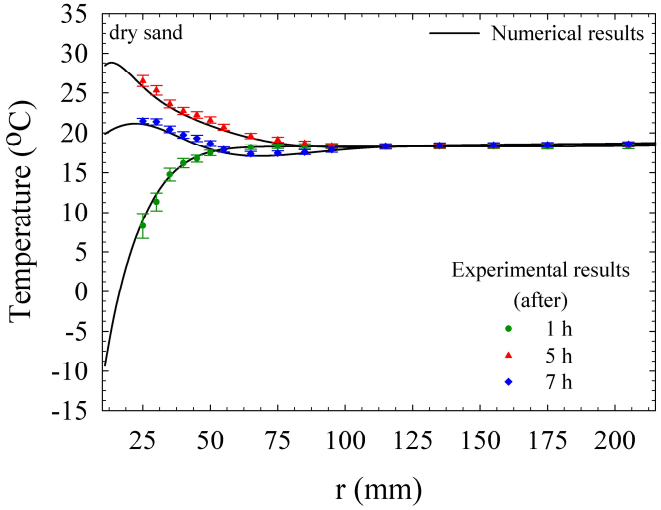

Figure 5-9: Temperature profile for the second test case (dry sand)

5.5.3 Third test case: saturated sand with freezing

In this case, the numerical ground model is validated against experimental data under freezing conditions. The initial sand temperature was 23.5 ºC. The inlet temperature of the working fluid to the inner pipe was first set to a constant value of -20ºC for the first 3.5 hours in order to freeze the saturated sand around the inner tube. Then, as shown in Figure 5-10(a), the fluid temperature was varied in order to have the inner tube temperature above and below the freezing point.

As shown in Figure 5-10(a), the temperature evolutions of the three measuring points (25, 35, and 75 mm from the center) are different. Points further from the center experience dampened oscillations which are shifted in time. At the end of the first heat extraction cycle (at t=3.5 hr), calculated temperatures of the first and third thermocouples reach -6.1ºC and -1.0ºC, respectively. This indicates that they are both located in the frozen region. At t=3.5 hr, the inner wall temperature is increased. As shown in the zoomed portion in Figure 5-10(b), the temperature of the frozen region (represented here by TC1) increases gradually up to -0.2ºC, close to the melting point. The temperature remains constant from t= 3.54 to 3.62 hr as the region melts. The

numerical model was able to capture this plateau. However, melting lasts about 0.01 hr longer in the numerical results when compared to experimental results.

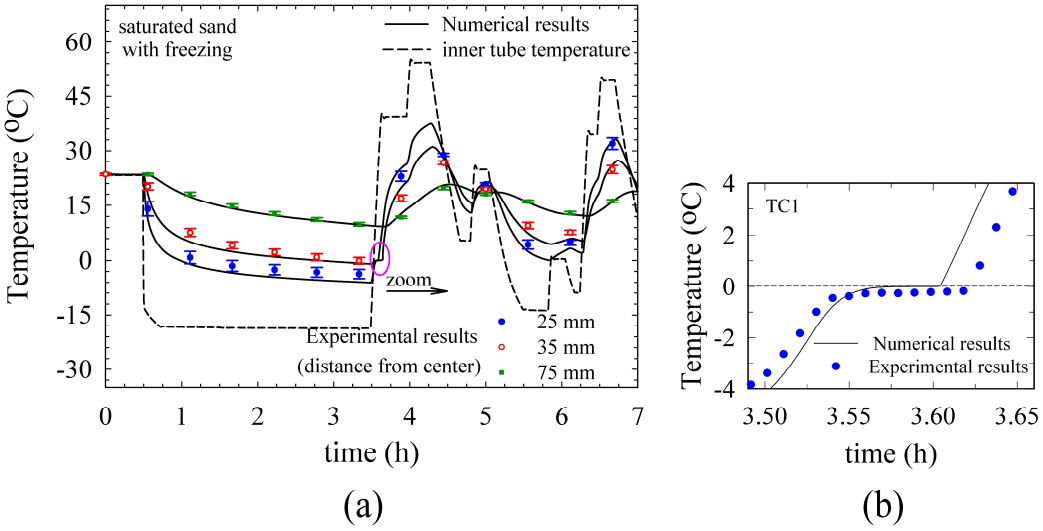

Figure 5-10: Temperature evolution for the third test case (saturated sand with freezing)

Figure 5-11 presents the temperature profiles after 3, 4.25, and 7 hours. As shown in this figure, the temperature profile after 3 hours indicates that the freezing front has progressed up to a radius of 35 mm. The other two curves show that the model is in very good agreement even after experiencing a few cycles of freezing and melting.

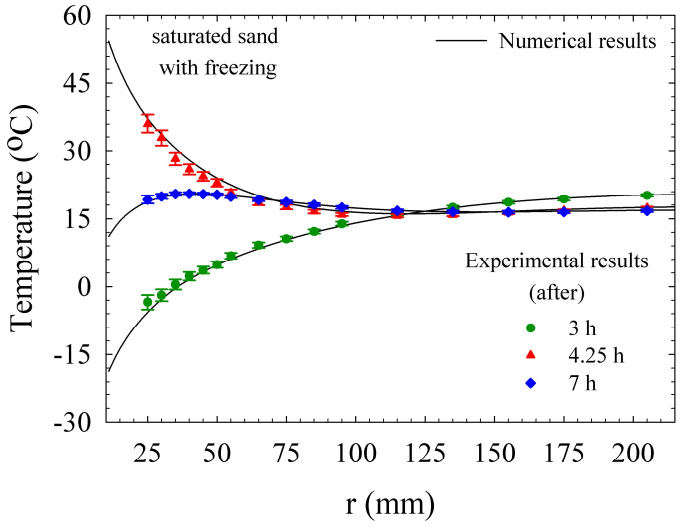

Figure 5-11: Temperature profile for the third test case (saturated sand with freezing)

The photo shown in Figure 5-12 has been taken with the top cap removed. It shows clearly the frozen ring after 3 hours of heat extractions (at t=3.5 hr).

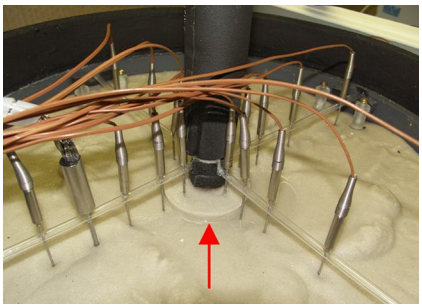

Figure 5-12: Photo showing the frozen ring in the third test case

5.6 Applications

In this section, GCHP system simulations are carried out over an entire heating season to examine the merits of the saturated sand ring. Two alternatives are compared and are shown in Figure 5-13. Case 1, which will be used as the reference case, represents a conventional GCHP system with a parallel double U-tube borehole. Case 2 involves solar recharging using a double U-tube borehole with two independent circuits. In this case, one circuit is linked to the heat pump (hp-circuit) and the other to thermal solar collectors (hs-circuit). Each circuit has its own circulating pump. Thus, both circuits can work simultaneously or independently.

These two cases have also been examined in a related study (without freezing) and the same GCHP system characteristics have been used here. These characteristics are summarized below; readers are referred to the study of Eslami nejad and Bernier (b2011) for more details. The simulated building corresponds to a well-insulated building located in Montréal, Canada. It has a peak space heating load of 5.2 kW and the annual space heating requirement is 11950 kWh. This building is heated with a 3-ton (10.5 kW) single-capacity GCHP. The heating capacity is sufficient to heat the building at peak conditions at the lowest recommended fluid inlet temperature, (i.e. -6 °C). Compressor power varies almost linearly from 1.65 to 1.85 kW for $T_{in,hp}$ between -6 °C and +30 °C . Finally, the mass flow rate on the evaporator side, $\dot{m}_{ref}$, is equal to 0.44 kg/s. For case 1, this flow rate is assumed to be split evenly between both circuits.

The solar collector is a standard single-glazed flat plate collector whose efficiency can be described by a second order curve relating the efficiency to $(T_{mean}-T_a)/G$ .The intercept of this curve is 0.78, and first and second order slope coefficients are 3.20 $W \cdot m^{-2} \cdot K^{-1}$ and 0.015 $W \cdot m^{-}$

$^{2}\cdot K^{-2}$, respectively. The collector area is set at 10 m^2 and the mass flow rate circulating in the hs-circuit is equal to $\dot{m}_{ref}$ /4.

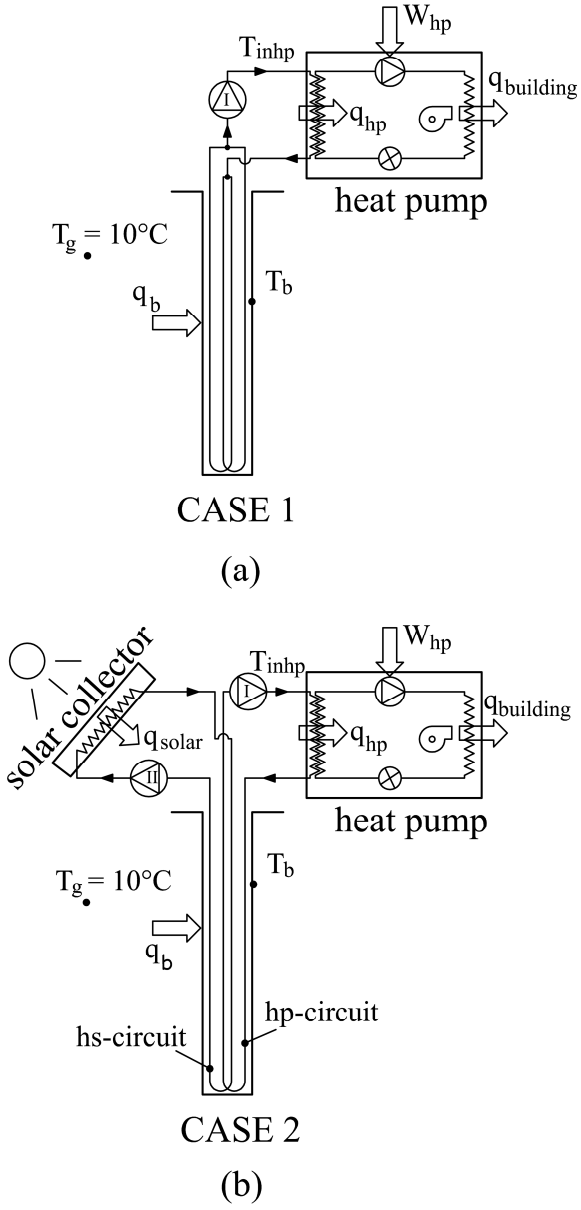

Figure 5-13: Schematic representation of Cases 1 and 2

Two borehole configurations are examined. They are shown in Figure 5-14 with characteristics given in Table 5-3. Configuration "a" represents a regular borehole while configuration "b" is the proposed borehole with a saturated sand ring. Both configurations have the same overall diameter of 15 cm and are equipped with four 3.34 cm diameter pipes. In configuration "b", both circuits

are in intimate contact and the sand ring thickness (r_{sr} - r_b) is 3.4 cm. Furthermore, it is assumed that the sand ring is in direct contact with the ground.

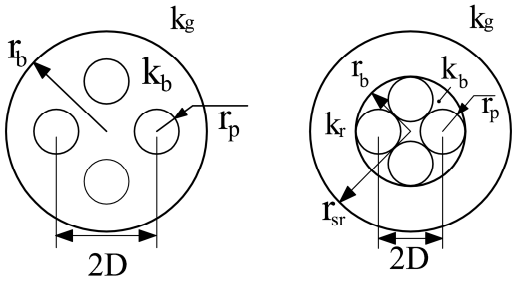

(a) Configuration "a" (b) Configuration "b"

Figure 5-14: Borehole cross sections

Table 5-3: Borehole characteristics

borehole types	r_b (cm)	r_p (cm)	D (cm)	r_{sr} (cm)	k_b ($W \cdot m^{-1} \cdot K^{-1}$)	k_r ($W \cdot m^{-1} \cdot K^{-1}$)
a	7.5	1.67	3.75	-	2	-
b	4.1	1.67	2.4	7.5	2	3

Four different cases, demoted as Cases 1a, 2a, 1b, and 2b, are examined. Each case has been simulated over a heating season. In all simulations, transient ground heat transfer from the borehole wall to the far-field (assumed here to be 3 meters away from the borehole center), including the saturated ring region, is evaluated using the ground model developed in this study. In each case it is coupled to a borehole model. For Case 1, the borehole model of Zeng et al. (2003) is used while Case 2 uses the double U-tube borehole model with two independent circuits developed by Eslami nejad and Bernier (b2011). An iterative solution is required at each time step in order to match the heat transfer rate at the borehole wall given by both the borehole and ground models. This results in a variation of the borehole wall temperature at each time step. Finally, the ground thermal conductivity and diffusivity are 2 $W \cdot m^{-1} \cdot K^{-1}$and 0.08 $m^2.day^{-1}$, respectively, and the undisturbed far-field ground temperature is set at 10 °C.

System simulations are performed using a 6 minute overall time step with the GCHP cycling on and off to meet the building load. Every 6 minutes, the building load and the available solar energy are calculated. These values are assumed to prevail over 360 inner time steps of the numerical model which, as indicated above, requires a 1 second time step. Calculations over the

entire heating season can take up to 10 hours of CPU (on a Intel Core 2 X6800 2.93GHz with 3.5 Gb of RAM).

Results, including required borehole length (H), cumulative heat pump energy consumption (W_{hp}), extracted energy from the ground (q_b), and injected solar energy to the borehole (q_{solar}) are presented in Table 5-4.

Table 5-4: Results of annual simulations

	Cases			
	1a	2a	1b	2b
H (m)	71	65	70	58
q_{build} (kWh)	11950			
W_{hp} (kWh)	3600	3430	3550	3440
q_b (kWh)	8350	2810	8400	2770
q_{solar} (kWh)	0	5710	0	5740

The resulting borehole lengths are 71, 65, 70, and 58 m for Cases 1a, 2a, 1b, and 2b, respectively. These values are the lengths required to keep T_{inhp} above -6ºC at all times during the heating season.

As shown in Table 5-4, for the reference case without the saturated ring (Case 1a) the heat pump extracts 8350 kWh from the ground (q_b) and uses 3600 kWh for the compressor (W_{hp}) to provide the required building load of 11950 kWh (q_{build}).

In case 2a, still without the saturated sand ring, 5710 kWh of solar heat is injected into the borehole which reduces the amount of energy extracted from the ground by 66% compared to Case 1a (from 8350 down to 2810 kWh). Furthermore, the heat pump energy consumption (W_{hp}) is reduced by 4.7% (from 3600 to 3430 kWh) and the required borehole length decreases by 6 m (8.5%). Both of these reductions are caused by solar heat injection which raises the inlet fluid temperature to the heat pump: The average annual value of T_{inhp} for Cases 1a and 2a are -1.7ºC and 0.7ºC, respectively. These reductions are, however, relatively modest and would probably not justify the extra cost associated with the thermal solar collectors. As pointed out by Eslami nejad and Bernier (b2011), these relatively small reductions are due to two factors. First, peak overnight building loads are not coincident with the available solar energy during the day. Secondly, in a single borehole geometry, the injected solar energy diffuses away from the

borehole and does not contribute to a significant increase in the ground temperature in the immediate vicinity of the borehole.

As shown in Table 5-4, using a saturated ring without solar injection (Case 1b) reduces the required length by a relatively small value of 1 m from 71 m (Case 1a) to 70 m. The heat pump energy consumption is also marginally reduced by 50 kWh. When solar heat injection is combined with a saturated ring (Case 2b), the borehole length required is reduced to 58 m (a 18 % reduction compared to Case 1a). The heat pump energy consumption for Cases 1b and 2b are not significantly different than their conventional borehole counterpart (Cases 1a and 2a).

Figure 5-15 presents the annual variations of: the inlet temperature to the heat pump, T_{inhp}; the borehole wall temperature, T_b; and the location of the radius of the frozen interface, r_{int}. The y-axis represents the number of hours from the start (mid-September) to the end of the heating season (mid-May), i.e. a total of 5800 hours.

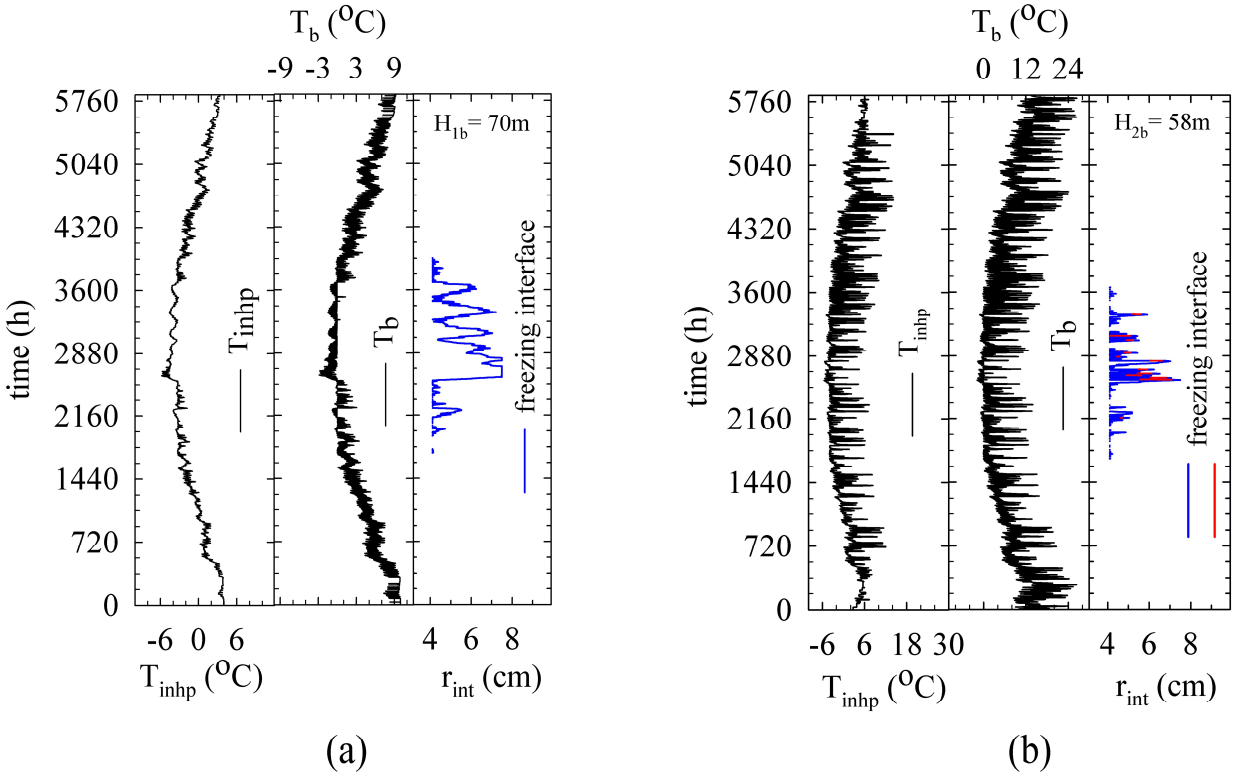

Figure 5-15: T_b, T_{inhp}, and the location of the freezing interface for cases 1b (a), and 2b (b)

For Case 1b (Figure 5-15(a)), the values of T_b and T_{inhp} decrease over time as heat is extracted for heat pump operation. At about t=1800 hours, T_b reaches the freezing point and freezing of the saturated sand ring starts. As indicated in the right graph of Figure 5-15(a), the thickness of the

frozen ring is relatively small, and remains small until t = 2600 hours. During that period, the borehole temperature, T_b, oscillates but does not often drop below 0ºC as the heat pump extracts the latent heat of fusion of the water in the saturated ring. Also, T_{inhp} remains above -3.4ºC most of the time. Starting at about t=2600 hours, the building load becomes important and the saturated ring remains frozen for about two months. During that period, the location of the frozen interface varies significantly and T_b and T_{inhp} fall below 0ºC and -3.4 ºC. The location of the frozen interface reaches a value of 7.5 cm (corresponding to the ring thickness of 3.4 cm) when the building load is at its peak. When the building load is small and heat pump operation is infrequent, the neighbouring ground (the far-field is at 10 ºC) warms the ring and r_{int} decreases. However, this process is insufficient to melt the whole region and T_b does not go above 0ºC until about t=3600 hours when the building load becomes small. Finally, as the building load is reduced further, T_b and T_{inhp} increase due to the net heat flow from the far-field to the borehole.

As shown in Figure 5-15(b), the borehole behaviour changes drastically when solar heat is injected. Except for short periods, for example at about t=2600 hours when the building load is maximum, T_b does not fall below 0 ºC because injected solar heat melts the frozen region. Furthermore, when the building load is small and solar availability is high, T_{inhp} reaches values around 14 ºC, significantly higher than for Case 1b.

Overall, the annual averages of T_{inhp} are -1.0 ºC and 1.0 ºC for Cases 1b and 2b, respectively. This leads to a 3.1% decrease in heat pump energy consumption (from 3550 down to 3440 kWh) despite the fact that the borehole is 17.1% shorter. When solar injection is present there are cases when there are two freezing interfaces. The radiuses of these two interfaces are indicated in blue and red in Figure 5-15(b).

This process is also illustrated in Figure 5-16 which shows a cross section of the borehole at four different times. At t=2564 hr, the saturated ring is completely melted and the interface is right on the borehole wall. Thirty-seven hours later, a 3.4 cm thick frozen ring is present. This coincides with a large building load and no solar heat injection. At t=2615 hr, conduction heat transfer from the far-field has reduced the thickness of the ring to 2.7 cm. Finally, solar heat injection at t = 2628 hr has melted the ice near the borehole wall up to the first freezing interface at 5.4 cm but a frozen ring is still present from this radius up to the second interface at 6.2 cm.

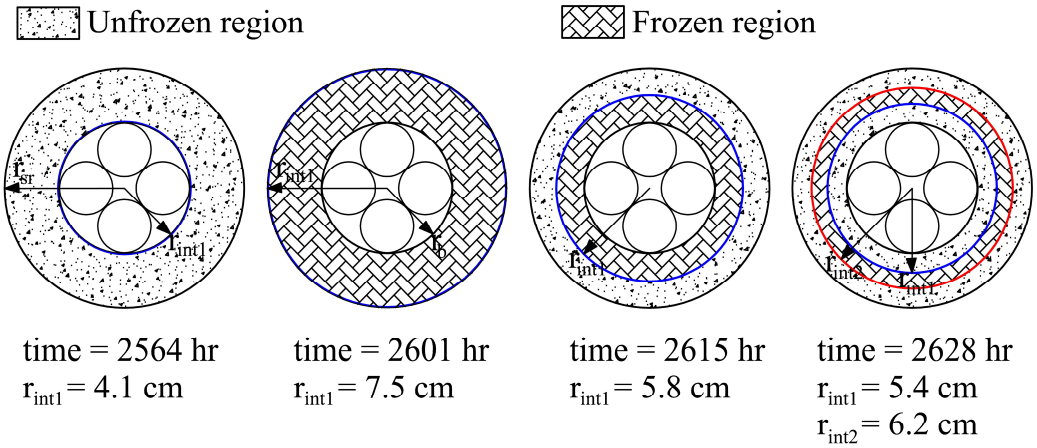

Figure 5-16: Schematic representation of a sequence of events leading to two freezing interfaces at t = 2628 hr

It is interesting to examine the effects of a variation of the saturated sand ring radius, r_{sr}, for Case 2b to evaluate the changes on H and the maximum radius of the freezing interface (r_{intmax}). The results of this analysis are presented in Figure 5-17.

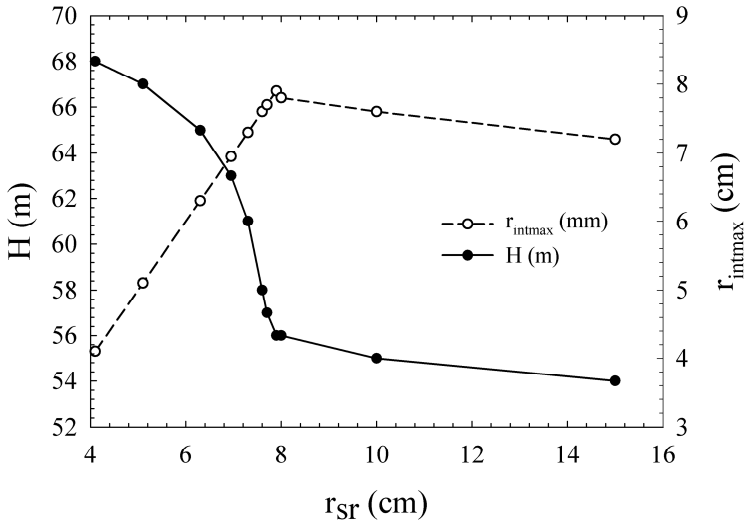

Figure 5-17: Optimum radius of the saturated ring for k_g= 2 W·m^{-1}·K^{-1}

The left axis presents the resulting borehole length H and values of r_{intmax} are given on the right axis. As shown on this Figure, the borehole length can be reduced from 68 m to 56 m (18% reduction) when r_{sr} is increased from 4.1 to 7.9 cm. However, it decreases by only 4% (from 56 m to 54 m) when r_{sr} increases from 7.9 to 15.0 cm.

As for r_{intmax} , it increases linearly with a slope of one as r_{sr} is increased from 4.1 to 7.9 cm. For this range of radius, the full thickness of the ring freezes at least once during the heating season.

At r_{sr} = 7.9 cm, there is a pivot point where r_{intmax} reaches its maximum. Any further increase of r_{sr} leads to a small gradual decrease of r_{intmax} from 7.9 cm to 7.2 cm when r_{sr} is varied from 7.9 cm to 15.0 cm. This is due to the increase of the thermal conductivity of the wider radius (the saturated ring has a thermal conductivity of 3 $W \cdot m^{-1} \cdot K^{-1}$ compared to a value of 2 $W \cdot m^{-1} \cdot K^{-1}$ for the ground) around the borehole which results in better conduction heat transfer from the borehole surroundings. In summary, given the modest advantages associated with thicker sand rings, a saturated sand ring radius of 7.9 cm appears to be the optimum radius for this case. In other words, r_{sr} should be selected such that it freezes entirely at least once during the heating season.

Finally, it is interesting to evaluate the changes on H, W_{hp}, and r_{intmax} when the ground thermal conductivity is reduced from 2 to 1 $W \cdot m^{-1} \cdot K^{-1}$ and increased from 2 to 3 $W \cdot m^{-1} \cdot K^{-1}$ while the other parameters remain the same. The results of this analysis are presented in Table 5-5. As mentioned above, the resulting borehole length is evaluated so that T_{inhp} is not allowed to fall below -6ºC during the heating season. For each thermal conductivity, five sets of results are presented: Cases 1a, 2a, 1b, 2b, and a modified Case 2b configuration where the radius of the saturated ring region has been optimized so that r_{sr} is equal to the maximum possible value of r_{int}.

Table 5-5: Simulation results for ground thermal conductivities of 1.0 and 3.0 $W \cdot m^{-1} \cdot K^{-1}$

	k_g= 1.0 ($W \cdot m^{-1} \cdot K^{-1}$) Cases				Opt. r_{sr}		k_g= 3.0 ($W \cdot m^{-1} \cdot K^{-1}$) Cases				Opt. r_{sr}
	1a	2a	1b	2b	2b		1a	2a	1b	2b	2b
H (m)	114	98	111	90	71		55	51	54	49	49
W_{hp} (KWh)	3540	3360	3510	3330	3460		3650	3510	3600	3450	3460
r_{intmax} (cm)	-	-	7.5	7.5	13.3		-	-	6.7	5.7	5.9
r_{sr} (cm)	-	-	7.5	7.5	13.3		-	-	7.5	7.5	5.9

The first thing to note in Table 5-5 is that borehole lengths are about twice as long when the thermal conductivity is reduced from 3.0 to 1.0 $W \cdot m^{-1} \cdot K^{-1}$ .This is no surprise as borehole length is heavily dependent on ground thermal conductivity. For a high ground thermal conductivity (right portion of Table 5-5), Case 2b shows the lowest heat pump energy consumption (3450 kWh) and the smallest borehole length (49 m). However, when compared to Case 1a, this represents modest reductions of 11% and 6 m. Thus, the use of a saturated ring with solar heat injection in a high ground thermal conductivity may not be economically advantageous because of this small decrease. It should also be noted that r_{intmax} is equal to 5.7 cm for case 2b

indicating that the saturated region does not freeze entirely and that smaller r_{sr} could be used. The last column of the right portion of Table 5-5 indicates the results for an optimum radius equals to 5.9 cm. However, the results are not much more different than for the non-optimum Case 2b.

Results for a low thermal conductivity ground are shown on the left portion of Table 5-5. The required borehole length for Case 2b is 21% lower than the reference case (90 m as opposed to 114 m). Moreover, the heat pump energy consumption decreases by 6% from 3540 kWh to 3330 kWh. For Case 2b, the freezing interface, r_{intmax}, has reached the radius of the saturated ring, r_{sr} (=7.5 cm). If r_{sr} is increased to its optimum value of 13.3 cm, then, as shown in Table 5-5, the required borehole length decreases to 71 m (a 38% difference when compared to Case 1a). Thus, the impact of the saturated sand ring is more significant in a low thermal conductivity ground.

5.7 Conclusion and recommendations

This study examines the thermal consequences of freezing the ground in the immediate vicinity of geothermal boreholes. A one-dimensional radial numerical heat transfer model is developed to evaluate heat transfer from the borehole wall to the far-field ground. The model accounts for multiple ground layers and phase change is handled using the effective capacity method. A small-scale experimental set-up has also been built to validate the numerical model. It is shown that the results of the numerical model are in very good agreement with the experimental results thus validating the numerical model.

In the application section, this model is used in a new proposed borehole system where a saturated sand ring is added between the borehole wall and the ground. This ring is allowed to freeze during peak heat load conditions to take advantage of the large constant-temperature storage capacity offered by the latent heat of fusion of the water. This saturated ring is used in conjunction with a double U-tube borehole with two independent circuits. Thermal solar collectors are connected to one circuit for solar recharging while a heat pump is linked to other circuit. With this approach solar energy can be injected, when available, to melt the saturated ring.

Typical borehole configurations are compared against this newly proposed borehole to examine the merits of this configuration. Results show that for configurations with a saturated sand ring, the borehole wall temperature remains around 0ºC for several days, during peak heating

conditions, while the borehole wall temperatures drops to much lower temperatures for typical boreholes without a saturated ring. Typically, freezing occurs within a thickness of 3-4 centimetres around the borehole. When solar energy is available and it is injected into one circuit of the borehole, it is shown that it is possible to melt the ice and "recharge" the saturated sand region for the next freezing cycle. With this approach, the borehole length can be reduced by as much as 38% in low ground thermal conductivity grounds.

Clearly, a parametric analysis for various building loads, solar availability, and ground conditions should be undertaken to cover the full spectrum of possible conditions. As shown in this paper, solar heat injection reduces the amount of energy required from the ground for heat pump operation. In multiple borehole installations, this means that borehole thermal interference is reduced and that boreholes could be placed closer together.

The numerical model presented here is based on a number of assumptions including the assumption of one-dimensional radial heat transfer. This is a good approximation to establish that freezing of a saturated ring has some potential while limiting calculation time over a heating season to reasonable values. However, it is clear that a 2-D model which would account for azimuthal variations is the next logical step. Finally, a full-scale experiment would enhance the understanding of the proposed system.

5.8 Nomenclature

$2D$ shank spacing between the U-tubes (m)

c_s soil pecific heat ($J \cdot kg^{-1} \cdot K^{-1}$)

c_i ice specific heat ($J \cdot kg^{-1} \cdot K^{-1}$)

c_w water specific heat ($J \cdot kg^{-1} \cdot K^{-1}$)

H required borehole length (m)

k thermal conductivity ($W \cdot m^{-1} \cdot K^{-1}$)

k_b grout thermal conductivity ($W \cdot m^{-1} \cdot K^{-1}$)

k_g ground thermal conductivity ($W \cdot m^{-1} \cdot K^{-1}$)

k_r Saturated sand ring thermal conductivity ($W \cdot m^{-1} \cdot K^{-1}$)

L latent heat per unit mass ($J \cdot kg^{-1}$)

$\dot{m}$ mass flow rate of the circulating fluid ($kg \cdot s^{-1}$)

N, S two adjacent neighbours of central control volume (shown in Figure 5-2)

n, s control volume faces (shown in Figure 5-2)

P central control volume represented by the node P at the center (shown in Figure 5-2)

q_b extracted energy from the ground (kWh)

q_{solar} solar energy injected into the borehole (kWh)

r radial distance from the center (m)

r_b borehole radius (m)

r_{int} freezing interface radius in the saturated region (m)

r_{intmax} maximum radius of the frozen region (m)

r_p pipe external radius (m)

r_{sr} saturated sand ring radius (m)

T_b borehole wall temperature (ºC)

TC thermocouples

T_{inhp} inlet fluid temperature to the heat pump (ºC)

T_m melting temperature (ºC)

$(U_T)_c$ uncertainty of the temperature measurement (ºC)

$(U_T)_r$ uncertainty associated with the probe location accuracy (ºC)

U_r uncertainty of the thermocouple tip location (m)

U_T global temperature uncertainty (ºC)

W_{hp} Annual heat pump energy consumption (kWh)

Δt time interval (s)

Greek symbols

2δ phase change temperature range (ºC)

ϕ soil porosity

ρc heat capacity ($J \cdot m^{-3} \cdot K^{-1}$)

ρ_{sp} density of soil particles ($kg \cdot m^{-3}$)

ρ_w density of water and ice ($kg \cdot m^{-3}$)

Subscripts

is bulk average values of the frozen regions

ws bulk average values of the unfrozen regions

1-3 1-3 circuit in the 1-3,2-4 configuration

2-4 2-4 circuit in the 1-3,2-4 configuration

5.9 Appendix

Linear interpolation of the nodal temperatures to account for the latent heat of fusion:

The specific heat of different phases is determined based on a linear interpolation of temperatures of neighbouring nodes as follows:

$$(\rho c)_1 = \frac{1}{2}\left[(\rho c)_{1,2} + (\rho c)_{1,0}\right]$$

for example to calculate $(\rho c)_{1,2}$

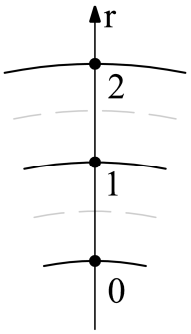

Figure 5-A-1: Typical portion of the calculation domain

if $T_2 < T_1 < T_m - \delta$

$$(\rho c)_{1,2} = \rho_{sp} c_s (1-\phi) + \rho_w c_i \phi$$

if $T_m + \delta < T_2 < T_1$

$$(\rho c)_{1,2} = \rho_{sp} c_s (1-\phi) + \rho_w c_w \phi$$

if $T_2 < T_m - \delta$ and $T_1 > T_m + \delta$

$$(\rho c)_{1,2} = \rho_{sp} c_s (1-\phi) + \rho_w \left\{ \frac{1}{T_1 - T_2} \left[2\delta \left(\frac{c_w + c_i}{2} + \frac{L}{2\delta} \right) + c_i (T_m - \delta - T_2) + c_w (T_1 - T_m - \delta) \right] \right\} \phi$$

if $T_m - \delta < T_2 < T_1 < T_m + \delta$

$$(\rho c)_{1,2} = \rho_{sp} c_s (1-\phi) + \rho_w \left(\frac{c_w + c_i}{2} + \frac{L}{2\delta} \right) \phi$$

if $T_2 < T_m - \delta$ and $T_m - \delta < T_1 < T_m + \delta$

$$(\rho c)_{1,2} = \rho_{sp} c_s (1-\phi) + \rho_w \left\{ \frac{1}{T_1 - T_2} \left[\left(\frac{c_w + c_i}{2} + \frac{L}{2\delta} \right) (T_1 - T_m + \delta) + c_i (T_m - \delta - T_2) \right] \right\} \phi$$

if $T_m - \delta < T_2 < T_m + \delta$ and $T_m + \delta < T_1$

$$(\rho c)_{1,2} = \rho_{sp} c_s (1-\phi) + \rho_w \left\{ \frac{1}{T_1 - T_2} \left[\left(\frac{c_w + c_i}{2} + \frac{L}{2\delta} \right) (T_m + \delta - T_2) + c_w (T_1 - T_m - \delta) \right] \right\} \phi$$

5.10 References

ASHRAE/ANSI (1986). Guide for engineering analysis of experimental data. American Society of Heating Refrigeration and Air-Conditioning Engineers/American National Standards Institute.

Bakirci, K., Ozyurt, O., Comakli, K., and Comakli, O. (2011). Energy analysis of a solar-ground source heat pump system with vertical closed-loop for heating application. *Energy*, 36(5), 3224-3232.

Baliga, B. R., and Atabaki, N. (2006). Control-volume-based finite difference and finite element methods. In Minkowycz, W. J., Sparrow, E. M., and Murthy, J. Y. (Eds.), *Handbook of Numerical Heat Transfer* (2nd ed). New York: John Wiley & Sons.

Bonacina, C., Comini, G., Fasano, A., and Primicerio, M. (1973). Numerical solution of phase-change problems. *International Journal of Heat and Mass Transfer*, 16(10), 1825-1832.

Carslaw, H. S., and Jaeger, J. C. (1993). Change of state. In *Conduction of Heat in Solids* (2nd ed). New York: Oxford University Press.

Chiasson, A. D., and Yavuzturk, C. (2003). Assessment of the viability of hybrid geothermal heat pump systems with solar thermal collectors. *ASHRAE Transactions*, 109 (2), 487-500.

Civan, F., and Sliepcevich, C. M. (1987). Limitation in the apparent heat capacity formulation for heat transfer with phase change. Proceeding of the Oklahoma Academy of Science, 67, 83-88.

Diao, N. R., Li, Q., and Fang, Z. H. (2004). Heat transfer in ground heat exchangers with groundwater advection. *International Journal of Thermal Science*, 43(12), 1203-1211.

Eskilson, P. (1987). Thermal analysis of heat extraction systems. Doctorial Thesis, University of Lund, Sweden.

(a) Eslami nejad, P., and Bernier, M. (2011). Heat transfer in double U-tube boreholes with two independent circuits. *ASME Journal of Heat Transfer*, 133(8).

(b) Eslami nejad, P., and Bernier, M. (2011). Coupling of geothermal heat pumps with thermal solar collectors using double U-tube borehole with two independent circuits. *Applied Thermal Engineering*, 31(14-15), 3066-3077.

Fan, R., Jiang, Y., Yao, Y., Shiming, D., and Ma, Z. (2007). A study on the performance of a geothermal heat exchanger under coupled heat conduction and groundwater advection. *Energy*, 32(11), 2199-2209.

Frivik, P. E., and Comini, G. (1982). Seepage and heat flow in soil freezing. *ASME Journal of Heat Transfer*, 104(2), 323-328.

Fukusako, S., Seki, N., and Yamada, M. (1987). Heat-removal characteristics of a combined system of concentric-tube thermosyphon and heat pump. *International Journal of JSME*, 30(264), 936-944.

Gong, Z. X., and Mujumdar, A. S. (1997). Non-convergence versus non-conservation in effective heat capacity methods for phase change problems. *International Journal of Numerical Methods for Heat Fluid Flow*, 7(6), 565-579.

Guidice, S. D., Comini, G., and Lewis, R. W. (1978). Finite element simulation of freezing processes in soils. *International Journal of Numerical Analytical Methods in Geomechanics*, 2(3), 223-235.

Han, Z., Zheng, M., Kong, F., Wang, F., Li, Z., and Bai, T. (2008). Numerical simulation of solar assisted ground-source heat pump heating system with latent heat energy storage in severely cold area. *Applied Thermal Engineering*, 28 (11-12), 1427-1436.

Hashemi, H. T., and Sliepcevich, C. M. (1973). Effect of seepage stream on artificial soil freezing. *ASCE Journal of the Soil Mechanics and Foundations Division*, 99(SM3), 267-289.

Hsiao, J. S. (1985). An efficient algorithm for finite-difference analyses of heat transfer with melting and solidification. *Numerical Heat Transfer*, 8(6), 653-666.

Hellström, G. (1991). Ground heat storage, thermal analysis of duct storage system. Doctorial Thesis, University of Lund, Sweden.

Ingersoll, L. R., Zobel, O. J., and Ingersoll, A. C. (1954). *Heat conduction with engineering geological and other applications* (2nd ed). New York: McGraw-Hill.

Kjellsson, E., Hellström, G., and Perers, B. (2010). Optimization of systems with the combination of ground-source heat pump and solar collectors in dwellings. *Energy*, 35 (6), 2667-2673.

Lee, C. K. (2011). Effects of multiple ground layers on thermal response test analysis and ground-source heat pump simulation. *Applied Energy*, 88(12), 4405-4410.

Lu, T., and Wang, K. S. (2008). Numerical analysis of the heat transfer associated with freezing/solidifying phase changes for a pipeline filled with crude oil in soil saturated with water during pipeline shutdown in winter. *Journal of Petroleum Science and Engineering*, 62(1-2), 52-58.

Marcotte, D., Pasquier, P., Sheriff, F., and Bernier, M. (2010). The importance of axial effects for borehole design of geothermal heat-pump systems. *Renewable Energy*, 35(4), 763-770.

Mei, V. C., and Emerson, C. J. (1985). New approach for analysis of ground-Coil design for applied heat pump systems. *ASHRAE Transactions*, 91(2B), 1216-1224.

Mikkola, M., and Hartikainen, J. (2001). Mathematical model of soil freezing and its numerical implementation. *International Journal of Numerical Methods in Engineering*, 52(5-6), 543-557.

Moffat, R. J. (1982). Contributions to the theory of single-sample uncertainty analysis. *Journal of Fluids Engineering Transaction ASME*, 104(2), 250-260.

Newman, G. P., and Wilson, G. W. (1997). Heat and mass transfer in unsaturated soils during freezing. *Canadian Geotechnical Journal*, 34(1), 63-70.

Nordell, B., and Ahlström, A. K. (2006). Freezing problems in borehole heat exchangers. *NATO Science Series II: Mathematics, Physics and Chemistry*, 234, 193-204.

Ozgener, O., and Hepbasli, A. (2005). Experimental performance analysis of a solar assisted ground-source heat pump greenhouse heating system. *Energy and Buildings*, 37(1), 101-110.

Patankar, S. V. (1980). *Numerical heat transfer and fluid flow* (2nd ed). New York: McGraw-Hill.

Penrod, E. B., and Prasanna, D. V. (1962). Design of flat-plate collector for solar earth heat pump. *Solar Energy*, 6 (1), 9-22.

Penrod, E. B., and Prasanna, D. V. (1969). Procedure for designing solar-earth heat pumps. *Heating, Piping and Air Conditioning*, 41 (6), 97-100.

Rattanadecho, P., and Wongwises, S. (2008). Moving boundary-moving mesh analysis of freezing process in water-saturated porous media using a combined transfinite interpolation and PDE mapping methods. *ASME Journal of Heat Transfer*, 130(1).

Raymond, J., Therrien, R., Gosselin, L., and Lefebvre, R. (2011). Numerical analysis of thermal response tests with a groundwater flow and heat transfer model. *Renewable Energy*, 36(1), 315-324.

Sres, A., Pimentel, E., and Anagnostou, G. (2006). Numerical and physical modeling of artificial ground freezing. Proceeding of International Conference of Numerical Simulation of Construction Processes in Geotechnical Engineering Urban Environment, 185-191.

Sres, A., and Anagnostou, G. (2007). Numerical modeling and the implementation of artificial ground freezing. Proceeding of International Symposium of Numerical Models in Geomechanics, 311-316.

Stefan, J. (1889). Über die Theorie der Eisbildung, insbesondere über die Eisbildung in Polarmeere, Sitzungsber. *Wien Akad Math Natur*, 98, 965–983.

Stojanovic, B., and Akander, J. (2010). Build-up and long-term performance test of a full-scale solar-assisted heat pump system for residential heating in Nordic climatic conditions. *Applied Thermal Engineering*, 30 (2-3), 188-195.

Tarnawski, V. R., Momose, T., Leong, W. H., Bovesecchi, G., and Coppa, P. (2009). Thermal Conductivity of Standard Sands. Part I. Dry-state Conditions. *International Journal of Thermophysics*, 30(3), 949-968.

Tarnawski, V. R., Momose, T., and Leong, W. H. (2011). Thermal Conductivity of Standard Sands II. Saturated Conditions. *International Journal of Thermophysics*, 32(5), 984-1005.

Trillat-Berdal, V., Souyri, B., and Achard, G. (2007). Coupling of geothermal heat pumps with thermal solar collectors. *Applied Thermal Engineering*, 27 (10), 1750-1755.

Voller, V. R. (1990). Fast implicit finite-difference method for the analysis of phase change problems. *Numerical Heat Transfer Part B Fundamentals*, 17(2), 155-169.

Wang, C. Y., Wu, C. Z., Tu, C. J., and Fukusako, S. (1990). Freezing around a vertical cylinder immersed in porous media incorporating the natural convection effect. *Waerme Stoffuebertrag*, 26(1), 7-15.

Wang, H., Qi, C., Wang, E., and Zhao, J. (2009). A case study of underground thermal storage in a solar-ground coupled heat pump system for residential buildings. *Renewable Energy*, 34(1), 307-314.

Wang, X., Zheng, M., Zhang, W., Zhang, S., and Yang, T. (2010). Experimental study of a solar-assisted ground-coupled heat pump system with solar seasonal thermal storage in severe cold areas. *Energy and Buildings*, 42 (11), 2104-2110.

Weaver, J. A., and Viskanta, R. (1985). Freezing of liquid-saturated porous media. *ASME, heat transfer division* (publication) HTD, 46, 1-8.

Xi, C., Lin, L., and Hongxing, Y. (2011). Long term operation of a solar-assisted ground coupled heat pump system for space heating and domestic hot water. *Energy and Buildings*, 43(8), 1835-1844.

Yang, H., Cui, P., and Fang, Z. (2010). Vertical- borehole ground-coupled heat pumps: A review of models and systems. *Applied Energy*, 87 (1), 16-27.

Yang W., Chen, Z., and Shi, M. (2010). Alternate operation characteristics of a solar-ground source heat pump system. *Journal of Southeast University English Edition*, 26(2), 327-332.

Yang, W., Shi, M., and Dong, H. (2006). Numerical simulation of the performance of a solar-earth source heat pump system. *Applied Thermal Engineering*, 26 (17-18), 2367-2376.

Yang, W., Shi, M., Liu, G., and Chen, Z. (2009). A two-region simulation model of vertical U-tube ground heat exchanger and its experimental verification. *Applied Energy*, 86 (10), 2005-2012.

Zeng, H., Diao, N., and Fang, Z. (2003). Heat transfer analysis of boreholes in vertical ground heat exchangers. *International Journal of Heat and Mass Transfer*, 46 (23), 4467-4481.

CHAPITRE 6 GENERAL DISCUSSION AND RECOMMENDATIONS

The main objective of this work is to assess the applicability and benefits of the double U-tube with two independent circuit configuration equipped with a saturated ring both in terms of heat pump energy consumption and borehole length reduction.

6.1 Review of the main contributions of this thesis

The system under study (presented in Figure 5-1) consists of a solar thermal collector, heat pump, and a new double U-tube borehole configuration with two independent circuits surrounded by a saturated sand ring. This borehole configuration is used for heat extraction in one circuit, combined with a heat pump, and thermal recharging in the other circuit using solar energy. The main benefit of this configuration is that, during peak heating conditions, the saturated ring will freeze. Thus, it is possible to take advantage of the relatively high energy content associated with the latent heat of fusion of water in the sand to keep the return fluid temperature above the recommended operating limit of the heat pump. When solar energy is available, solar heat is injected in the second circuit to melt the frozen saturated ring and recharge the ground for the next freezing cycle. The first study (Article I) is devoted to the development of an analytical model to predict steady-state heat transfer in double U-tube geothermal boreholes equipped with two independent circuits. The model accounts for thermal interaction among pipes and predicts the fluid temperature profiles of both circuits along the borehole depth, including the exit fluid temperature. Laplace transforms are used to solve the governing dimensionless heat flow balance equations. Different circuit arrangements are assessed under typical borehole operating conditions and the 1-3,2-4 arrangement is found to provide superior performance compared to the 1-2,3-4 and 1-2,4-3 configurations. A parametric analysis of dimensionless borehole wall temperature, dimensionless pipe spacing, and grout thermal conductivity is performed to evaluate the effect of these parameters on borehole required length.

The second study (Article II) improves the previous borehole model so that it can account for unequal mass flow rates and inlet temperatures in the two independent circuits. Simulations over 20 years are performed to examine the impact of thermal recharging a single-borehole residential system under dry ground conditions. Results indicate that winter solar recharging using the proposed configuration reduces the amount of energy extracted from the ground significantly.

However, the effects on the required borehole length and heat pump energy consumption are relatively marginal.

The final study (Article III) focuses on the thermal consequences of freezing the ground in the immediate vicinity of geothermal boreholes. First, a one-dimensional radial numerical heat transfer model is developed to evaluate heat transfer from the borehole wall to the far-field ground. The model accounts for multiple cylindrical layers in the ground and phase change is handled using the effective capacity method. A small-scale experimental set-up is also built. It was used to successfully validate the numerical model over several freezing/thawing cycles. The numerical ground model is coupled to the borehole model developed in the previous two studies to examine various scenarios involving typical heat pump operation. Typical borehole configurations are compared against this new configuration to examine its merits. Results show that for configurations with a saturated sand ring, the borehole wall temperature remains around 0ºC for several days, during peak heating conditions, while the borehole wall temperatures drops to much lower temperatures for typical boreholes without a saturated ring. Typically, freezing occurs within a thickness of 3-4 centimetres around the borehole. When solar energy is available and it is injected into one circuit of the borehole, it is shown that it is possible to melt the ice and "recharge" the saturated sand region for the next freezing cycle. With this approach the borehole length can be reduced by as much as 38% in low ground thermal conductivity grounds. However, the effect of the new borehole configuration on the heat pump energy consumption is still relatively small with heat pump energy consumption reductions of less than 5%.

The optimum saturated sand ring radius for different ground thermal conductivities was evaluated. Results indicate that higher ground thermal conductivities require smaller saturated sand ring radius. For example, for a relatively high ground thermal conductivity of 3 $W \cdot m^{-1} \cdot K^{-1}$, the optimum saturated sand ring radius is about 2 cm thick while it is about 9 cm thick when the ground thermal conductivity is 1 $W \cdot m^{-1} \cdot K^{-1}$. For these two examples, the borehole length reduction is 11% and 38%, respectively. Therefore, based on these results, the use of a saturated sand ring combined with a double U-tube borehole and solar heat injection in a low thermal conductivity ground could be more economically advantageous.

6.2 Recommendation for future studies

It is clear from the work presented in this thesis that the new borehole configuration with two independent circuits surrounded by a saturated sand ring shows some potential to reduce borehole lengths and heat pump energy consumption. In order to confirm these findings, it is recommended to perform an extensive parametric analysis that would cover the full spectrum of possible conditions including various building loads, different climates and ground conditions. As shown in this study, solar heat injection reduces the amount of energy required from the ground for heat pump operation. In multiple borehole installations, this means that borehole thermal interference is reduced and that boreholes could be placed closer together. Therefore, evaluating the effect of using this borehole configuration on multiple borehole installations in terms of overall required space and borehole length would be interesting.

The numerical ground model elaborated in the present work is based on a number of simplifying assumptions including one-dimensional radial heat transfer. This is a good approximation to establish that freezing of a saturated ring has some potential while limiting simulation time over a heating season to reasonable values. However, it is clear that a two-dimensional model which would account for azimuthal variations is the next logical step.

Implementation of the combined borehole/ground model in a commercially available simulation software such as TRNSYS would certainly make it readily available to design engineers.

Finally, it is recommended to proceed to a full-scale experimental validation of the combined double U-tube and saturated sand ring configuration. Once this is done and the results look promising, construction and implementation of such boreholes in the field should be envisioned.

LIST OF REFERENCES

Al-Khoury, R., and Bonnier, P. G. (2006). Efficient finite element formulation for geothermal heating systems. Part II: Transient. *International Journal of Numerical Methods in Engineering*, 67 (5), 725-745.

Al-Khoury, R., Bonnier, P. G., and Brinkgreve, R. B. J. (2005). Efficient finite element formulation for geothermal heating systems. Part I: Steady state. *International Journal of Numerical Methods in Engineering*, 63 (7), 988-1013.

ASHRAE/ANSI (1986). Guide for engineering analysis of experimental data. American Society of Heating Refrigeration and Air-Conditioning Engineers/American National Standards Institute.

Bakirci, K., Ozyurt, O., Comakli, K., and Comakli, O. (2011). Energy analysis of a solar-ground source heat pump system with vertical closed-loop for heating application. *Energy*, 36(5), 3224-3232.

Baliga, B. R., and Atabaki, N. (2006). Control-volume-based finite difference and finite element methods. In Minkowycz, W. J., Sparrow, E. M., and Murthy, J. Y. (Eds.), *Handbook of Numerical Heat Transfer* (2nd ed). New York: John Wiley & Sons.

Bennet, J., Claesson, J., and Hellström, G. (1987). Multipole method to compute the conductive heat flows to and between pipes in a composite cylinder. University of Lund, Department of Building Technology and Mathematical Physics. Lund, Sweden.

Bernier, M. (2000). A Review of the Cylindrical Heat Source Method for the Design and Analysis of Vertical Ground-Coupled Heat Pump Systems. 4th International Conference of Heat Pumps in Cold Climates, 14 pages.

Bernier, M., Labib, R., Pinel, P., and Paillot, R. (2004). A multiple load aggregation algorithm for annual hourly simulations of GCHP systems. *HVAC&R Research*, 10 (4), 471-487.

Bernier, M., and Salim Shirazi, A. (2007). Solar heat injection into boreholes: a preliminary analysis. Proceeding of 2nd Canadian Solar Building Conference, T1-1-1, 8 pages.

Bonacina, C., Comini, G., Fasano, A., and Primicerio, M. (1973). Numerical solution of phase-change problems. *International Journal of Heat and Mass Transfer*, 16(10), 1825-1832.

Carslaw, H. S., and Jaeger, J. C. (1993). Change of state. In *Conduction of Heat in Solids* (2nd ed). New York: Oxford University Press.

Carslaw, H. S., and Jaeger, J. C. (1947). *Conduction of heat in solids* (1st ed). Oxford, U.K.: Claremore Press.

Chapuis, S., and Bernier, M. (2008). Étude préliminaire sur le stockage solaire saisonnier par puits géothermique. Proceeding of 3rd Canadian Solar Building Conference, 14-23.

Chapuis, S., and Bernier, M. (2009). Seasonal storage of solar energy in borehole heat exchangers. Proceeding of 11th International IBPSA Conference, 599-606.

Chiasson, A. D., and Yavuzturk, C. (2003). Assessment of the viability of hybrid geothermal heat pump systems with solar thermal collectors. *ASHRAE Transactions*, 109 (2), 487-500.

Civan, F., and Sliepcevich, C. M. (1987). Limitation in the apparent heat capacity formulation for heat transfer with phase change. Proceeding of the Oklahoma Academy of Science, 67, 83-88.

Diao, N. R., Zeng, H. Y., and Fang, Z. H. (2004). Improvement in modeling of heat transfer in vertical ground heat exchangers. *HVAC&R Research*, 10 (4), 459-470.

Diao, N. R., Li, Q., and Fang, Z. H. (2004). Heat transfer in ground heat exchangers with groundwater advection. *International Journal of Thermal Science*, 43(12), 1203-1211.

Eskilson, P. (1987). Thermal analysis of heat extraction systems. Doctorial Thesis, University of Lund, Sweden.

(a) Eslami nejad, P., and Bernier, M. (2011). Heat transfer in double U-tube boreholes with two independent circuits. *ASME Journal of Heat Transfer*, 133(8).

(b) Eslami nejad, P., and Bernier, M. (2011). Coupling of geothermal heat pumps with thermal solar collectors using double U-tube borehole with two independent circuits. *Applied Thermal Engineering*, 31(14-15), 3066-3077.

Eslami nejad, P., Bernier, M., Kummert, M. (2010). Réalisation d'un logiciel d'évaluation des performances thermiques de géométrise innovantes de capteurs enterers. Rapport confidentiel soumis à Électricité de France, Contrat: P3907, 30 pages.

Eslami nejad, P., Langlois, A., Chapuis, S., Bernier, M., and Faraj, W. (2009). Solar heat injection into boreholes. Proceeding of 4th Canadian Solar Building Conference, 237-246.

Fan, R., Jiang, Y., Yao, Y., Shiming, D., and Ma, Z. (2007). A study on the performance of a geothermal heat exchanger under coupled heat conduction and groundwater advection. *Energy*, 32(11), 2199-2209.

Frivik, P. E., and Comini, G. (1982). Seepage and heat flow in soil freezing. *ASME Journal of Heat Transfer*, 104(2), 323-328.

Fontaine, P. O., Marcotte, D., Pasquier, P., and Thibodeau, D. (2011). Modeling of horizontal geoexchange systems for building heating and permafrost stabilization. *Journal of Geothermics*, 40 (3), 211-220.

Fukusako, S., Seki, N., and Yamada, M. (1987). Heat-removal characteristics of a combined system of concentric-tube thermosyphon and heat pump. *International Journal of JSME*, 30(264), 936-944.

Georgiev, A., Busso, A., and Roth, P. (2006). Shallow borehole heat exchanger: Response test and charging-discharging test with solar collectors. *Renewable Energy*, 31 (7), 971-985.

Gong, Z. X., and Mujumdar, A. S. (1997). Non-convergence versus non-conservation in effective heat capacity methods for phase change problems. *International Journal of Numerical Methods for Heat Fluid Flow*, 7(6), 565-579.

Gu, Y., and O'Neal, D. (1998). Development of an equivalent diameter expression for vertical U-tubes used in ground coupled heat pumps. *ASHRAE Transactions*, 104(2), 347-355.

Guidice, S. D., Comini, G., and Lewis, R. W. (1978). Finite element simulation of freezing processes in soils. *International Journal of Numerical Analytical Methods in Geomechanics*, 2(3), 223-235.

Han, Z., Zheng, M., Kong, F., Wang, F., Li, Z., and Bai, T. (2008). Numerical simulation of solar assisted ground-source heat pump heating system with latent heat energy storage in severely cold area. *Applied Thermal Engineering*, 28 (11-12), 1427-1436.

Hashemi, H. T., and Sliepcevich, C. M. (1973). Effect of seepage stream on artificial soil freezing. *ASCE Journal of the Soil Mechanics and Foundations Division*, 99(SM3), 267-289.

Hsiao, J. S. (1985). An efficient algorithm for finite-difference analyses of heat transfer with melting and solidification. *Numerical Heat Transfer*, 8(6), 653-666.

He, M., Rees, S., and Shao, L. (2009). Simulation of a domestic ground source heat pump system using a transient numerical borehole heat exchanger model. Proceeding of 11th International IBPSA Conference, 607-614.

Hellström, G. (1989). Duct ground heat storage model. Manual for Computer Code, Department of Mathematical Physics, University of Lund, Sweden.

Hellström, G. (1991). Ground heat storage, thermal analysis of duct storage system. Doctorial Thesis, University of Lund, Sweden.

Ingersoll, L. R., Zobel, O. J., and Ingersoll, A. C. (1954). *Heat conduction with engineering geological and other applications* (2nd ed). New York: McGraw-Hill.

Kjellsson, E., Hellström, G., and Perers, B. (2010). Optimization of systems with the combination of ground-source heat pump and solar collectors in dwellings. *Energy*, 35 (6), 2667-2673.

Kummert, M., and Bernier, M. (2008). Analysis of a combined photovoltaic-geothermal gas-fired absorption heat pump system in a Canadian climate. *Journal of Building Performance Simulation*, 1 (4), 245-256.

Lamarche, L., and Beauchamp, B. (2007). New solutions for the short-time analysis of geothermal vertical boreholes. *International Journal of Heat and Mass Transfer*, 50(7-8), 1408-1419.

Lamarche, L., Kajl, S., and Beauchamp, B. (2010). A review of methods to evaluate borehole thermal resistances in geothermal heat-pump systems. *Journal of Geothermics*, 39 (1), 187-200.

Lee, C. K. (2011). Effects of multiple ground layers on thermal response test analysis and ground-source heat pump simulation. *Applied Energy*, 88(12), 4405-4410.

Lu, T., and Wang, K. S. (2008). Numerical analysis of the heat transfer associated with freezing/solidifying phase changes for a pipeline filled with crude oil in soil saturated with water during pipeline shutdown in winter. *Journal of Petroleum Science and Engineering*, 62(1-2), 52-58.

Man, Y., Yang, H., Diao, N., Liu, J., and Fang, Z. (2010). A new model and analytical solutions for borehole and pile ground heat exchangers. *International Journal of Heat and Mass Transfer*, 53 (13-14), 2593-2601.

(a) Marcotte, D., and Pasquier, P. (2008). Fast fluid and ground temperature computation for geothermal ground-loop heat exchanger systems. *Journal of Geothermics*, 37 (6), 651-665.

(b) Marcotte, D., and Pasquier, P. (2008). On the estimation of thermal resistance in borehole thermal conductivity test. *Renewable Energy*, 33 (11), 2407-2415.

Marcotte, D., Pasquier, P., Sheriff, F., and Bernier, M. (2010). The importance of axial effects for borehole design of geothermal heat-pump systems. *Renewable Energy*, 35(4), 763-770.

Mei, V. C., and Emerson, C. J. (1985). New approach for analysis of ground-Coil design for applied heat pump systems. *ASHRAE Transactions*, 91(2B), 1216-1224.

Mikkola, M., and Hartikainen, J. (2001). Mathematical model of soil freezing and its numerical implementation. *International Journal of Numerical Methods in Engineering*, 52(5-6), 543-557.

Moffat, R. J. (1982). Contributions to the theory of single-sample uncertainty analysis. *Journal of Fluids Engineering Transaction ASME*, 104(2), 250-260.

Muraya, N. K., O'Neal, D. L., and Heffington, W. M. (1996). Thermal interference in adjacent legs in a vertical U-tube heat exchanger for a ground coupled heat pump. *ASHRAE Transactions*, 102(2), 12-21.

Newman, G. P., and Wilson, G. W. (1997). Heat and mass transfer in unsaturated soils during freezing. *Canadian Geotechnical Journal*, 34(1), 63-70.

Nordell, B., and Ahlström, A. K. (2006). Freezing problems in borehole heat exchangers. *NATO Science Series II: Mathematics, Physics and Chemistry*, 234, 193-204.

Ozgener, O., and Hepbasli, A. (2005). Experimental performance analysis of a solar assisted ground-source heat pump greenhouse heating system. *Energy and Buildings*, 37(1), 101-110.

Patankar, S. V. (1980). *Numerical heat transfer and fluid flow* (2nd ed). New York: McGraw-Hill.

Paul, N. D. (1996). The effect of grout thermal conductivity on vertical geothermal heat exchanger design and performance. Master of Science Thesis. South Dakota State University.

Penrod, E. B., and Prasanna, D. V. (1962). Design of flat-plate collector for solar earth heat pump. *Solar Energy*, 6 (1), 9-22.

Penrod, E. B., and Prasanna, D. V. (1969). Procedure for designing solar-earth heat pumps. *Heating, Piping and Air Conditioning*, 41 (6), 97-100.

Philippacopoulos, A. J., and Berndt, M. L. (2001). Influence of debonding in ground heat exchangers used with geothermal heat pumps. *Journal of Geothermics*, 30 (5), 527-545.

Rattanadecho, P., and Wongwises, S. (2008). Moving boundary-moving mesh analysis of freezing process in water-saturated porous media using a combined transfinite interpolation and PDE mapping methods. *ASME Journal of Heat Transfer*, 130(1).

Raymond, J., Therrien, R., Gosselin, L., and Lefebvre, R. (2011). Numerical analysis of thermal response tests with a groundwater flow and heat transfer model. *Renewable Energy*, 36(1), 315-324.

Remund, C. P. (1999). Borehole thermal resistance: laboratory and field studies. *ASHRAE Transaction*s, 105 (1), 439-445.

Rottmayer, S. P., Beckman, W. A., and Mitchell, J. W. (1997). Simulation of a single vertical U-tube ground heat exchanger in an infinite medium. ASHRAE, Atlanta, GA, USA.

Sibbitt, B., Onno, T., McClenahan, D., Thornton, J., Brunger, A., Kokko, J., and Wong, B. (2007). The Drake Landing Solar Community Project – Early Results. Proceeding of 2nd Canadian Solar Building Conference, M2-1-3, 11 pages.

Sres, A., Pimentel, E., and Anagnostou, G. (2006). Numerical and physical modeling of artificial ground freezing. Proceeding of International Conference of Numerical Simulation of Construction Processes in Geotechnical Engineering Urban Environment, 185-191.

Sres, A., and Anagnostou, G. (2007). Numerical modeling and the implementation of artificial ground freezing. Proceeding of International Symposium of Numerical Models in Geomechanics, 311-316.

Stefan, J. (1889). Über die Theorie der Eisbildung, insbesondere über die Eisbildung in Polarmeere, Sitzungsber. *Wien Akad Math Natur*, 98, 965–983.

Stojanovic, B., and Akander, J. (2010). Build-up and long-term performance test of a full-scale solar-assisted heat pump system for residential heating in Nordic climatic conditions. *Applied Thermal Engineering*, 30 (2-3), 188-195.

Tarnawski, V. R., Momose, T., Leong, W. H., Bovesecchi, G., and Coppa, P. (2009). Thermal Conductivity of Standard Sands. Part I. Dry-state Conditions. *International Journal of Thermophysics*, 30(3), 949-968.

Tarnawski, V. R., Momose, T., and Leong, W. H. (2011). Thermal Conductivity of Standard Sands II. Saturated Conditions. *International Journal of Thermophysics*, 32(5), 984-1005.

Trillat-Berdal, V., Souyri, B., and Achard, G. (2007). Coupling of geothermal heat pumps with thermal solar collectors. *Applied Thermal Engineering*, 27 (10), 1750-1755.

Voller, V. R. (1990). Fast implicit finite-difference method for the analysis of phase change problems. *Numerical Heat Transfer Part B Fundamentals*, 17(2), 155-169.

Wang, C. Y., Wu, C. Z., Tu, C. J., and Fukusako, S. (1990). Freezing around a vertical cylinder immersed in porous media incorporating the natural convection effect. *Waerme Stoffuebertrag*, 26(1), 7-15.

(a)Wang, H., Qi, C., Du, H., and Gu, J. (2009). Thermal performance of borehole heat exchanger under ground water flow: A case study from Baoding. *Energy and Buildings*, 41(12), 1368-1373.

(b)Wang, H., Qi, C., Wang, E., and Zhao, J. (2009). A case study of underground thermal storage in a solar-ground coupled heat pump system for residential buildings. *Renewable Energy*, 34(1), 307-314.

Wang, X., Zheng, M., Zhang, W., Zhang, S., and Yang, T. (2010). Experimental study of a solar-assisted ground-coupled heat pump system with solar seasonal thermal storage in severe cold areas. *Energy and Buildings*, 42(11), 2104-2110.

Weaver, J. A., and Viskanta, R. (1985). Freezing of liquid-saturated porous media. ASME, heat transfer division (publication) HTD, 46, 1-8.

Wetter, M., and Huber, A. (1997). TRNSYS Type 451: Vertical Borehole Heat Exchanger (3.1 ed).

Xi, C., Lin, L., and Hongxing, Y. (2011). Long term operation of a solar-assisted ground coupled heat pump system for space heating and domestic hot water. *Energy and Buildings*, 43(8), 1835-1844.

Yang, H., Cui, P., and Fang, Z. (2010). Vertical- borehole ground-coupled heat pumps: A review of models and systems. *Applied Energy*, 87 (1), 16-27.

Yang W., Chen, Z., and Shi, M. (2010). Alternate operation characteristics of a solar-ground source heat pump system. *Journal of Southeast University English Edition*, 26(2), 327-332.

Yang, W., Shi, M., and Dong, H. (2006). Numerical simulation of the performance of a solar-earth source heat pump system. *Applied Thermal Engineering*, 26 (17-18), 2367-2376.

Yang, W., Shi, M., Liu, G., and Chen, Z. (2009). A two-region simulation model of vertical U-tube ground heat exchanger and its experimental verification. *Applied Energy*, 86 (10), 2005-2012.

Yavuzturk, C., Spitler, J. D., and Rees, S. J. (1999). A transient two dimensional finite volume model for the simulation of vertical U-tube ground heat exchanger. *ASHRAE Transactions*, 105, 465-474.

Young, T. R. (2004). Development, verification, and design analysis of the borehole fluid thermal mass model for approximating short-term borehole thermal response. Master of Science Thesis, Oklahoma State University, United States.

Zeng, H., Diao, N., and Fang, Z. (2003). Heat transfer analysis of boreholes in vertical ground heat exchangers. *International Journal of Heat and Mass Transfer*, 46 (23), 4467-4481.

Zeng, H., Diao, N., and Fang, Z. (2002). A finite line-source model for boreholes in geothermal heat exchangers. *Heat Transfer - Asian Research*, 31**,** 558-567.